Thesis Report

Thickness-Tailored Flexible Airfoil for Improved Aeroelastic Stability Behaviour

R. de Vries

Technische Universiteit Delft

TU Delft

Thesis Report

Thickness-Tailored Flexible Airfoil for Improved Aeroelastic Stability Behaviour

by

R. de Vries

to obtain the degree of Master of Science
at the Delft University of Technology,
to be defended publicly on Thursday December 1, 2016 at 2:00 PM.

Student number:	1522183	
Project duration:	March 1, 2015 – December 1, 2016	
Thesis committee:	Dr. ir. R. De Breuker,	TU Delft, supervisor
	Dr. J. Sodja	TU Delft, supervisor
	Dr. M. M. Abdallah,	TU Delft
	Dr. ir. O. K. Bergsma,	TU Delft

TU Delft

Delft University of Technology
Faculty of Aerospace Engineering
Department of Aerospace Structures and Materials

GRADUATION COMMITTEE

Dated: 1-12-2016

Committee chair:

Dr. M. M. Abdallah

Committee members:

Dr. ir. R de Breuker

Dr. ir. O. K. Bergsma

Dr. J. Sodja

Acknowledgements

First of all I would like to thank Roeland and Jurij for their daily support during the project. They were always very helpful and I could trust on their knowledge in cases I had questions. The regular meetings we had I experienced as very motivational which is something I needed from time to time. Furthermore I want to thank Dr. M. M. Abdallah and Dr. ir. O. K. Bergsma for their willingness to participate in the graduation committee.

Furthermore I want to thank the department for facilitating me during my thesis. Especially I want to thank Johan, Adriaan, Stefan, Maarten, Krishna, Twan, and Juliette for the useful discussions on aeroelasticity and also for the time we spent during the coffee breaks or when doing activities together.

Lastly and most importantly, I want to thank my parents for always motivating and supporting me during my entire studies. Without them it would not have been possible to finish university.

R. de Vries
Delft, December 2016

Abstract

The general trend in the aerospace industry is to optimise lightweight and highly flexible wing structures made of composite materials. This flexibility gives rise to static and dynamic aeroelastic instability problems. Research by Kim and Lee, Murua et al., and Drazumeric et al. have proven that chord-wise flexibility has a significant effect on the aeroelastic characteristics of an airfoil [1–3]; including the aeroelastic instability boundaries. Drazumeric et al. have numerically and experimentally shown that by adding chord-wise flexibility the stability boundaries could be increased up to 79.2% in the region of bimodal flutter behaviour, meaning that conventional section flutter and plate flutter occur simultaneously.

It has been identified that the two-dimensional aeroelastic characteristics of flexible airfoil has been studied for constant stiffness flexible airfoils only. The present project will take the next step by assuming a piecewise constant thickness distributed flexible trailing edge. An elastically supported rigid airfoil shaped leading edge with attached a flexible composite plate was considered. The piecewise constant thickness distribution of the flexible plate was optimized for increasing the critical flow velocity at which the aeroelastic instabilities occur.

An aeroelastic model has been developed to determine the aeroelastic characteristics of an elastically supported airfoil with attached a flexible piecewise constant thickness distributed trailing edge. The thin airfoil is assumed to harmonically oscillate with small amplitudes. The aerodynamic forces and moments are calculated by adopting the Küssner and Schwarz model which relates the pressure distribution over the airfoil to the downwash [4]. The transverse motion of the plate is modelled as an Euler-Bernoulli beam under the assumption that no span-wise deformations in the flexible trailing edge occur. The aeroelastic stability boundary is obtained by solving a complex eigenvalue problem in matrix form. The solutions to the system of equations are obtained as couples of the reduced frequency with the corresponding critical flow speed.

The aeroelastic model is used to tailor the thickness distribution of the flexible trailing edge to optimise for the critical flow speed. Optimisations are executed for airfoil sections with conventional sectional parameters and with unconventional sectional parameters. In all cases it can be seen that a convergence in critical flow velocities was obtained for a trailing edge divided in two sections with a constant thickness. Depending on the length of the flexible trailing edge an increase up to 76% was achieved for airfoils with unconventional parameters, while for airfoils with conventional parameters a limited increase up to 4.1% was achieved.

Contents

Nomenclature

Greek Symbols

Symbol	Description	Units
α	Non-dimensional damping coefficient	$-$
α_0	Pitching degree of freedom	rad
ϵ	Strain	$-$
ϵ_x	Strain in x direction	$-$
θ	Ply angle	deg
λ_j	j^{th} eigenvalue of the freely vibrating plate	$-$
μ	Mass ratio of the plate	$-$
μ_m	Material viscosity	$kg/(sm)$
ρ	Air density	kg/m^3
σ_{dp}	Stress due to viscoelastic material damping	N/m^2
σ_p	Areal density of the flexible plate	kg/m^2
ϕ	Velocity potential	$-$
ω	Angular frequency	rad/s
ω_α	Natural frequency pitching motion	s^{-1}
ω_h	Natural frequency plunging motion	s^{-1}

Latin Symbols

Symbol	Description	Units
A_0	Amplitude of the pitching degree of freedom	$-$
A_F	Aeroelastic matrix	$-$
a_j	Transverse displacement mode series coefficient	$-$
b	Width of the airfoil	m
C	Theodorsen function	$-$
C_p	Viscoelastic material damping along the plate	Nms
D_p	Flexural rigidity along the plate	Nm
d_α	Damping coefficient for pitching	Nms/rad
d_y	Damping coefficient for plunging	Ns/m
G	Function for pressure distribution determination	$-$
h	Thickness of the plate	m
I	Identity matrix	$-$
J_0	Mass moment of inertia of the rigid part around the axis of rotation	kgm^2
J_α	Mass moment of inertia of the system around the axis of rotation	kgm^2
k	Reduced frequency	$-$
k_α	Pitch stiffness	Nm/rad
k_y	Plunge stiffness	N/m
l	Length of the chord	m
l_p	Length of the flexible plate	m
M_{dp}	Bending moment due to viscoelastic material damping	Nm
m	Mass of the rigid part	kg
m_0	Mass involved in plunge only	kg
m_y	Mass of the system	kg
n_p	Number of plies	$-$
p	Total pressure distribution	N/m^2
p_w	Pressure distribution due out-of-plane plate motion	N/m^2
p_y	Pressure distribution due to plunging	N/m^2
p_α	Pressure distribution due to pitching	N/m^2
$S_{y\alpha}$	Static moment of mass for plunging due to pitching	kgm
$S_{\alpha y}$	Static moment of mass for pitching due to plunging	kgm
S	Number of plate sections	$-$
s	Section number	$-$
T	Kinetic energy	Nm
t	Time	s
U	Internal potential energy	Nm
U_c	Non-dimensional critical flow speed	$-$
u	Horizontal displacement component	m
V	External potential energy	Nm
v	Vertical displacement component	m
v_{af}	Airfoil flutter speed	m/s
v_{cr}	Critical speed	m/s
v_{div}	Divergence speed	m/s
v_F	Flutter speed	m/s
v_{pf}	Plate flutter speed	m/s
v_y	Downwash	m/s
v_∞	Free-stream velocity	m/s
W	Transverse displacement mode of the plate	Nm
W_{0j}	j^{jt} eigenmode of a freely vibrating plate	$-$
W_{NC}	Work done due to non-conservative forces	Nm
w	Transverse displacement of the plate	m
x	Longitudinal position on the airfoil	m
x_0	Distance between the elastic axis and the leading edge	m
x_T	Distance between the center of gravity and the elastic axis	m
Y_0	Amplitude of the plunging degree of freedom	$-$
y_0	Plunging degree of freedom	m
z	Through the thickness direction	m

1 Introduction

Aeroelasticity is the field of physics or engineering that studies the interaction between inertial, elastic, and aerodynamic forces [5]. The aeroelastic field of study is summarised by the Collar aeroelastic triangle (Collar 1978), shown in Figure 1.1. The triangle visualises the relation between two or more forces to the corresponding discipline in engineering. Aeroelasticity can have undesirable effects on the performance of flexible structures, which may subsequently lead to structural failures. In order to prevent this type of constructional default it is essential to include aeroelastic phenomena during the design phase of flexible structures.

Aeroelasticity is not solely significant for the aerospace industry. Aeroelastic research has been carried out on structures like wind turbines [6–8], turbomachinery blades [9, 10], bridges [11, 12], and even Formula One cars [13]. A disaster like the collapse of the Tacoma bridge due to aeroelastic instabilities confirms the necessity of considering aeroelastic effects during the design phase of these structures.

Aeroelastic phenomena are divided into static and dynamic aeroelasticity. Static aeroelasticity is concerned with non-oscillatory effects of aerodynamic forces on the structure, which involves the interaction between elastic and aerodynamic forces (Figure 1.1). Whereas dynamic aeroelasticity considers the oscillatory effects of aeroelastic interactions, which are a result of coupling between inertial, elastic, and aerodynamic forces (Figure 1.1). The main area of interest in the field of dynamic aeroelasticity is

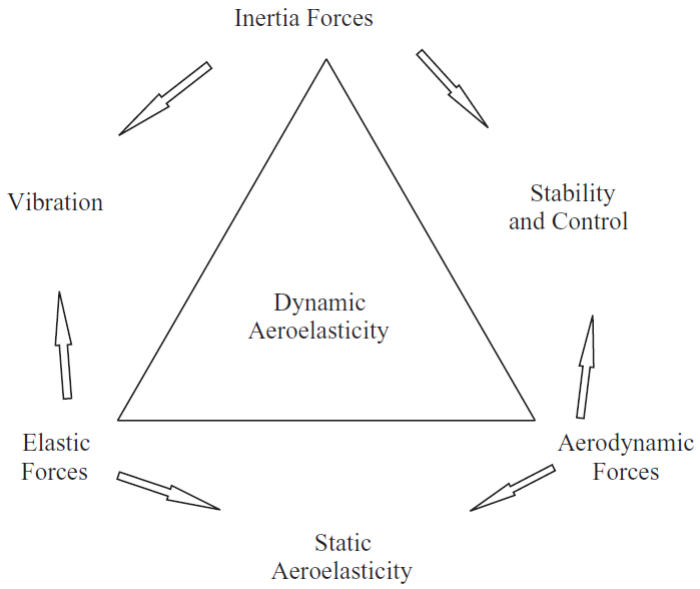

Figure 1.1: Collar's aeroelastic triangle (Collar 1978).

the flutter phenomenon [14]. The flutter point is defined as the flow speed whereas oscillating motion with a decaying amplitude transitions into an unstable oscillation with a growing amplitude.

Aerospace companies are continuously looking for possibilities to reduce the weight of an aircraft which is beneficial for reducing the fuel consumption. One of the possibilities for weight reduction recognised by the industry is the introduction of composite materials, which increased the possibilities to further optimise aircraft structures by tailoring material properties. In many cases a reduction in structural weight goes hand in hand with increased flexibility. Optimisation of an aircraft structure however may not affect the safety of flight within the flight envelope.

Problems of aeroelasticity commonly occur during the optimisation of lightweight and highly flexible wing structures made of advanced composite materials. Wing flexibility gives the opportunity to use wing surfaces for controlling an aircraft. However, above the critical airspeed undesired static and dynamic instabilities arise. Advantages of using a morphing wing compared to a traditional rigid flap for control of the aircraft are, potential weight savings, and reduction in aerodynamic drag and noise [15].

In Section 1.1 current literature on the aeroelastic analysis of flexible airfoils and plates is presented. Also stuctural and aerodynamic models used in these papers are discussed. The gap in the body of knowledge that is filled with this research project is identified in Section 1.2. Based on the identified gap research objectives and questions are formulated in Section 1.3. Consequently in Section 1.4 the steps taken in the research project and the outcomes of the project are discussed. Finally the outline of the report is drafted in Section 1.5.

1.1. State-of-the-art

This section is meant to give insight in the current understanding on the effects of adding flexibility to an airfoil on the aeroelastic characteristics of the airfoil. Additionally an overview is given which structural and aerodynamic models are used for the aeroelastic models described in current literature.

1.1.1. Aeroelastic analysis flexible airfoil

Considerable research has been executed to determine the aeroelastic stability boundary of two-dimensional elastically supported lifting surfaces. Theodorsen and Küssner & Schwarz were the first to determine the non-stationary forces acting on an airfoil section oscillating with small amplitudes [4, 16]. Numerous studies have been done to perform stability analysis on airfoils and flexible plates by Kornecki and Dowell, Huang, and Tang et al. which are described in more detail later in this section [17–19]. More recently, the book *A Modern Course in Aeroelasticity* by Dowell et al. presents an extensive literature review of elastically supported rigid airfoils [5].

An extra degree of freedom was added to the classical two-dimensional aeroelastic model in the work of Murua et al. [2]. The research numerically investigated the effects of chordwise flexibility of fully flexible airfoils on the dynamic stability. The research has proven that camber deformations influence the stability limits of a classic aeroelastic system. However no quantitative comparison is made of the critical velocity between the classic system and the system including chordwise flexibility. A comparison between a fully flexible airfoil section and a rigid section was made by Kim and Lee [1]. The main conclusion is that the chordwise flexibility effect becomes significant for pitch to plunge stiffness ratios greater than one.

Drazumeric et al. investigated the aeroelastic behaviour of an elastically supported rigid airfoil section with attached a flexible composite plate [3]. The paper shows for a configuration with a high plunge to pitch stiffness ratio, an increase of 40% in critcal flow speed can be achieved in the bimodal region compared to the most rigid trailing edge. The bimodal region is the flow speed at which classical airfoil flutter and plate flutter occur simultaniously. Gjerek et al. used the same flexible airfoil system focussing on the chordwise flexibility only [20]. The goal was to increase the dynamic stability limits due to introducing airfoil flexibility. Two main conclusions drawn from the research are that flexibility can be used to increase the instability boundary and significantly lower the amplitudes of the system response at critical flutter speed.

The flexible trailing edge in the papers by Drazumeric et al. and Gjerek et al. is considered to be a flexible plate whose stability has been thoroughly investigated [3, 20]. The aeroelastic stability of two-dimensional panels with various boundary conditions in uniform incompressible flow was studied by Kornecki and Dowell [17]. The paper shows that a panel fixed at both ends loses stability by divergence, while a cantilevered panel shows flutter when exposed to subsonic uniform flow. Shayo extended this work for finite panels and demonstrated that a two-dimensional analysis may lead to an overestimation of the critical velocity for finite panels [21]. This work was further extended by Huang [18]. Huang studied the flutter phenomenon quantitatively and concluded that the circulatory flow, attributed to the wake vortices, is key to flutter as it does positive work, while the non-circulatory flow almost does no positive work. Positive work means that energy is put into the (aeroelastic) system.

The plate stability problem was further investigated in the work of Tang and Dowell and Tang et al. where structural non-linearities (in the bending stiffness and mass inertia terms) and three-dimensional aerodynamics were incorporated in the model [19, 22]. In the latter paper a very good agreement between theory and experiments was obtained for the velocity at which flutter and limit cycle oscillations (LCO) initiate. However, for large amplitude LCO differences between theory and experiment are observed which are likely a result of aerodynamic non-linearities not being included in the model.

Few research has been done on the influence of the flexible versus rigid fraction of a plate on the instability boundary. In the papers by Tang and Païdoussis and De Breuker et al. the influence of the rigid part has been investigated [15, 23]. It is evinced that the critical velocity at which flutter occurs depends on the flexible plate length to total plate length ratio and the mass ratio (air mass to flexible plate mass). The presence of a rigid part stabilises or destabilises the aeroelastic behaviour of the plate depending on a combination of the previously mentioned ratios.

The stability limits of a two-dimensional airfoil section with variable geometry trailing edge was further investigated by Bergami and Gaunaa [7]. It was found that for a section with an uncontrolled flexible trailing edge, the stability boundaries significantly depend on the mass distribution of the airfoil section and bending stiffness of the trailing edge. Quantitatively these results are in agreement with the results obtained in the paper by Gjerek et al. [20]. For the controlled trailing edge the stability limits are also dependent on the control algorithm, control inputs, gain parameters and time lag in the control.

1.1.2. Structural Models

In this research an elastically supported two-dimensional airfoil with attached a flexible composite plate is considered. The elastic support represents the bending and torsional stiffness of a wing. The values for the bending and torsional stiffness are input for the aeroelastic matrix, which will be analysed to determine the aeroelastic characteristics of the wing. A suitable model needs to be chosen to realistically model the behaviour of the flexible composite plate. The structural properties of the flexible composite plate will be calculated by using the classical laminated plate theory as explained in the book by Kassapoglou [24].

The problem considered is two-dimensional, therefore beam and plate theories can be used to model the flexible plate. In the paper by De Breuker et al. the structure is modelled using a semi-analytical approach [15]. The structural mass and stiffness matrices are derived employing Hamilton's variational principle, structural damping however is neglected. The structure is discretised using the Rayleigh-Ritz assumed modes method. In the papers by Tang and Dowell and Tang et al. the same approach is used and extended the models by including non-linear stiffness and inertia effects [19, 22]. It is shown that the non-linear mass inertia effects have a significant influence on Limit Cycle Oscillations (LCO).

The non-linear Euler-Bernoulli dynamic beam equation was derived in the paper by Semler et al. [25]. In the derivation the in-extensibility condition is applied, implying that the deformation of the beam is limited to bending. The in-extensibility condition is applicable for thin beams subject to low axial forces. The non-linear Euler-Bernoulli beam model was used by Tang and Païdoussis for determination of the instability boundary and analysis of post-critical behaviour of a two-dimensional flexible cantilevered plate [23]. It was concluded that the latter theory has better agreement with available experimental

data compared to other theories. Furthermore results show that the critical velocity is sensitive to variations in length of the rigid upstream element when the upstream element is short, while it is almost constant for sufficiently long upstream elements. Longer upstream elements appear to have a lower critical velocity.

Drazumeric et al. modelled the dynamic behaviour of the flexible plate with a thin viscoelastic plate model [3]. The Kelvin-Voigt material model was used to define the material properties of the plate. It is assumed that the pressure distribution does not vary in spanwise direction, hence chordwise transverse motion is considered only. The largest deviations between theory and experiments are observed in the bimodal region, where the measured critical flutter speeds measured where lower than predicted by the numerical model. The four main reasons given for the deviations are

- very low sensitivity of the airfoil flutter to critical speed and reduced frequency in the bimodal region,
- number of plies of flexible plate in practice is an integer, while for obtaining maximum critical flutter speed a fraction of an integer is needed,
- variations between flexural rigidity due to the fact that it is handmade,
- the assumption of a viscous damping law for the elastic support is just a first order approximation.

However outside the bimodal region, the theoretical and experimental results show similar trends.

A non-linear equation of motion for plates was derived by Tang et al. using Hamilton's variational principle and Lagrange's equations based on non-linear Von Karman plate equations [26]. Structural non-linearities in this structure occurred due to double bending in the chordwise and spanwise directions. Since the model considered in the present research is two-dimensional, double plate bending will not be considered.

1.1.3. Aerodynamic Models

An aerodynamic model has to be selected which will be used to determine the two-dimensional pressure distribution of a thin airfoil oscillating with small constant amplitudes.

Theodorsen proposed a two-dimensional aeroelastic model to estimate flutter speeds for slender wings [16]. An exact solution for the unsteady aerodynamic loads on an oscillating airfoil is arrived at based on potential flow and the Kutta condition. The theory considers infinitesimal oscillations about the position of equilibrium, large oscillations are neglected. Finite span, section shape, deviations from potential flow, and bending and twisting of wing sections are not taken into account. In the paper by De Breuker et al. the aerodynamic pressure on an partially rigid plate is determined by following Theodorsen's theory [15].

In the same period Küssner and Schwarz derived a solution for unsteady pressure distribution for the similar problem as Theodorsen [4]. The airfoil was substituted by an aerodynamically equivalent mean line. The pressure distribution due to downwash is given by an integral representation in complex form. The downwash consists of the gliding of a fluid particle along the mean line and a non-stationairy portion due to the oscillating mean line. The work of Küssner and Schwarz is used by Drazumeric et al. in their research to study the influence of airfoil flexibility on the stability boundaries [4, 27].

An extension of Theodorsen's model was given by Gaunaa [28]. Gaunaa derived analytical expressions for distributed and integral unsteady two-dimensional forces on a variable geometry undergoing arbitrary motion. The main difference between Theodorsen's model and Gaunaa's model is the way airfoil deformation and rigid body motions are described; in the model of Gaunaa the airfoil deformation and rigid body motions are described by assuming mode shapes while Theodorsen defined a pitching, plunging, and flap deflection. Buhl et al. used the aerodynamic model to investigate load reduction using variable trailing edge geometry for the two-dimensional attached-flow case [6]. The aerodynamic model is later used in a study by Bergami and Gaunaa in which a method is proposed to determine the flutter and divergence limits of a two-dimensional airfoil section equipped with deformable trailing edge

flap control [7]. Verification of the aerodynamic model in these studies show reasonable predictions of aerodynamic forces compared to other theories.

A solution to a similar problem as in the paper by Gaunaa [28] was found by Mesaric and Kosel [29]. A closed form analytical solution has been obtained for the unsteady aerodynamic load due to camber variation only. The solution is derived in the frequency and time domain and is computationally efficient, therefore it is suitable for active control of the airfoil camber for the purpose of flutter suppression. Results show that the location of the maximum camber has significant effect on the lift and moment amplitude. However no solution has been presented for the pressure distribution on an airfoil or for unsteady loads due to a combination of airfoil rigid body motions (pitch and plunge) and camber variation.

In their papers on limit cycle oscillations of two-dimensional panels Tang and Dowell and Tang et al. used the vortex lattice lattice method to determine the pressure distribution over the panel [19, 22]. Very good agreement between theory and experiment was obtained for the prediction of flutter and LCO initiation. In the latter paper it was observed that for large LCO significant differences between theory and experiments occur which are thought to be result of the aerodynamic non-linearities not taken into account in the model.

1.2. Progress Beyond State-of-the-art

The general trend in the aerospace industry is to optimise lightweight and highly flexible wing structures made of composite materials. This flexibility increases static and dynamic aeroelastic instability problems. Research by Kim and Lee, Murua et al., and Drazumeric et al. have proven that chordwise flexibility has a significant effect on the aeroelastic characteristics of an airfoil; including the aeroelastic instability boundaries [1, 2, 27]. Drazumeric et al. have numerically and experimentally shown that by adding chordwise flexibility the stability boundaries could be increased up to 79.2% in the region of bimodal flutter behaviour, meaning that conventional section flutter and plate flutter occur simultaneously [27].

It has been identified that the two-dimensional aeroelastic characteristics of flexible airfoil has been studied for constant stiffness flexible airfoils only. The present project will take the next step by assuming a variable thickness distribution of a flexible trailing edge. An elastically supported rigid airfoil shaped leading edge with attached a flexible composite plate will be considered. The variable thickness distribution of the flexible plate will be optimised for increasing the critical flow velocity at which the aeroelastic instabilities occur. This will be accomplished by developing a numerical aeroelastic model.

1.3. Research Objectives

Multiple researches have concluded that adding chordwise flexibility to a two-dimensional airfoil significantly influences the aeroelastic stability boundary. However, only a few researchers considered partly flexible airfoils. As mentioned earlier one of those studies was carried out by Drazumeric et al., who considered an elastically supported rigid airfoil shaped leading edge with attached a flexible plate with constant properties along the chord [3]. This research will be taken to the next step by adding a thickness distribution to the flexible composite plate instead of a constant stiffness trailing edge. The objective of the research project can thus be stated as

"Optimising the chordwise thickness distribution of a flexible composite trailing edge to postpone the onset of aeroelastic instabilities. For the optimisation a two-dimensional numerical model will be developed."

The stability boundaries that will be considered are section divergence, section flutter, and plate flutter. The main objective is split into three sub-objectives that must be completed to satisfy the main objective and is stated as follows

1. Development of a two-dimensional numerical aeroelastic analysis methodology that accounts for airfoil flexibility and thickness-tailoring
2. Executing a verification of the developed aeroelastic analysis tool

3. Carrying out an optimization which will provide an optimal stiffness distribution of the flexible trailing edge

Based on the objective, the research question can be formulated. The main research question is formulated as follows

"To what extent can tailoring the chordwise thickness distribution of a two-dimensional airfoil section with a thickness distributed flexible trailing edge postpone the critical flow speed at which aeroelastic instabilities occur?"

The main research question is divided into three sub-questions.

1. Which theories are most suitable to model the aeroelastic response of a two-dimensional airfoil with a variable stiffness flexible composite trailing edge efficiently and with sufficient accuracy?
2. What is the optimal chordwise thickness distribution of the trailing edge for improved aeroelastic characteristics?
3. What can be concluded from the results of the numerical model regarding the effects of a variable thickness distribution of the trailing edge on the aeroelastic characteristics?

1.4. Research Plan

The objective of the research project is to find the optimal thickness distribution of the flexible composite trailing edge to postpone aeroelastic instability boundaries and to obtain a benign flutter onset. A two-dimensional numerical model simulating the aeroelastic behaviour of a flexible airfoil will be developed for the optimisation. In this section the steps that are taken to answer the research questions and fulfill the research objectives are presented in chronological order. Also the outcomes of the research project are discussed in more detail.

1.4.1. Methodology

As mentioned in Section 1.1 airfoil flexibility has significant effects on the aeroelastic characteristics. It is therefore interesting to test if this flexibility can be used to improve these aeroelastic characteristics. The main hypothesis that will be investigated can be formulated as

"Tailoring the chordwise thickness distribution of the flexible trailing edge can postpone the onset of aeroelastic instabilities."

This research project is an extension of the work carried out by Drazumeric et al. who investigated the effects of trailing edge flexibility on the flutter behaviour of the elastically supported airfoil for a constant stiffness trailing edge [3].

The steps that have to be taken to test the hypothesis and achieve the objectives set in Section 1.3 are listed in chronological order of execution.

- **Develop aeroelastic model for constant thickness trailing edge**
  A numerical model that simulates the aeroelastic behaviour of an elastically supported rigid airfoil shaped leading edge with attached a constant thickness flexible composite trailing edge will be developed in Matlab. The model will be based on the paper by [3].
- **Verification of the constant thickness model**
  The aeroelastic model developed in the previous step will be verified with the results presented in the paper by [3], which should be in agreement for similar inputs. This step will verify the response of the elastic support, the constant plate response, and the aerodynamics.
- **Implement variable thickness**
  The next step will be the implementation of a variable thickness distributed trailing edge into the aeroelastic model developed in the first step. For the optimisation a piecewise constant thickness distributed plate is assumed.

- **Optimise variable thickness distribution**
  The goal of the optimisation is to tailor the chordwise thickness distribution of the composite trailing edge as such that the aeroelastic instability boundaries are postponed. The composite trailing edge will be described by laminate parameters to convert the discrete optimisation problem into a continuous problem, which allows the use of a gradient based optimiser ([30]).

1.4.2. Structural and aerodynamic models used

The numerical aeroelastic model is developed to determine the stability boundaries and to simulate the benignity of flutter onset of the aeroelastic system. Hence post-critical behaviour is not subject of study in the present project; small amplitude oscillations will be considered only. Therefore it is not necessary to use the non-linear beam equation to model the flexible plate as used in the paper by Tang and Païdoussis[23]. Furthermore a two-dimensional system is considered where no deformations in spanwise direction are to be expected, it is therefore not necessary to use the non-linear plate equations derived by Tang et al. [26]. The plate equation in the paper by Drazumeric et al. is derived as such that a variable thickness distribution can be implemented relatively easy [27]. The flexible plate will therefore be modelled as a thin viscoelastic plate with the Kelvin-Voigt material model.

The pressure distribution on a flexible airfoil oscillating harmonically with small amplitudes is required for determination of the stability boundaries. The aerodynamic theories derived in the papers by Theodorsen and Küssner and Schwarz are pretty much similar and can both be derived for flexible airfoils or plates [4, 16]. De Breuker et al. and Gaunaa showed an extension of Theodorsen's model for flexible plates and flexible airfoils respectively [15, 28], while Drazumeric et al. extended the model by Küssner and Schwarz for flexible airfoils. For verification purposes it is chosen to use the model derived in the paper by Küssner and Schwarz since this is used by Drazumeric et al. [27], where the present research is based on.

1.4.3. Outcomes

The outcomes of the research fulfill the research objectives and give an answer to the research questions formulated in section 1.3. The outcomes of the research are listed here.

- **State-of-the-art effects of airfoil flexibility on aeroelastic characteristics**
  The state-of-the-art on airfoils containing flexibility is presented in section 1.1. Multiple researches showed the effects of airfoil flexibility on the aeroelastic characteristics. No evidence was found of a research considering a varying thickness distribution along the chord, hence confirming the relevance of the main objective of the present research to investigate the possibility of optimising the chordwise thickness distribution of the flexible trailing edge to improve aeroelastic instability behaviour.

- **Aeroelastic model that accounts for a variable thickness distributed trailing edge**
  A numerical model that simulates the aeroelastic response of an elastically supported rigid airfoil with attached a composite plate with a variable thickness distribution will be build. For the aeroelastic system substituted in the model the critical flow speeds for each of the instability modes considered (section divergence, section flutter, plate flutter) are determined.

- **Tailored thickness distribution for improved aeroelastic behaviour**
  The aeroelastic code will be used to tailor the thickness distribution of the flexible trailing edge. During the optimisation, the trailing edge will be tailored to postpone the instability boundaries.

- **Analysis on the effects of a variable thickness distributed trailing edge**
  The most significant outcome of the research reflects back to the main objective as set in section 1.3. An analysis will be given what the effects on the aeroelastic characteristics of an airfoil are when a flexible trailing edge with a variable thickness distribution is added to the elastically supported airfoil shaped rigid leading edge.

1.5. Report Outline

The report is structured as follows. Firstly, in Chapter 2 the aeroelastic model is defined followed by the main assumptions made in the modelling. Consequently the equations of motion are derived starting with the modified Euler-Lagrange equations. The chapter ends with a detailed verification of the aeroelastic model described. Next, Chapter 3 shows the results of the optimisations in which the verified aeroelastic model described in the previous chapter is used. The chapter initiates with a description of the optimisation strategy, where the program structure is explained. In the second section the influence of important design variables is shown and declared. In the remaining sections the airfoil configurations used for the optimisations and the results of the optimisations are presented. The report is finalised by drawing conclusions on the basis of the observations made during analysis. Lastly, recommendations are given for further considerations.

2

Aeroelastic Model

This chapter describes the aeroelastic analysis tool developed for the analysis of the aeroelastic behaviour of a partially flexible airfoil. This analysis tool is later used during the optimisation procedure which is outlined in Chapter 3.

The chapter starts with defining the aeroelastic system and the most important assumptions made to describe the aeroelastic behaviour of the system in Sections 2.1 and 2.2. Consequently the structural model is elaborated in Section 2.3 and the assumptions made in the aerodynamic model in Section 2.4. The general equations of motion are derived in Section 2.5. The derivation starts with the modified Euler-Lagrange equation of which the derivation is shown in Appendix A. Next the solution method to the general equations of motion is described in Section 2.6. Section 2.7 shows the methods used to calculate the critical flow speeds at which aeroelastic instabilities occur. Consequently a convergence study is executed to determine the number of plate modes that need to be considered during analysis. Lastly, Section 2.10 presents a detailed verification of the aeroelastic model described in the current chapter.

2.1. Definition Aeroelastic System

The aeroelastic system studied consists of an elastically supported rigid airfoil shaped leading edge with attached a cantilevered flexible composite plate as shown in figure 2.1. The (partially) flexible airfoil is placed in a uniform flow with a flow speed v_∞ causing a pressure distribution $p(x,t)$ on the airfoil. The airfoil has a chord of length l and is considered to be two-dimensional with a span b. The system studied possesses two rigid degrees of freedom: plunge or heave displacement $y_0(t)$, and pitch angle rotation $\alpha_0(t)$. In addition to the rigid motion, the model allows for out-of-plane plate deformation $w(x,t)$ which provides airfoil flexibility. The flexible plate has a length of l_p. The axis of rotation is located at a distance x_0 from the leading edge and the distance between the axis of rotation and the center of gravity of the rigid part is listed as x_T.

The dynamic properties of the system are given by k_y and k_α, the plunge and pitch stiffness of the system, and d_y and d_α, the plunge and pitch damping coefficients. The mass m_0 is involved in plunge motion only, the mass of the airfoil shaped rigid leading edge m is involved in plunge and pitch motion, and J_0 the mass moment of inertia of the rigid part around the axis of rotation.

The objective of the research is to investigate effects of a variable thickness distribution of the flexible composite plate along the chord of the plate on the aeroelastic characteristics of an airfoil. The plate properties that are subject to change are the specific mass, stiffness, and damping coefficient and are assumed to be constant in span-wise direction. The flexible composite plate is modelled as a thin viscoelastic plate using the Kelvin-Voigt material model. Basically the plate is modelled as a Euler-Bernoulli beam since a two-dimensional system is considered. The dynamic properties are given by the areal density $\sigma_p(x)$, the flexural rigidity $D_p(x)$, and the viscoelastic damping coefficient $C_p(x)$, the values of those coefficients are allowed to vary along the plate in chordwise direction. The structural

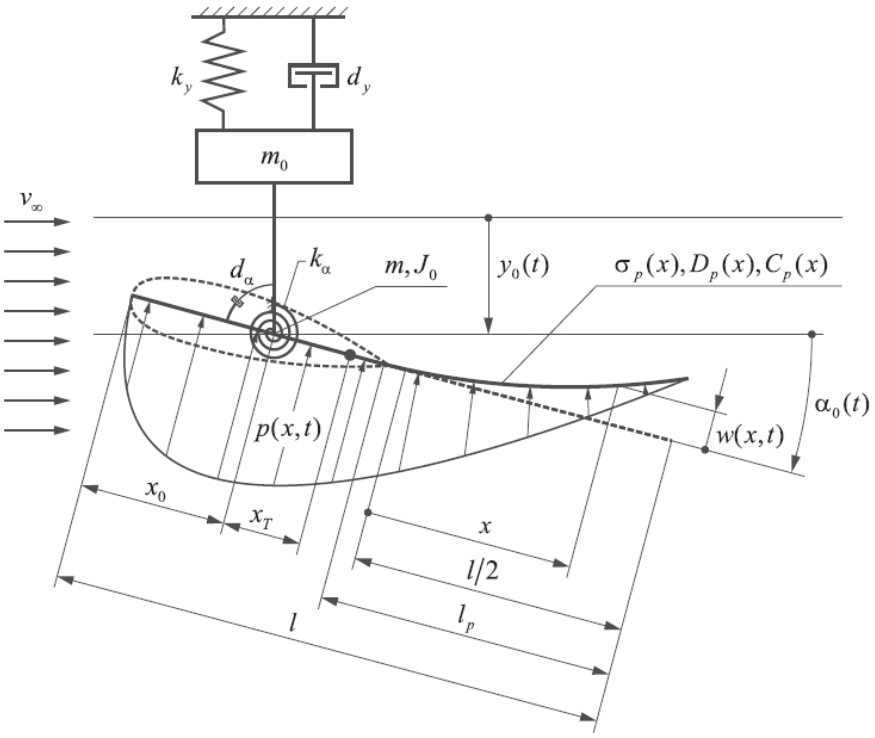

Figure 2.1: Elastically supported flexible airfoil section [3].

model is explained in more detail in Section 2.3.

A brief reflection on how the described system could represent reality is given here. The previously described flexible airfoil configuration could represent a two-dimensional wind tunnel model that is elastically mounted in the wind tunnel setup. Also it could correspond to a typical airfoil section along a finite wing. In this case the translational and torsional springs represent the wing structural bending and torsional stiffnesses. The axis of rotation in that case represents the elastic axis [31].

2.2. Assumptions

In modelling usually a trade-off has to be made between accuracy and computational effort. In order to speed up the calculations executed by the aeroelastic model, simplifications are made. Making assumptions in the model however leads to limitations in applicability of the model or to a reduction in accuracy. In other words, how well the model is able to represent reality. In the aeroelastic model for investigation of the aeroelastic behaviour of an elastically supported partially flexible airfoil simplifications are made. In this section the main assumptions made in the model are elaborated.

The main assumption made is that we are dealing with a two-dimensional system, implying that we can use a two dimensional beam for modelling of the flexible plate and two-dimensional aerodynamics for modelling the fluid loads on the aeroelastic structure. Since a two-dimensional aerodynamic model is considered, the pressure distribution in span-wise direction is considered to be constant. Hence it is assumed that no bending occurs in span-wise direction. Both the plunging and pitching rigid motions are assumed to be restrained by linear strings.

The objective of the research is to investigate the effects of flexibility on the aeroelastic instability points. In the instability points the response of the aeroelastic system is assumed to be harmonic with small amplitudes. Meaning that the system is oscillating with a small and constant amplitude. In complex form the motions can be written as

$$y_0(t) = Y_0 e^{i\omega t} \tag{2.1}$$

$$\alpha_0(t) = A_0 e^{i\omega t} \tag{2.2}$$

$$w(\bar{x}, t) = W(\bar{x}) e^{i\omega t} \tag{2.3}$$

where $Y_0(t)$ is the amplitude of the plunge motion, A_0 the amplitude of the pitch motion, $W(\bar{x})$ the transverse displacement amplitude of the plate, and ω the angular frequency of the motion. It can be seen that there is no real part in the denominator of the exponent, this is because as mentioned above the motion is assumed to harmonically oscillate and therefore the real part representing the damping of the motion is zero. A second important assumption made for the motion is that the aeroelastic system is oscillating with small amplitudes at the onset of the instabilities. Based on this assumption the displacement components are approximated as

$$\left.\begin{aligned} u &= x\left[\cos\left(\alpha_0\right) - 1\right] \approx 0 \\ v = y_0 + \sin\left(\alpha_0\right)\left(x + \tfrac{l}{2} - x_0\right) - w &\approx y_0 + \alpha_0\left(x + \tfrac{l}{2} - x_0\right) - w \end{aligned}\right\} for\ \alpha_0 \ll 1 \tag{2.4}$$

A more detailed discussion on the effects of this assumption on the equations of motion is found in Appendix A. The assumptions in the structural and aerodynamic model are evaluated in detail in Sections 2.3 and 2.4.

2.3. Structural Model

In this section the structural model is described. Basically only a model needs to be determined for deformation of the flexible plate, since for the rigid body motions conventional linear force-displacement equations can be used. In the previous section the assumption was made that during this researcha two-dimensional airfoil section is considered and thus no bending deformations occur in span-wise direction. Hence no double bending in the plate will occur through which structural non-linearities may occur in the structure, according to Tang et al. [26].

In the current research the instability point itself is concerned solely. Hence post-critical behaviour where large deformations might occur does not need to be modelled [23]. The previously mentioned limitation of the model in combination with the fact that a thin plate is considered, relatively simple Euler-Bernoulli beam equations are suitable for to be used for calculation of the flexible plate deflections.

Material Model

The flexible plate is modelled as a thin viscoelastic plate using the Kelvin-Voigt material model or alternatively the Voigt model. In the model the behaviour of the material is governed by a parallel connection of a spring element and a dashpot element [32]. The total stress in a Kelvin-Voigt material model is a summation of the stress in the spring and the dash-pot and is given by

$$\sigma = E\epsilon + \mu_m \frac{d\epsilon}{dt} \tag{2.5}$$

where σ is the material stress, E is the bending stiffness, μ_m the material viscosity, ϵ the strain, and $\frac{d\epsilon}{dt}$ the strain rate. The first term represents the stress due to bending, while the second term is the stress due to viscoelastic damping in the plate. The bending moment due to viscoelastic material damping is derived here. The total strain in a plate in pure bending is given by

$$\epsilon_x(x,t) = -z\frac{d^2w}{dx^2}(x,t) \tag{2.6}$$

where ϵ_x is the strain in the length direction, z the location in thickness direction in the plate, and w the out-of-plane beam deflection. Substitution of the strain definition given in equation 2.6 into the second term of equation 2.5, results in the stress due to viscoelastic material damping.

$$\sigma_{dp}(x,t) = -z\mu_m \frac{d}{dt}\left(\frac{d^2w}{dx^2}(x,t)\right) \tag{2.7}$$

where σ_{dp} is the stress due to viscoelastic damping. The resultant bending moment due to viscoelastic plate damping M_{dp} is determined by integrating the product of the stress and the through the thickness location. This is formulated as,

$$M_{dp}(x,t) = -\mu_m \int_{-h/2}^{h/2} z^2 dz \frac{d}{dt}\left(\frac{d^2w}{dx^2}(x,t)\right) \tag{2.8}$$

where the integral can be recognised as the second area moment of inertia usually denoted as I with units m^3. Substitution gives

$$M_{dp}(x,t) = -\mu_m I \frac{d}{dt}\left(\frac{d^2w}{dx^2}(x,t)\right) \tag{2.9}$$

Replacing μI by the viscoelastic damping coefficient $C_p(x)$ with units Nms simplifies equation 2.10 to

$$M_{dp}(x,t) = -C_p(x) \frac{d}{dt}\left(\frac{d^2w}{dx^2}(x,t)\right) \tag{2.10}$$

Equation 2.10 is used to determine the work on the aeroelastic system by the bending moment due to viscoelastic material damping.

2.4. Aerodynamic Model

In this section the aerodynamic model is discussed. A model is needed to determine the aerodynamic forces and moments on a flexible harmonically oscillating airfoil. The aerodynamic model used is derived by Kussner and Schwarz, for a detailed derivation the reader is encouraged to read the paper *The Oscillating Wing with Aerodynamically Balanced Elevator* by the here for mentioned researchers [4]. In this section there is elaborated on the assumptions made during the derivation of the model.

Aerodynamic theories are based on the three conservation laws; conservation of mass, conservation of momentum, and conservation of energy. The Navier-Stokes equations are the most extensive form of these laws. The Navier-Stokes equations are however computationally expensive to solve. In many cases however it is not necessary to treat the Navier-Stokes equations. In these cases assumptions can be made in order to simplify these equations.

The Küssner and Schwarz aerodynamic theory used in this research is based on the potential theory. The potential flow theory assumes inviscid, incompressible, and irrotational flow. The assumption of an inviscid flow implies that there is no friction in the flow. This is most noticeable by the absence of the boundary layer where the flow slows down from the velocity in the free stream to zero at the airfoil surface [14]. A solution to a potential flow is usually obtained by applying the well-known Laplace equation *Laplace equation*. The Laplace equation is denoted as:

$$\nabla^2 \phi = 0 \tag{2.11}$$

where ϕ is the velocity potential. Solutions to the Laplace equations are called harmonic functions. As stated in Section 2.2 at the instability point it is assumed that the airfoil is harmonically oscillating with small amplitudes. This assumption is thus in agreement with the solutions to the Laplace equation. A boundary condition that needs to be satisfied is the flow tangency condition which ensures no air is flowing through the airfoil. Furthermore the airfoil is assumed to be thin, hence it can be represented by an equivalent mean line.

The Kutta condition ensures the flow is smoothly leaving the top and bottom surfaces of the airfoil. The condition is a boundary condition to the potential flow theory since it defines the circulation around the airfoil such that the flow leaves the trailing edge smoothly [33]. The Kutta condition ensures that no infinite velocity gradients occur at the trailing edge and that a stagnation point is located at the trailing edge tip. In order to compensate for the circulation around the airfoil Kelvin's circulation theorem is adopted which states that circulation in an enclosed volume consisting of the same fluid particles is

constant.

The Küssner and Schwarz aerodynamic theory relates the pressure distribution to the downwash which is a result of the airfoil shape and motion. The downwash is the vertical velocity of the air with respect to the coordinate system. It consists of a steady portion due to gliding past the mean line of the airfoil $\partial y/\partial x$ and of a unsteady portion due to oscillation of the airfoil $\partial y/\partial t$. The total downwash v_y is therefore given as

$$v_y = v_\infty \frac{\partial v}{\partial \bar{\xi}} + \frac{\partial v}{\partial t} \tag{2.12}$$

where v is given by equation 2.4. The first term represents the steady portion of the downwash and the second term the unsteady portion. The relation between the total pressure distribution of a flexible harmonically oscillating airfoil is defined as

$$p(\bar{x}, t) = \rho v_\infty \frac{2}{\pi} \int_{-1}^{1} v_y(\bar{\xi}, t) G(k, \bar{x}, \bar{\xi}) d\bar{\xi} \tag{2.13}$$

where ρ is the air density and $G(k, \bar{x}, \bar{\xi})$ is a complex function defined as

$$G(k, \bar{x}, \bar{\xi}) = \left(C(k) - 1 - \frac{1}{\bar{x} - \bar{\xi}} \right) \sqrt{\frac{1 - \bar{x}}{1 + \bar{x}}} \sqrt{\frac{1 + \bar{\xi}}{1 - \bar{\xi}}} + \frac{ik}{2} ln \frac{1 - \bar{x}\bar{\xi} + \sqrt{1 - \bar{x}^2}\sqrt{1 - \bar{\xi}^2}}{1 - \bar{x}\bar{\xi} - \sqrt{1 - \bar{x}^2}\sqrt{1 - \bar{\xi}^2}} \tag{2.14}$$

In this equation $C(k)$ is the complex Theodorsen function derived in the paper [16]. The pressure distribution is denoted as a linear superposition of the partial pressure distributions due to the plunging motion, pitching motion, and deformation of the flexible trailing edge.

$$p(\bar{x}, t) = p_y(\bar{x}, t) + p_\alpha(\bar{x}, t) + p_w(\bar{x}, t) \tag{2.15}$$

where the individual terms are described by

$$p_y(\bar{x}, t) = \rho v_\infty \frac{2}{\pi} \int_{-1}^{1} \dot{y}_0(t) G(k, \bar{x}, \bar{\xi}) d\bar{\xi} \tag{2.16a}$$

$$p_\alpha(\bar{x}, t) = \rho v_\infty \frac{2}{\pi} \int_{-1}^{1} \left[\frac{l}{2} (\bar{\xi} + 1 - \bar{x}_0) \dot{\alpha}_0(t) + v_\infty \alpha_0(t) \right] G(k, \bar{x}, \bar{\xi}) d\bar{\xi} \tag{2.16b}$$

$$p_w(\bar{x}, t) = -\rho v_\infty \frac{2}{\pi} \int_{1-\bar{l}_p}^{1} \left(\frac{\partial w}{\partial t}(\bar{\xi}, t) + v_\infty \frac{2}{l} \frac{\partial w}{\partial \bar{\xi}}(\bar{\xi}, t) \right) G(k, \bar{x}, \bar{\xi}) d\bar{\xi} \tag{2.16c}$$

The partial pressure distributions given in equation 2.16 are used to describe the aerodynamic forces and moments on the system by integration over the airfoil along the chord.

Comparison to Theodorsen

Both the aerodynamic theories are based on the same assumptions. The main difference between both theories lies in the way the pressure distribution over the airfoil is solved. The Theodorsen theory relates the pressure distribution to velocity potentials. The velocity potentials themselves are expressed in terms of the airfoil motion and geometry. The aerodynamic theory by Küssner and Schwarz on the other hand expresses the pressure distribution as function of the downwash velocity. The downwash in turn is solved using a Fourier series with respect to a spatial variable.

2.5. Derivation Equations of Motion

In order to derive the equations of motion using the modified Euler-Lagrange equation, the total kinetic energy, internal potential energy, and external potential energy of the aeroelastic system are needed and the work due to the non-conservative forces on the aeroelastic system have to be determined as function of the generalised coordinates. The derivation of the modified Euler-Lagrange equations is demonstrated in Appendix A. The derivation of the equations of motion starts with the modified Euler-Lagrange equation given in Equation A.21.

2.5.1. Kinetic energy of the aeroelastic system

The kinetic energy of a flexible aerofoil for small rotations and no motion in the horizontal direction can be written as

$$T = \frac{1}{2} m \left(\frac{dv}{dt} \right)^2 \tag{2.17}$$

where the vertical displacement component v is defined in equation 2.4. Since v is a function of the generalised coordinates, one should be careful to multiply the moving mass or inertia with the corresponding generalised coordinate that causes this motion. Substituting equation 2.4 into 2.17 and considering the afore mentioned, the variation of the total kinetic energy of the flexible airfoil system can be formulated as,

$$T = \frac{1}{2} \Bigg(m_y \dot{y}_0^2(t) + J_\alpha \dot{\alpha}_0^2(t) + \int_{l/2-l_p}^{l/2} \sigma_p(x) \left(\frac{dw}{dt} \right)^2 (x,t) dx + S_{y\alpha} \dot{y}_0(t) \dot{\alpha}_0(t) + S_{\alpha y} \dot{y}_0(t) \dot{\alpha}_0(t)$$
$$-2\dot{y}_0(t) \int_{l/2-l_p}^{l/2} \sigma_p(x) \left(\frac{dw}{dt} \right)(x,t) dx - 2\dot{\alpha}_0(t) \int_{l/2-l_p}^{l/2} \sigma_p(x) \left(x + \frac{l}{2} - x_0 \right) \left(\frac{dw}{dt} \right)(x,t) dx \Bigg) \tag{2.18}$$

where m_y is the total mass, $S_{y\alpha}$ and $S_{\alpha y}$ the static moments of mass, and J_α the mass moment of inertia. These can be obtained by

$$m_y = m_0 + m + b \int_{l/2-l_p}^{l/2} \sigma_p(x) dx, \quad S_{y\alpha} = m x_T + b \int_{l/2-l_p}^{l/2} \sigma_p(x) \left(x + \frac{l}{2} - x_0 \right) dx$$
$$S_{\alpha y} = S_{y\alpha}, \quad J_\alpha = J_0 + b \int_{l/2-l_p}^{l/2} \sigma_p(x) \left(x + \frac{l}{2} - x_0 \right)^2 dx \tag{2.19}$$

where J_0 is the mass moment of inertia of the rigid section around the axis of rotation.

2.5.2. Potential energy of the aeroelastic system

The potential energy in the aeroelastic system occurs due to deformation of the springs opposing the plunging and pitching motions of the rigid leading edge and due to bending of the flexible plate. The internal potential energy or strain energy of the aeroelastic system due to plate bending is given by

$$U = \frac{1}{2} \int_0^l D_p(x) \left(\frac{d^2 w}{dx^2} \right)^2 dx \tag{2.20}$$

where $D_p(x)$ is the flexural rigidity usually notated as EI [34]. The flexible plate is attached to the rigid leading edge at $l/2 - l_p$ and ends at $l/2$ these are therefore the integration limits. The external potential energy originates from both springs.

$$V = \frac{1}{2}k_y y_0^2(t) + \frac{1}{2}k_\alpha \alpha_0^2(t) \tag{2.21}$$

where k_y is the plunge stiffness, and k_α the pitch stiffness. The conservative energies (kinetic energy and total potential energy) are derived and can be substituted into the Lagrangian which is defined defined as:

$$\mathcal{L}(q_i, \dot{q}_i, t) = T - (U + V) \tag{2.22}$$

Substituting the kinetic energy, internal and external potential energy of the flexible aeroelastic system, the Lagrangian $\mathcal{L}$ is given by:

$$\begin{aligned}\mathcal{L} = \frac{1}{2}\Bigg(& m_y \dot{y}_0^2(t) + J_\alpha \dot{\alpha}_0^2(t) + \int_{l/2-l_p}^{l/2} \sigma_p(x)\left(\frac{dw}{dt}\right)^2 (x,t)dx + S_{y\alpha}\dot{y}_0(t)\dot{\alpha}_0(t) + S_{\alpha y}\dot{y}_0(t)\dot{\alpha}_0(t) \\ & -2\dot{y}_0(t)\int_{l/2-l_p}^{l/2} \sigma_p(x)\left(\frac{dw}{dt}\right)(x,t)dx - 2\dot{\alpha}_0(t)\int_{l/2-l_p}^{l/2} \sigma_p(x)\left(x + \frac{l}{2} - x_0\right)\left(\frac{dw}{dt}\right)(x,t)dx\Bigg) \\ & + \frac{1}{2}\int_0^l D_p(x)\left(\frac{d^2w}{dx^2}\right)^2 dx + \frac{1}{2}k_y y_0^2(t) + \frac{1}{2}k_\alpha \alpha_0^2(t)\end{aligned} \tag{2.23}$$

2.5.3. Work due to non-conservative forces

In aeroelastic problems the work due to non-conservative forces originates from damping in the system and aerodynamic loading acting on the system. The damping in the system originates from the dampers attached to the rigid airfoil-shaped leading edge and viscoelastic material damping in the plate. The virtual work done due to the non-conservative forces is given by:

$$\delta W_{NC} = -Q_i \cdot \delta q_i \tag{2.24}$$

The non-conservative work done by the dampers attached to the rigid leading edge expresses in system parameters is defined as:

$$\delta W_{NC,y} = -d_y \dot{y} \cdot \delta y_0 \tag{2.25a}$$

$$\delta W_{NC,\alpha} = -d_\alpha \dot{\alpha} \cdot \delta \alpha_0 \tag{2.25b}$$

where d_y and d_α are the damping coefficients for the plunging and pitching motion. The viscoelastic damping moment in the plate is derived in Section 2.3. The corresponding work done by the plate damping is the last internal damping term of the aeroelastic system.

$$\delta W_{NC,Cp} = -\int_{l/2-l_p}^{l/2} C_p(x)\frac{d}{dt}\left(\frac{d^2w}{dx^2}(x,t)\right)\cdot\delta\left(\frac{d^2w}{dx^2}\right)dx \tag{2.26}$$

To get rid of the variation of the second order derivative of the plate deflection and obtain the non-conservative virtual work due to the viscoelastic plate damping, equation 2.26 has to be integrated by parts twice. First integration by parts yields:

$$\begin{aligned}-\int_{l/2-l_p}^{l/2} C_p(x)\frac{d}{dt}\left(\frac{d^2w}{dx^2}(x,t)\right)\cdot\delta\left(\frac{d^2w}{dx^2}\right)dx = & -\cancel{C_p(x)\frac{d}{dt}\left(\frac{d^2w}{dx^2}(x,t)\right)\delta\left(\frac{dw}{dx}\right)\Bigg|_{l/2-l_p}^{l/2}} \\ & + \int_{l/2-l_p}^{l/2}\frac{d}{dx}\left(C_p(x)\frac{d}{dt}\left(\frac{d^2w}{dx^2}(x,t)\right)\right)\delta\left(\frac{dw}{dx}\right)dx\end{aligned} \tag{2.27}$$

The first term is zero since the variations at the starting point and end point are equal to zero. Second integration by parts yields:

$$\int_{l/2-l_p}^{l/2} \frac{d}{dx}\left(C_p(x)\frac{d}{dt}\left(\frac{d^2w}{dx^2}(x,t)\right)\right)\delta\left(\frac{dw}{dx}\right)dx = \cancel{\frac{d}{dx}\left(C_p(x)\frac{d}{dt}\left(\frac{d^2w}{dx^2}(x,t)\right)\right)\Big|_{l/2-l_p}^{l/2}} - \int_{l/2-l_p}^{l/2} \frac{d^2}{dx^2}\left(C_p(x)\frac{d}{dt}\left(\frac{d^2w}{dx^2}(x,t)\right)\right)\delta w dx \tag{2.28}$$

Again the first term cancels out for similar reason as in the previous integration. At this point the energy contributions due to internal damping in the aeroelastic system are derived.

Lastly the energy contribution due to the aerodynamic pressure distribution $p(x,t)$ must be determined. The equation for the virtual work done by the aerodynamic pressure is is defined as [5]:

$$\delta W_{NC,aero} = b\int p(x,t)\cdot\delta v dx \tag{2.29}$$

where the vertical displacement component is defined in equation 2.4. Substituting equation 2.4 into 2.29 and integrating over their respective lengths gives

$$\delta W_{NC,aero} = -b\int_{-l/2}^{l/2} p(x,t)\cdot\delta y_0 dx - b\int_{-l/2}^{l/2} p(x,t)\left(x+\frac{l}{2}-x_0\right)\cdot\delta\alpha_0 dx + b\int_{l/2-l_p}^{l/2} p(x,t)\cdot\delta w dx \tag{2.30}$$

Adding the damping and the aerodynamic terms leads to the final formulation of the work due to the non-conservative forces in the aeroelastic system.

$$\begin{aligned}\delta W_{NC} = {} & -b\int_{-l/2}^{l/2} p(x,t)\delta y_0 dx - b\int_{-l/2}^{l/2} p(x,t)\left(x+\tfrac{l}{2}-x_0\right)\delta\alpha_0 dx + b\int_{l/2-l_p}^{l/2} p(x,t)\delta w dx \\ & -d_y\dot{y}_0(t)\cdot\delta y_0 - d_\alpha\dot{\alpha}_0(t)\cdot\delta\alpha_0 - \int_{l/2-l_p}^{l/2}\tfrac{d^2}{dx^2}\left(C_p(x)\tfrac{d}{dt}\left(\tfrac{d^2w}{dx^2}(x,t)\right)\right)\delta w dx\end{aligned} \tag{2.31}$$

The non-conservative force contributions to the system in the modified Euler-Lagrange equations A.21 are represented by the generalised forces Q_i. Using equation A.18 the generalised forces can easily be obtained from 2.31.

$$Q_y = -b\int_{-l/2}^{l/2} p(x,t)dx - d_y\dot{y}_0(t) \tag{2.32a}$$

$$Q_\alpha = -b\int_{-l/2}^{l/2} p(x,t)\left(x+\frac{l}{2}-x_0\right)dx - d_\alpha\dot{\alpha}_0(t) \tag{2.32b}$$

$$Q_w = b\int_{l/2-l_p}^{l/2} p(x,t)\delta w dx - \int_{l/2-l_p}^{l/2}\frac{d^2}{dx^2}\left(C_p(x)\frac{d}{dt}\left(\frac{d^2w}{dx^2}(x,t)\right)\right)dx \tag{2.32c}$$

It has been shown how energy and force contributions to the aeroelastic system are determined as function of the generalised coordinates. Evaluation of the modified Euler-Lagrange equations (given

by equation A.21) after substitution of equations 2.23 and 2.32 results in the equations of motion of the aeroelastic system. The general form of the equilibrium equations can be written as

$$m_y \ddot{y}_0(t) + S_{y\alpha}\ddot{\alpha}_0(t) - \int_{l/2-l_p}^{l/2} \sigma_p(x)\left(\frac{d^2w}{dt^2}\right)(x,t)\,dx + d_y\dot{y}_0(t) + k_y y_0(t) = -b\int_{-l/2}^{l/2} p(x,t)\,dx \tag{2.33a}$$

$$S_{\alpha y}\ddot{y}_0(t) + J_\alpha\ddot{\alpha}_0(t) - \int_{l/2-l_p}^{l/2} \sigma_p(x)\left(x+\frac{l}{2}-x_0\right)\left(\frac{d^2w}{dt^2}\right)(x,t)\,dx + d_\alpha\dot{\alpha}_0(t) + k_\alpha\alpha_0(t) = -b\int_{-l/2}^{l/2} p(x,t)\left(x+\frac{l}{2}-x_0\right)dx \tag{2.33b}$$

$$\sigma_p(x)\left[-\ddot{y}_0(t) - \left(x+\frac{l}{2}-x_0\right)\ddot{\alpha}_0(t) + \frac{d^2w}{dx^2}(x,t)\right] + \frac{d^2}{dx^2}\left[\left(D_p(x) + C_p(x)\frac{d}{dt}\right)\frac{d^2w}{dx^2}(x,t)\right] = p(x,t) \tag{2.33c}$$

where the plunge motion is described by equation 2.33a, the pitch equation by 2.33b, and the plate motion by equation 2.33c. The total mass and inertia properties of the system are given by

$$m_y = m_0 + m + b\int_{l/2-l_p}^{l/2} \sigma_p(x)dx \tag{2.34a}$$

$$S_{y\alpha} = mx_T + b\int_{l/2-l_p}^{l/2} \sigma_p(x)\left(x+\frac{l}{2}-x_0\right)dx; S_{\alpha y} = S_{y\alpha} \tag{2.34b}$$

$$J_\alpha = J_0 + b\int_{l/2-l_p}^{l/2} \sigma_p(x)\left(x+\frac{l}{2}-x_0\right)^2 dx \tag{2.34c}$$

2.6. Solution Method

As discussed in the previous sections it is assumed that at the flutter point the aeroelastic system is harmonically oscillating with small amplitudes. In complex form the harmonic response can be written as

$$y_0(t) = Y_0 e^{i\omega t} \tag{2.35a}$$

$$\alpha_0(t) = A_0 e^{i\omega t} \tag{2.35b}$$

$$w(\overline{x},t) = W(\overline{x})e^{i\omega t} \tag{2.35c}$$

where ω is the angular frequency of the system response. In aeroelasticity however, it is common to use the reduced frequency k, which is a non-dimensional parameter. The non-dimensional reduced

frequency is defined as $k = (\omega/v_F)(l/2)$. Substituting the definition for the reduced frequency into equation 2.35 results in

$$y_0(t) = Y_0 e^{ikv_F \frac{2}{l} t} \tag{2.36a}$$

$$\alpha_0(t) = A_0 e^{ikv_F \frac{2}{l} t} \tag{2.36b}$$

$$w(\overline{x}, t) = W(\overline{x}) e^{ikv_F \frac{2}{l} t} \tag{2.36c}$$

2.6.1. Eigenfunction Expansion Approach

A solution has to be found for the mathematical equations of motion in Equations 2.33 which describe the aeroelastic response of the system. The assumed form for the rigid motions plunge and pitch shown in equation 2.35 are directly substituted into the equations of motion. The motion of the plate is approximated using an eigenfunction expansion approach. The flexible plate is rigidly attached to the airfoil-shaped leading edge. Therefore the motion of the plate can be described by the well known equation for a freely vibrating elastic cantilever beam using the Euler-Bernoulli beam theory. The motion is described using mode shapes, therefore a differential equation of a freely vibrating beam for every j^{th} mode shape is defined

$$W_{0j}''''(x) - (\lambda_j/\bar{l}_p)^4 W_{0j}(\overline{x}) = 0 \tag{2.37}$$

This equation is solved using a harmonic general solution presented in equation 2.38.

$$W_{0j}(x) = C_{1j} cos(\lambda_j \overline{x}/\bar{l}_p) + C_{2j} sin(\lambda_j \overline{x}/\bar{l}_p) + C_{3j} cosh(\lambda_j \overline{x}/\bar{l}_p) + C_{4j} sinh(\lambda_j \overline{x}/\bar{l}_p) \tag{2.38}$$

In order to solve for the coefficients C_{1j}, C_{2j},C_{3j}, and C_{4j} a set of boundary conditions is needed. For a cantilevered beam it is known that the displacement and gradient of the deflection is zero at the root, while the moment and shear force are zero at the tip of the beam. These boundary conditions yield for every single eigenmode. The boundary conditions for every j^{th} eigenmode are written as

$$W_{0j}(1 - \bar{l}_p) = 0, W_{0j}'(1 - \bar{l}_p) = 0, W_{0j}''(1) = 0, W_{0j}'''(1) = 0 \tag{2.39}$$

and an additional one $W_{0j}(x) = l/2$ to obtain unique solutions for every eigenmode $W_{0j}(\bar{x})$. Using these boundary conditions the general solution can straightforwardly be obtained. Solving the general solution for the boundary conditions leads to the relations $C_{1j} = -C_{3j}$ and $C_{2j} = -C_{4j}$. Eventually setting C_{2j} equal to the one and normalizing with the additional boundary condition leads to the spatial solution being

$$W_{0j}(\bar{x}) = \frac{l}{2} \frac{1}{2sin\lambda cos\lambda - 2cos\lambda sin\lambda} \left[\left(cos\lambda_j + cosh\lambda_j\right) \left(sin\left(\frac{\lambda_j}{\bar{l}_p} \left(\bar{x} - 1 + \bar{l}_p \right) \right) - sinh\left(\frac{\lambda_j}{\bar{l}_p} \left(\bar{x} - 1 + \bar{l}_p \right) \right) \right) \right.$$
$$\left. - \left(sin\lambda_j + sinh\lambda_j\right) \left(cos\left(\frac{\lambda_j}{\bar{l}_p} \left(\bar{x} - 1 + \bar{l}_p \right) \right) - cosh\left(\frac{\lambda_j}{\bar{l}_p} \left(\bar{x} - 1 + \bar{l}_p \right) \right) \right) \right] \tag{2.40}$$

The eigenvalues of boundary value problem given in equation 2.37 straightforwardly be obtained by applying the boundary conditions which leads to the relationship given in equation 2.41 for the eigenvalues.

$$1 + cos\lambda_j cosh\lambda_j = 0 \tag{2.41}$$

This relationship has an infinite number of solutions for λ_j. The first four solutions for the eigenvalues are $\lambda_1 = 1.875$, $\lambda_2 = 4.694$, $\lambda_3 = 7.855$, and $\lambda_4 = 10.996$. In Section 2.8 a convergence study is performed to determine the number of eigenmodes that need to be considered for analysis of the instability modes.

The boundary value problem in equation 2.37 together with the boundary conditions in equation 2.39 were recognised as a self-adjoint eigenvalue problem in the book *Methods of Mathematical Physics* by Courant and Hilbert [35]. For a self-adjoint eigenvalue problem it is known that the eigenfunctions $W_{0j}(\overline{x})$ are orthogonal. This leads to:

$$\int_{1-\bar{l}_p}^{1} W_{0j}(\overline{x})W_{0k}(\overline{x})d\overline{x} = 0, j \neq k; \int_{1-\bar{l}_p}^{1} W_{0j}^2(\overline{x})d\overline{x} = \frac{\bar{l}_p\bar{l}^2}{16} \tag{2.42}$$

Now every function $f(\overline{x})$ with continuous first, second, third, and fourth derivatives and satisfying the boundary conditions can be expanded in terms of the eigenfunctions as:

$$f(\overline{x}) = \sum_{j=1}^{\infty} \gamma_j W_{0j}(\overline{x}), \gamma_j = \frac{16}{\bar{l}_p\bar{l}^2} \int_{1-\bar{l}_p}^{1} f(\overline{x})W_{0j}(\overline{x})d\overline{x} \tag{2.43}$$

Using the assumed form of the flutter response defined in equation 2.35, the boundary values for the plate motion can be written as:

$$W(1-\bar{l}_p) = 0, W'(1-\bar{l}_p) = 0, W''(1) = 0, W'''(1) = 0 \tag{2.44}$$

Consequently, the out-of-plane motion of the plate can be expanded into a series expression as:

$$W(\overline{x}) = \sum_{j=1}^{\infty} a_j W_{0j}(\overline{x}) \tag{2.45}$$

where a_j are the series coefficients that have to be determined by solving the aeroelastic system.

2.6.2. Constant thickness

In the papers by Drazumeric et al. and Gjerek et al. the aeroelastic behaviour of an elastically supported aifoil-shaped leading edge with attached a constant thickness flexible plate is studied [3, 20, 27, 36]. The results presented in these papers are used as a verification for the constant thickness model. In the constant thickness model the plate properties D_p, C_p, and σ_p in equation 2.33 are constant and therefore no longer function of x. The equations of motion for the aeroelastic system with a constant plate is used for verification and for comparison of aeroelastic behaviour with the piecewise constant plate model.

At this point all ingredients are present to determine a set of equations with whom the instability points of the aeroelastic system can be determined. Obviously for a constant plate the plate properties D_p, C_p, and σ_p are no longer a function of x, the spatial coordinate along the chord. As a consequence of constant plate properties, the derivatives of the plate properties with respect to x vanish from the plate equation given in equation 2.33c.

Now the assumed form of the flutter response from equation 2.35 with the eigenfunction expansion from equation 2.45 is substituted into the general equations of motion presented in equation 2.33 together with the expressions for the partial pressure distributions from equation 2.16. This results in a conditional set of equations for the series coefficients. Finally the conditional equations for plunging, pitching, and the transverse plate motion can be written as

$$\left(k^2 m_y - \frac{i\omega}{v_F}\frac{l}{2}d_y - \frac{1}{v_F^2}\frac{l^2}{4}k_y - \frac{bl}{2}\int_{-1}^{1} I_y(k,\overline{x})\,d\overline{x}\right)Y_0 + \left(k^2 S_{y\alpha} - \frac{bl}{2}\int_{-1}^{1} I_\alpha(k,\overline{x})\,d\overline{x}\right)A_0$$
$$-\sum_{k=1}^{\infty} a_k \frac{bl}{2}\left(k^2\sigma_p \int_{1-\bar{l}_p}^{1} W_{0k}(k,\overline{x})\,d\overline{x} - \int_{-1}^{1} I_{wk}(k,\overline{x})\,d\overline{x}\right) = 0 \tag{2.46a}$$

$$\left[k^2 S_{\alpha y} - \frac{bl^2}{4}\int_{-1}^{1} I_y(k,\overline{x})\,(\overline{x}+1-\overline{x}_0)\,d\overline{x}\right] Y_0$$

$$+\left[k^2 J_\alpha - \frac{ik}{v_F}\frac{l}{2}d_\alpha - \frac{1}{v_F^2}\frac{l^2}{4}k_\alpha - \frac{bl^2}{4}\int_{-1}^{1} I_\alpha(k,\overline{x})\,(\overline{x}+1-\overline{x}_0)\,d\overline{x}\right] A_0$$

$$-\sum_{k=1}^{\infty} a_k \frac{bl^2}{4}\left[k^2\sigma_p \int_{1-\bar{l}_p}^{1} W_{0k}(\overline{x})\,(\overline{x}+1-\overline{x}_0)\,d\overline{x} - \int_{-1}^{1} I_{wk}(k,\overline{x})\,(\overline{x}+1-\overline{x}_0)\,d\overline{x}\right] = 0 \tag{2.46b}$$

$$\int_{1-\bar{l}_p}^{1} \left(k^2\sigma_p - I_y(k,\overline{x})\right) W_{0j}(\overline{x})\,d\overline{x} Y_0 + \int_{1-\bar{l}_p}^{1} \left[k^2\sigma_p \frac{l}{2}(\overline{x}+1-\overline{x}_0) - I_\alpha(k,\overline{x})\right] W_{0j}(\overline{x})\,d\overline{x} A_0$$

$$-\sum_{k=1}^{\infty} a_k \int_{1-\bar{l}_p}^{1} \left[k^2\sigma_p W_{0k}(\overline{x}) - \frac{4}{l^2}\left[\left(\frac{1}{v_F^2}D_p + \frac{ik}{v_F}\frac{2}{l}C_p\right) W_{0k}''''(\overline{x})\right] - I_{wk}(k,\overline{x})\right] W_{0j}(\overline{x})\,d\overline{x} = 0 \tag{2.46c}$$

The areal density for the aeroelastic system with a constant plate is no longer dependent on x, therefore σ_p in total mass and inertia properties given in 2.34 can be treated as a constant value. Of course the dependency on the number of plies remains. The pressure distribution around the airfoil appear in the integral functions

$$I_y(k,\bar{x}) = \rho\frac{l}{2}\frac{2}{\pi}\int_{-1}^{1} ikG(k,\bar{x},\bar{\xi})d\bar{\xi} \tag{2.47a}$$

$$I_\alpha(k,\bar{x}) = \rho\frac{l^2}{4}\frac{2}{\pi}\int_{-1}^{1} \left[ik(\bar{\xi}+1-\bar{x}_0)+1\right] G(k,\bar{x},\bar{\xi})d\bar{\xi} \tag{2.47b}$$

$$I_{wj}(k,\bar{x}) = \rho\frac{l}{2}\frac{2}{\pi}\int_{1-\bar{l}_p}^{1} \left(ikW_{0j}(\bar{\xi}) + W_{0j}'\right) G(k,\bar{x},\bar{\xi})d\bar{\xi} \tag{2.47c}$$

2.6.3. Piecewise constant

The objective of this research is to investigate the effects on the aeroelastic behaviour a stiffness distribution on the flexible trailing edge. Therefore in this section the equations of motion for an aeroelastic system with a piecewise constant flexible trailing edge are presented.

One of the consequences of assuming a piecewise constant stiffness distribution is that the plate properties are no longer constant over the chord, but vary per section. An extra subscript s is added to the plate properties indicating the section and are therefore denoted as $D_{p,s}$, $C_{p,s}$, and $\sigma_{p,s}$. The numbering for the plate section starts at side of the plate that is clamped. However since the plate properties per section are constant the derivatives of these properties are still zero. As a result of the assumed property distribution the plate properties need to be integrated over each section separately and an extra summation appears in each equation of motion for the summation of the plate properties. The

condition equations for plunging, pitching, and transverse plate motion for a piecewise constant plate can be written as

$$\left(k^2 m_y - \frac{i\omega}{v_F}\frac{l}{2}d_y - \frac{1}{v_F^2}\frac{l^2}{4}k_y - \frac{bl}{2}\int_{-1}^{1} I_y\,(k,\overline{x})\,d\overline{x}\right)Y_0 + \left(k^2 S_{y\alpha} - \frac{bl}{2}\int_{-1}^{1} I_\alpha\,(k,\overline{x})\,d\overline{x}\right)A_0$$
$$-\sum_{k=1}^{\infty} a_k \frac{bl}{2}\left(k^2 \sum_{s=1}^{S}\int_{s_1}^{s_2} \sigma_{p,s} W_{0k}\,(k,\overline{x})\,d\overline{x} - \int_{-1}^{1} I_{wk}\,(k,\overline{x})\,d\overline{x}\right) = 0 \tag{2.48a}$$

$$\left[k^2 S_{\alpha y} - \frac{bl^2}{4}\int_{-1}^{1} I_y\,(k,\overline{x})\,(\overline{x}+1-\overline{x}_0)\,d\overline{x}\right]Y_0$$
$$+\left[k^2 J_\alpha - \frac{ik}{v_F}\frac{l}{2}d_\alpha - \frac{1}{v_F^2}\frac{l^2}{4}k_\alpha - \frac{bl^2}{4}\int_{-1}^{1} I_\alpha\,(k,\overline{x})\,(\overline{x}+1-\overline{x}_0)\,d\overline{x}\right]A_0$$
$$-\sum_{k=1}^{\infty} a_k \frac{bl^2}{4}\left[\sum_{s=1}^{S} k^2 \int_{s_1}^{s_2} \sigma_{p,s} W_{0k}\,(\overline{x})\,(\overline{x}+1-\overline{x}_0)\,d\overline{x} - \int_{-1}^{1} I_{wk}\,(k,\overline{x})\,(\overline{x}+1-\overline{x}_0)\,d\overline{x}\right] = 0 \tag{2.48b}$$

$$\left[\sum_{s=1}^{S} k^2 \int_{s_1}^{s_2} \sigma_{p,s} W_{0j}\,(\overline{x})\,d\overline{x} - \int_{1-\bar{l}_p}^{1} I_y\,(k,\overline{x})\,W_{0j}\,(\overline{x})\,d\overline{x}\right]Y_0$$
$$+\left[\sum_{s=1}^{S} k^2 \int_{s_1}^{s_2} \sigma_{p,s}\frac{l}{2}\,(\overline{x}+1-\overline{x}_0)\,d\overline{x} - \int_{1-\bar{l}_p}^{1} I_\alpha\,(k,\overline{x})\,W_{0j}\,(\overline{x})\,d\overline{x}\right]A_0$$
$$-\sum_{k=1}^{\infty} a_k \sum_{s=1}^{S}\int_{s_1}^{s_2}\left(k^2 \sigma_{p,s} W_{0k}\,(\overline{x}) - \frac{4}{l^2}\left[\left(\frac{1}{v_F^2}D_{p,s} + \frac{ik}{v_F}\frac{2}{l}C_{p,s}\right)W_{0k}''''\,(\overline{x})\right]\right)W_{0j}\,(\overline{x})\,d\overline{x}$$
$$-\int_{1-\bar{l}_p}^{1} I_{wk}\,(k,\overline{x})\,W_{0j}\,(\overline{x})\,d\overline{x} = 0 \tag{2.48c}$$

where s_1 indicates the side of the section closest to the clamp and s_2 the side closest to the free trailing edge. Remember that the tot total mass ans inertia's are determined by integrating the plate properties. These equations now also need to be split and summed up, resulting in the following equations

$$m_y = m_0 + m + b\sum_{s=1}^{S}\int_{s_1}^{s_2}\sigma_{p,s}dx \tag{2.49a}$$

$$S_{y\alpha} = mx_T + b\sum_{s=1}^{S}\int_{s_1}^{s_2}\sigma_{p,s}\left(x+\frac{l}{2}-x_0\right)dx; S_{\alpha y} = S_{y\alpha} \tag{2.49b}$$

$$J_\alpha = J_0 + b\sum_{s=1}^{S}\int_{s_1}^{s_2}\sigma_{p,s}\left(x+\frac{l}{2}-x_0\right)^2 dx \tag{2.49c}$$

2.7. Flutter Calculation

There are multiple methods to determine the flutter points of an aeroelastic system. In the paper by Drazumeric et al. the characteristic equation of the aeroelastic system matrix is used for calculation of the instability points [3]. This method of solving the aeroelastic system however gives no information about the physical mechanism causing the instability. The information of the physical mechanism can be used by engineers to make design changes that could postpone, alleviate or even eliminate the instability.

Other popular flutter calculation methods are the *p method*, *p-k method*, and *k method*. By using the *p method* flutter diagrams which are accurate over the complete range of the conditions can be constructed and therefore can give valuable insight in the physical mechanism causing the instability. The complicating factor in the p method is that an unsteady aerodynamic expression must be formulated which accounts for growing or decaying motions. However the aerodynamic theory by Küssner and Schwarz used in the current model assumes simple harmonic motion and therefore the p method can not be employed for finding the instability modes with this model. The assumption of simple harmonic motions is in accordance with finding the stability boundary at which the motion is assumed to be harmonic.

Both the *k method* and the *p-k method* make use of purely harmonic aerodynamic data for flutter analysis. Hassig applied the *p method* and *k method* to perform a flutter analysis for a realistic aircraft using similar purely harmonic aerodynamic data [37]. Comparing the results it was noted that the modal coupling is predicted wrongly and the wrong mode is predicted to become unstable when using the *k method* [37]. Doing a comparison for the similar case between but now using the *p method* and the *p-k method*, much better agreement was obtained and previously mentioned discrepancies were not observed. For the here fore mentioned reasons the *p-k method* is used to get a deeper understanding in the physical mechanics behind the aeroelastic instability behaviour of specific designs of the flexible airfoil.

2.7.1. Characteristic equation

The equations given by equation 2.46 can be written in matrix form. As can be seen in the equations, the complex coefficients of the aeroelastic matrix $\mathbf{A_F}(v_F, k)$ are a function of the flow speed v_F and the reduced frequency k. The aeroelastic matrix $\mathbf{A_F}(v_F, k)$ is a $n+2$ by $n+2$ square matrix, where n represents the number of mode shapes taken into account. The 'additional' two equations originate from the rigid body motions plunging and pitching.

The flutter problem can now be written as a complex eigenvalue value problem in matrix form. In matrix form the eigenvalue problem is described as

$$\mathbf{A_F} x = \lambda \mathbf{I} x \tag{2.50}$$

where λ is the vector of complex eigenvalues where the real parts are the flutter velocities and the imaginary parts the flutter frequencies, x is the eigenvector corresponding to the eigenvalues, and $\mathbf{I}$ a diagonal unit matrix.

$$(\mathbf{A_F} - \lambda \mathbf{I})\, x = 0 \tag{2.51}$$

For the trivial solution yields

$$|\mathbf{A_F} - \lambda \mathbf{I}| = 0 \tag{2.52}$$

The system has $n+2$ complex eigenvalues which are obtained by solving equation 2.52. Substitution of a single eigenfunction gives the aeroelastic response of the system in the substituted instability point. The aeroelastic matrix is complex, hence the characteristic equation and determinant are complex also. The complex determinant however, can be rewritten into two real equations which both need to be zero in an instability point.

$$Re(\left|\mathbf{A_F}(v_F, k)\right|) = 0, Im(\left|\mathbf{A_F}(v_F, k)\right|) = 0 \tag{2.53}$$

Since we are dealing with two equations, the solutions of the system of equations come in pairs. The solution to the real part of the characteristic equation given in equation 2.53 represents the critical flow velocity, while the imaginary solution represents the frequency of the motion. The solutions to the aeroelastic equations are obtained in pairs. When sorting the solutions by the frequency of the motion, the first solution is the airfoil divergence mode, the second the airfoil flutter mode, the remaining solutions are the plate modes taken into account.

2.7.2. p-k method

The *p-k method* is a compromise of the *p method* and the *k method*. It is based on conducting a *p method* type of analysis with the restriction that the unsteady aerodynamic matrix is for simple harmonic motion similarly to the *k method* [31]. It is sufficient to assume harmonic motion at the flutter speed, but above and below this speed it is not true. However for slowly growing or decaying amplitudes it is assumed that we may approximate the aerodynamic loads using purely harmonic motions. The structural motion is assumed to be of the form

$$y_0(t) = Y_0 e^{pt}, \alpha_0(t) = A_0 e^{pt}, w(\bar{x}, t) = W(\bar{x}) e^{pt} \tag{2.54}$$

where

$$p = \frac{1}{v_F}\frac{l}{2}(\sigma + i\omega) = \delta + ik \tag{2.55}$$

The complex value p consists of a real part representing the non-dimensional damping in the system and is symbolised by δ while the imaginary part represents the reduced frequency symbolised by k. Using the assumed form from equation 2.54 with the assumed form of the aerodynamic forces and moments, the equations for plunge, pitch, and plate motion for the aeroelastic system with a constant thickness distributed trailing edge can be written as

$$-\left(p^2 m_y + \frac{p}{v_F}\frac{l}{2}d_y + \frac{1}{v_F^2}\frac{l^2}{4}k_y + \frac{bl}{2}\int_{-1}^{1} I_y(k,\overline{x})\,d\overline{x}\right)Y_0 - \left(p^2 S_{y\alpha} + \frac{bl}{2}\int_{-1}^{1} I_\alpha(k,\overline{x})\,d\overline{x}\right)A_0 + \sum_{k=1}^{\infty} a_k \frac{bl}{2}\left(p^2\sigma_p \int_{1-\bar{l}_p}^{1} W_{0k}(k,\overline{x})\,d\overline{x} + \int_{-1}^{1} I_{wk}(k,\overline{x})\,d\overline{x}\right) = 0 \tag{2.56a}$$

$$-\left(p^2 S_{\alpha y} + \frac{bl^2}{4}\int_{-1}^{1} I_y(k,\overline{x})(\overline{x}+1-\overline{x}_0)\,d\overline{x}\right)Y_0 - \left(p^2 J_\alpha + \frac{p}{v_F}\frac{l}{2}d_\alpha + \frac{1}{v_F^2}\frac{l^2}{4}k_\alpha + \frac{bl^2}{4}\int_{-1}^{1} I_\alpha(k,\overline{x})(\overline{x}+1-\overline{x}_0)\,d\overline{x}\right)A_0 + \sum_{k=1}^{\infty} a_k \frac{bl^2}{4}\left(p^2\sigma_p \int_{1-\bar{l}_p}^{1} W_{0k}(\overline{x})(\overline{x}+1-\overline{x}_0)\,d\overline{x} + \int_{-1}^{1} I_{wk}(k,\overline{x})(\overline{x}+1-\overline{x}_0)\,d\overline{x}\right) = 0 \tag{2.56b}$$

$$-\int_{1-\bar{l}_p}^{1}\left(p^2\sigma_p + I_y(k,\overline{x})\right)W_{0j}(\overline{x})\,d\overline{x}Y_0 - \int_{1-\bar{l}_p}^{1}\left(p^2\sigma_p\frac{l}{2}(\overline{x}+1-\overline{x}_0) + I_\alpha(k,\overline{x})\right)W_{0j}(\overline{x})\,d\overline{x}A_0 + \sum_{k=1}^{\infty} a_k \int_{1-\bar{l}_p}^{1}\left\{p^2\sigma_p W_{0k}(\overline{x}) + \frac{4}{l^2}\left[\left(\frac{1}{v_F^2}D_p + \frac{p}{v_F}\frac{2}{l}C_p\right)W_{0k}^{IV}(\overline{x})\right] + I_{wk}(k,\overline{x})\right\}W_{0j}(\overline{x})\,d\overline{x} = 0 \tag{2.56c}$$

where again $p = \delta + ik$. A similar approach can be used to determine the equations for an airfoil system with a piecewise constant thickness distributed trailing edge. The equations in 2.56 are used to determine the complex value p for a range of flow velocities. In order to get non-trivial solutions for the equations of motion for every flow speed, the determinant of the aeroelastic matrix needs to be zero. The only unknowns in the aeroelastic matrix are the flow speed v_F, the non-dimensional assumed form of the motion p, and the reduced frequency k. The flow speed v_F is an input, therefore for every v_F a combination of p and k has to be found for which the determinant vanishes. This is done by making use of a determinant iteration technique.

The procedure starts with choosing a value v_F close to $v_F = 0$. As an initial guess for p_1 the natural frequency in absence of aerodynamic damping is used. This is a reasonable guess since the flow speed is near zero. The other initial guess p_2 is made by adding a small damping term to p_1. Substituting the flow speed chosen and the initial guesses, two determinants F_1 and F_2 for the matrices $A_{F,1}(v_{F,1}, p_1)$ and $A_{F,2}(v_{F,2}, p_2)$ can be computed. Next the non-dimensional motion p is updated using

$$p_3 = \frac{p_2 F_1 - p_1 F_2}{F_1 - F_2} \tag{2.57}$$

Now the new guesses are updated to $p_1 = p_2$ and $p_2 = p_3$. For a single flow speed the determinant iteration is repeated until the solution is converged, meaning that the real and imaginary part of the determinant equal zero. Consequently a new flow speed is chosen with initial guesses are based on the results obtained for the previous flow speed. This process is executed over the entire flow speed range for every independent degree of freedom to construct the p-k plots. The flutter speed is found when the real part of the assumed motion $\delta = 0$.

2.8. Convergence Study

The significance of a convergence study is twofold; most importantly it must be made sure the solution has converged such that the correct solution is obtained and secondly it is desirable to take into account the least number of modes for describing the plate deformation since this reduces the calculation time. Convergence is determined by calculating the relative difference between the critical flow speed obtained when taking into account n modeshapes to describe the transverse plate motion and the critical flow speed obtained for $n + 1$ modeshapes.

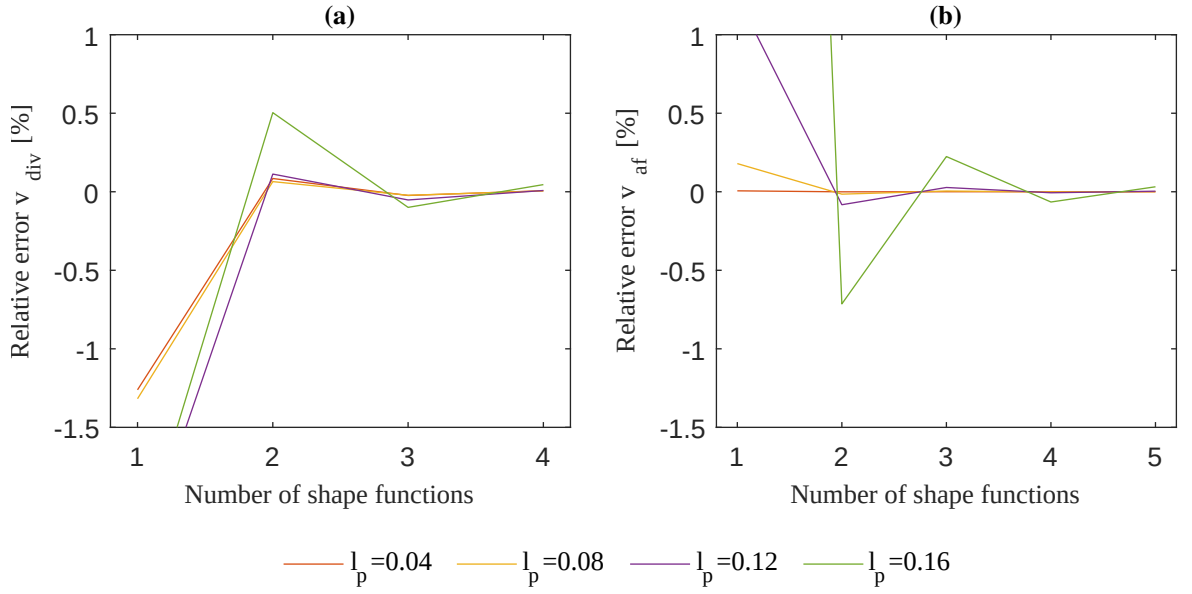

Figure 2.2: Convergence study for (a) divergence and (b) airfoil flutter.

The convergence studies have been performed for systems with properties as stated in Table 2.1. The

convergence study for the divergence mode is executed for an aeroelastic system where the elastic axis is location is $x_0 = 0.25$ with $n_p = 4.00$ and $l_p = 0.04m$, $l_p = 0.08m$, $l_p = 0.12m$, and $l_p = 0.16m$. The results are shown in Figure 2.2(a). The divergence speed converges quickly as expected since there is dealt with a static mode and deformation will mainly be in the first bending mode. A second reason to take into account the least number of modes necessary in the divergence mode is that the reduced frequency used as an input is $k = 1e^{-5}$ resulting in values approaching the limits of Matlab when using too many plate modes. In the remainder of the report two mode shapes are considered for determination of the divergence speed.

Table 2.1: Constant parameters.

l [m]	b [m]	m_0 [kg]	m [kg]	$J_0[kgm^2]$	k_y [N/m]	k_α [Nm/rad]	d_y [Ns/m]	d_α [Nms/rad]
0.18	0.355	0.80	0.50	0.0006	2200	0.50	1.00	0.001

A similar method is used for the convergence study for the airfoil flutter speed. An aeroelastic system is chosen as such that airfoil flutter is observed for all plate lengths considered. The system parameters used are $x_0 = 0.18$, $x_T = 0.21$, and $n_p = 6.00$. The results of the convergence study for airfoil flutter are shown in Figure 2.2(b). In the calculation of airfoil flutter very small reduced frequencies are not encountered. For determination of airfoil flutter four mode shapes are used in the remainder of the report.

In the verification section 2.10 it will be shown that a mode jump occurs at a mass ratio $\mu = 1.2$ for a non dimensional viscoelastic damping coefficient $\alpha = 0.004$. The mass ratio is determined using Equation 2.60. Therefore a convergence study is done before the mode jump for $\mu = 0.5$ and behind the mode jump for $\mu = 1.5$. The results of the convergence study for plate flutter are shown in Figure 2.3. It can be seen that for both mass ratios the critical flow speed is converged when four modes are taken into account. Four mode shapes will therefore be considered for calculation of the plate flutter speed.

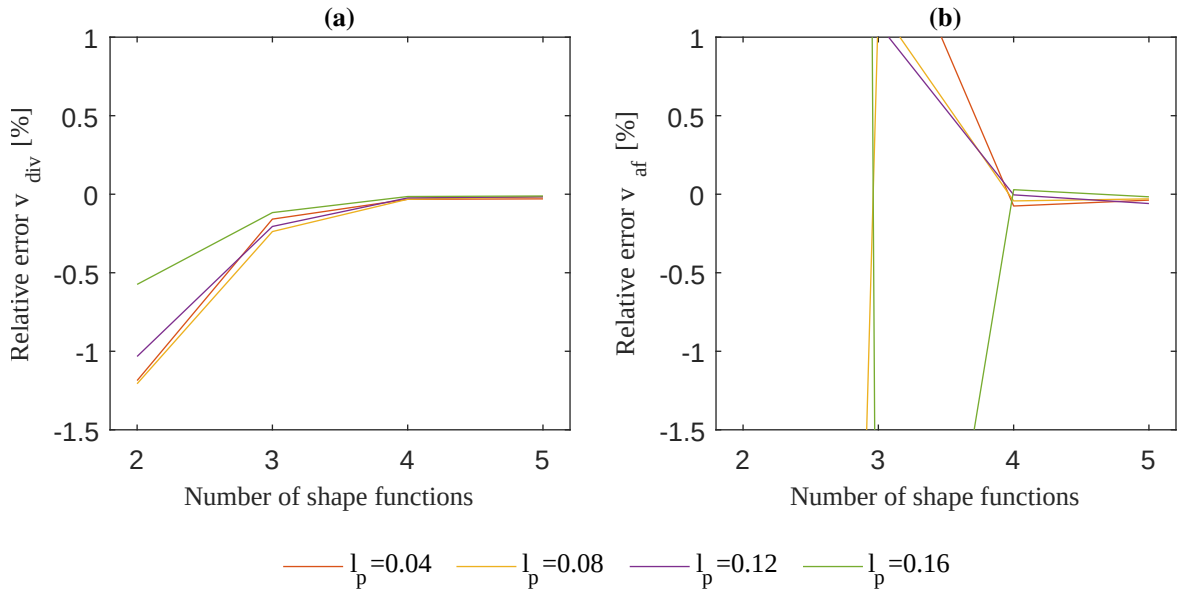

Figure 2.3: Convergence study plate flutter for (a) $\mu = 0.5$ and (b) $\mu = 1.5$.

2.9. Plate Damping Study

In this section the effects of viscoelastic material damping in the flexible plate on the critical flutter speed and benignity of flutter onset is studied. Benignity of the flutter onset is obtained by determination of the gradient of the damping at the instability point of the corresponding mode in the p-k plot. Viscoelastic plate damping is implemented using the Kelvin-Voigt material model. The amount of viscoelastic

damping in the material is symbolised by the non dimensional coefficient α defined in the paper by Tang and Païdoussis [23]. The damping in the plate is defined by

$$C_p = \alpha \sqrt{\frac{\sigma_p l_p^4}{D_p}} D_p \tag{2.58}$$

The areal density σ_p and flexural rigidity D_p are dependent on the number of plies, so this is one way to vary the absolute value of the viscoelastic material damping. The other method is by varying the non dimensional damping coefficient α. For investigation of the viscoelastic damping α is varied, however in the real world this is a constant material property. After this section a constant value for the non-dimensional damping coefficient is used.

In Figure 2.4 the airfoil flutter speed v_{af}, plate flutter speed v_{pf}, and benignity of plate flutter η are plotted against α for $n_p = 4.00$ and $n_p = 6.00$. It can be seen that the plate damping does not alter the airfoil flutter speed. Plate flutter behaviour is however very sensitive to a varying α. Obviously plate damping increases the critical plate flutter speed significantly and decreases the flutter frequency which can be seen in Figure 2.5. These results are in agreement with the papers by Chen et al. [38, 39]. Considering benignity of plate flutter it can be seen that although the critical speed is significantly higher for a plate with $n_p = 6.00$, while the benignity of plate flutter is lower. This implies that benignity of plate flutter is governed by the absolute damping value of the plate.

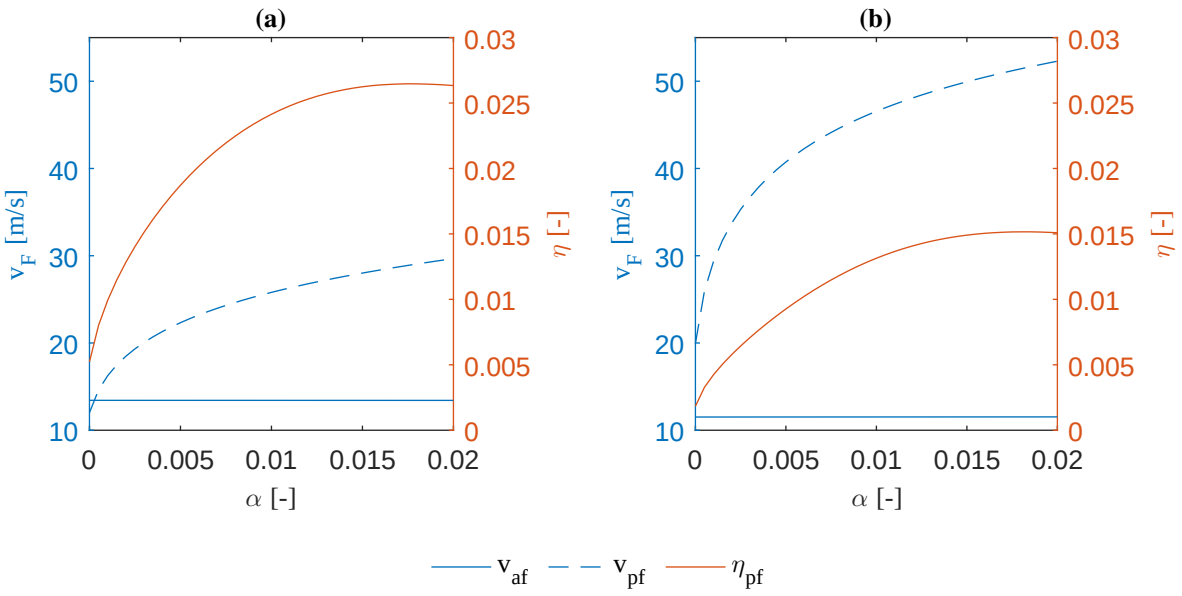

Figure 2.4: Flutter speeds and benignity of plate flutter for an aeroelastic system with $x_0 = 0.15$, $x_t = 0.25$, and $l_p = 0.12$ for (a) $n_p = 4.00$ and (b) $n_p = 6.00$.

By visualisation of the plate modes for multiple values of α it can be seen how the viscoelastic material damping alters the motion of the plate. Figure 2.6 shows the for a plate with $n_p = 3.00$ for $\alpha = 0.0$, $\alpha = 0.010$, $\alpha = 0.020$, and $\alpha = 0.050$ at their corresponding critical flow velocities $v_{pf} = 8.70m/s$, $v_{pf} = 17.33m/s$, $v_{pf} = 20.22m/s$, and $v_{pf} = 25.56m/s$ respectively. From the figures it can be concluded that by adding damping to the plate, the node at approximately $\bar{x} = 0.7$ disappears due to the first bending mode becoming the dominant bending mode. Looking at Figure 2.6(a) where the plate does not posses any damping. It can be seen that there is still damping in the system since the plate is not purely vibrating in the second mode. The damping in the system is a result from aerodynamics and is therefore aerodynamic damping.

The paper by Chen et al. shows a study to the effects of material viscoelasticity on the dynamics of a flag in flow [38]. Figure 2.7 shows the vibration modes of a flag or plate for an increasing viscoelastic

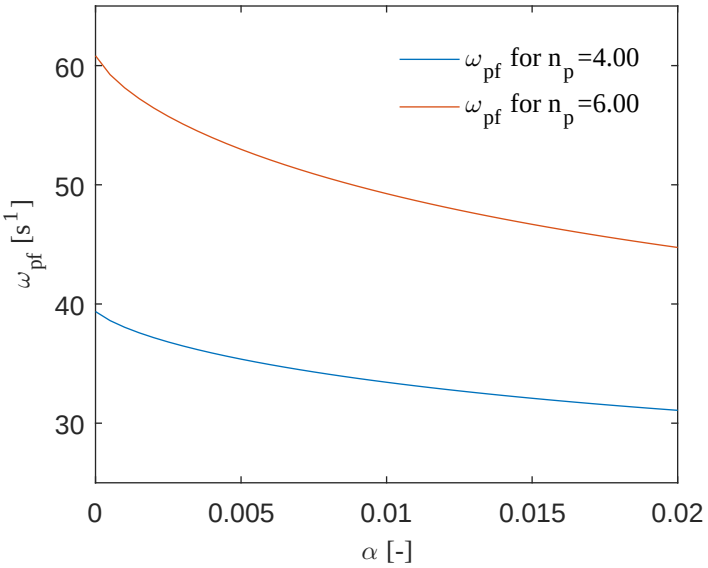

Figure 2.5: Plate flutter frequency versus α for a plate of length $l_p = 0.12$ with $n_p = 4.00$ and $n_p = 6.00$.

damping coefficient. Comparing Figures 2.6 and 2.7 similar trends are observed; in both figures the system transitions from a higher frequency state to a lower frequency state, resulting in a decreasing mean curvature of the plate. Note that the plate mass ratio's are not equal, the goal is to qualitatively show that a similar trend is obtained for an increasing viscoelastic damping coefficient.

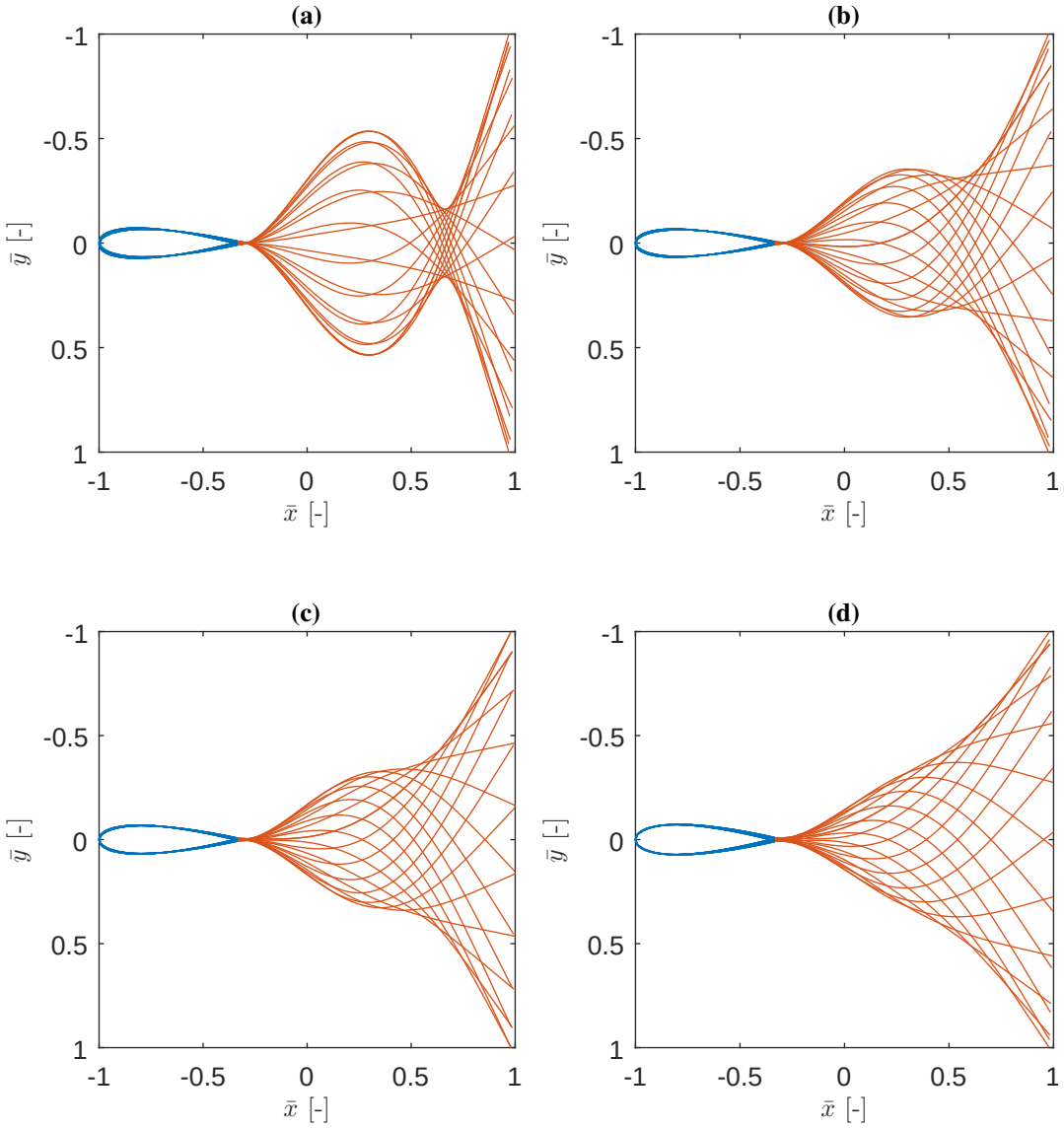

Figure 2.6: Plate flutter modes for an aeroelastic system with $l_p = 0.12$ and $n_p = 3.00$ for: (a) $\alpha = 0.0$, (b) $\alpha = 0.010$, (c) $\alpha = 0.020$, and (d) $\alpha = 0.050$.

2.10. Verification

Verification is an important step in development of a software tool. Verification is the process of determining if the model is built correctly. This can be checked by comparing to the results of models presented in other literature. Successful verification helps building confidence that the model is solved correctly. Verification does not address the relation between the model and the real world.

The verification for the model described in this chapter will be twofold. Firstly the model itself will be compared with the models described in literature, where potential discrepancies in results have to be explained. The second part of the verification consists of checking the optimization procedure by comparison with the results found in the paper by Drazumeric et al. [3].

2.10.1. Verification of the Model

The model is verified by comparison of the flutter boundary results found in the papers by Huang [18], De Breuker et al. [15], and Tang and Païdoussis [23]. Two non dimensional parameters for the reduced critical flow velocity and the mass ratio are introduced by following the non dimensionalisation equations by Tang and Païdoussis [23]. Where the reduced critical flow velocity is defined as

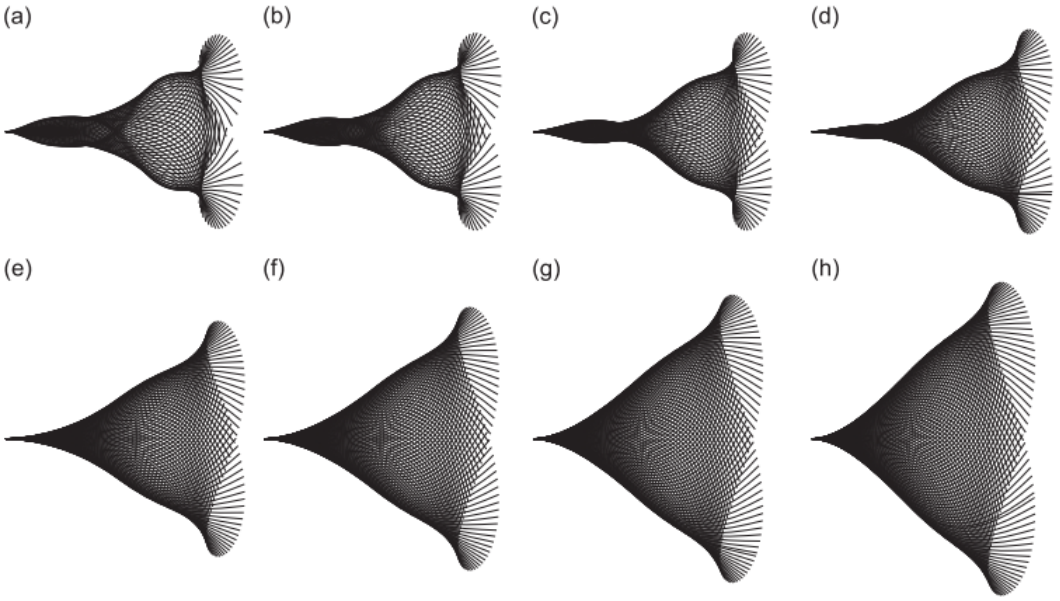

Figure 2.7: Figure from the paper by Chen et al. which shows the vibration modes for an increasing viscoelastic material damping coefficient [38].

$$\bar{U}_c = v_F l_p \sqrt{\sigma_p / D_p} \tag{2.59}$$

where v_F is the dimensional flutter speed, l_p the length of the flexible plate, σ_p the areal density of the plate, and D_p the flexural rigidity along the plate. The mass ratio of the plate is given by

$$\mu = \frac{\rho_f l_p}{\sigma_p} \tag{2.60}$$

where ρ_f is the fluid density. The critical reduced flow speed is plotted against the mass ratio in Figure 2.8. The flutter boundary obtained with the current theory and $\alpha = 0$ is compared with the results found in the papers by Huang [18] and De Breuker et al. [15] while for $\alpha = 0.004$ it is compared to the results by Tang and Païdoussis [23].

As shown in Figure 2.8 the critical reduced flow velocity is dependent on the material damping coefficient α. A very good agreement between the results of the current model and the results by the Tang and Païdoussis [23] model is found for $\alpha = 0.004$. In the model by Tang and Païdoussis [23] an unsteady lumped vortex model is used which is fundamentally different than the aerodynamic theory used in the current model. In order to obtain confidence in the response to a changing viscoelastic material damping coefficient two cases are compared. For the cases $\mu = 0.2$ and zero viscous drag, $\bar{U}_c = 7.05$ when $\alpha = 0.001$, and $\bar{U}_c = 9.20$ when $\alpha = 0.004$, are reported in the paper by Tang and Païdoussis [23]. Using the current model with similar plate properties we find reduced flow velocities of $\bar{U}_c = 6.85$ when $\alpha = 0.001$ and $\bar{U}_c = 9.10$ when $\alpha = 0.004$. These differences are within 3% and again a very good agreement is found for a small viscoelastic material damping coefficient.

Now looking at the results for zero damping, some discrepancies can be observed. As expected the flutter boundary is lower over the complete domain when comparing to the flutter boundary for a viscoelastically damped plate. However two differences can be seen between the flutter boundary results of the verifications and the current model. Firstly, for low mass ratios the current model predicts a lower flutter boundary whereas the results of Huang [18] and De Breuker et al. [15] show very good agreement. Secondly, when comparing to De Breuker et al. [15] the location of the mode jump is predicted for a lower mass ratio by the current mode. However in Figure 8 in the same paper where flutter boundaries of different models are compared, variations in the location of the mode jump are

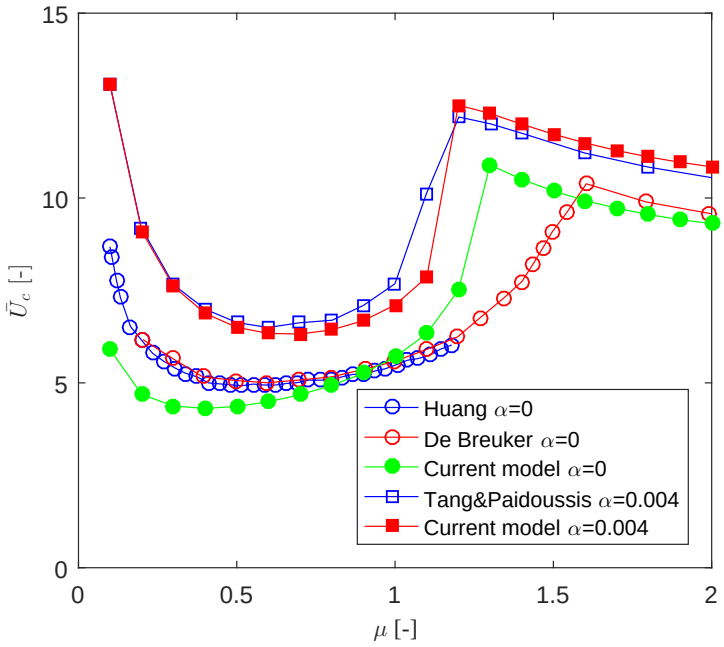

Figure 2.8: Comparison flutter boundary with results found in literature from Huang [18], De Breuker et al. [15], and Tang and Païdoussis [23]. Where α represents the non dimensional material damping coefficient.

observed. So far these discrepancies can not be explained, it was expected to obtain identical results since similar models for the structure and aerodynamics are used.

Vibration modes can give valuable insights in the behaviour of an aeroelastic system. By visualising the motion of the aeroelastic system the dominant modes can be observed giving insight how the aeroelastic system can be altered to improve aeroelastic behaviour. The paper by Tang and Païdoussis [23] shows the vibration modes for a wide range of mass ratios for a material damping coefficient $\alpha = 0.004$. The vibration modes are compared for mass ratios far away from the mode jump one before and the other far behind, and for mass ratios close to the mode jump again one just before and the other just after. The results for mass ratios of 0.5, 1.1, 1.2, and 2.0 can be seen in Figure 2.9. It can be seen that for increasing mass ratios (relatively long and thin plates) higher vibration modes become more important which is supported by the conclusions in the paper by Tang et al. [40]. A very good agreement is found for all mass ratios comparing both the locations of the nodes and the maximum amplitude of the vibrations.

2.10.2. Verification of the p-k method

The added value of the p-k method lies in the fact that it can be seen which degree of freedom becomes unstable and how different modes interact with each other. In Figure 2.10 for example it can be seen that the second plate mode becomes unstable while first plate mode never becomes unstable. Also it can be seen that a clamped-free plate in subsonic flow does not show divergence, which is in agreement with the paper by Kornecki and Dowell [17]. The interaction between modes can be seen most clearly in Figure 2.11(d) where the first and second plate mode show interaction. These kind of observations can give a deeper understanding of the aeroelastic behaviour of a certain configuration of the aeroelastic system in an instability point.

Figure 2.10 shows the p-k plots for $n_p = 6.0$, $n_p = 5.2$, $n_p = 4.22$, and $n_p = 3.0$ plies. The flutter solutions to exactly similar systems are presented in the paper by Drazumeric et al. [3]. The onset of aeroelastic instability in the p-k method occurs for the flow velocity where the damping becomes zero. The results from the verification paper and the p-k method are shown in Table 2.2. It can be seen that the results obtained with the p-k method are almost identical to the verification case. Similar agreement is observed for the reduced frequency comparison.

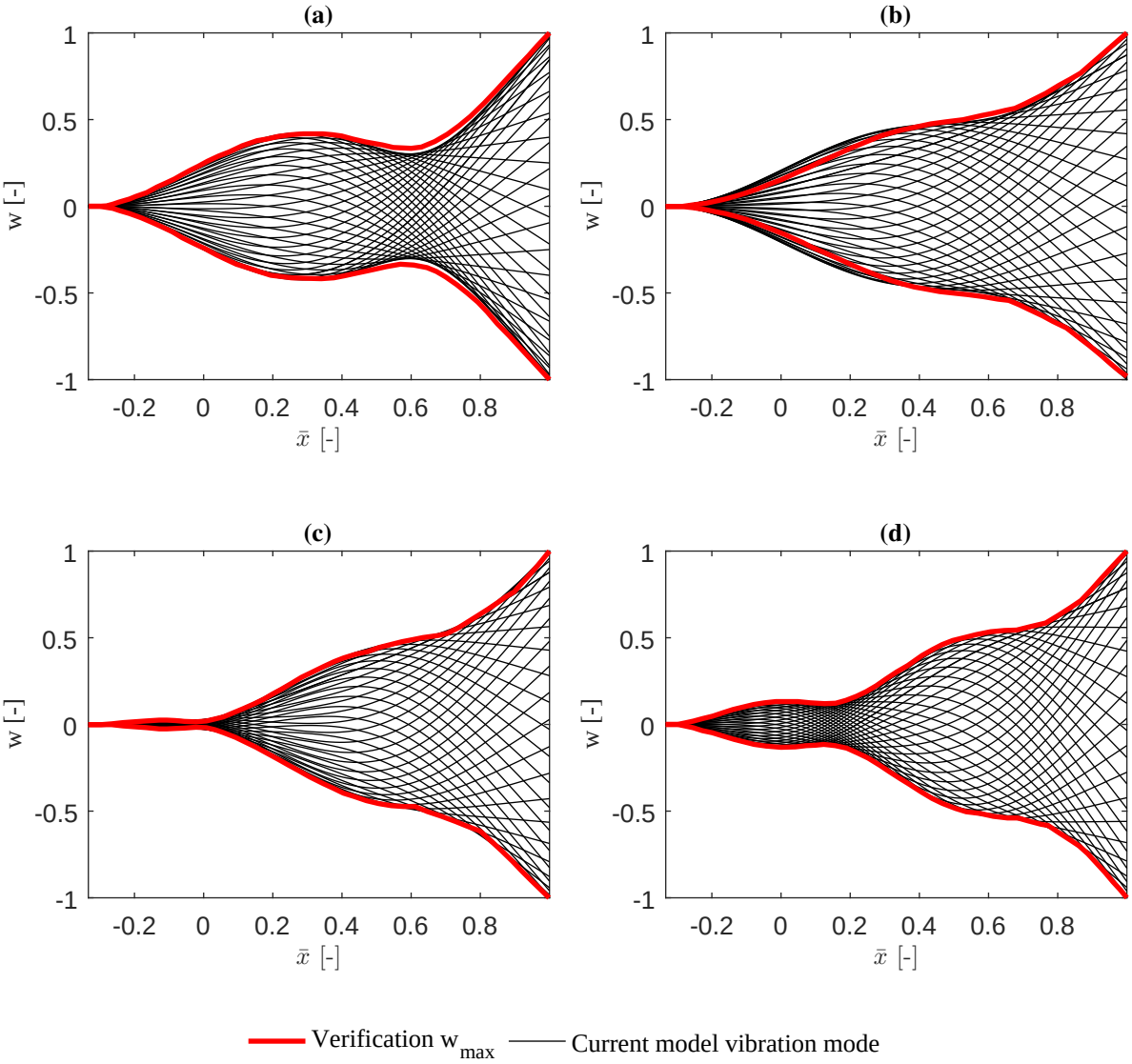

Figure 2.9: Visualisation of the vibration modes for $\alpha = 0.004$ and different values of the mass ratio μ at the corresponding critical points: (a) $\mu = 0.5$, (b) $\mu = 1.1$, (c) $\mu = 1.2$, and (d) $\mu = 2.0$.

Table 2.2: Comparison instability points between the results found in the paper by Drazumeric et al. [3] and the results determined with the p-k method.

	$n_p = 6.0$			$n_p = 5.2$			$n_p = 4.22$			$n_p = 6.0$		
	v_{div}	v_{af}	v_{pf}	v_{div}	v_{af}	v_{pf}	v_{div}	v_{af}	v_{pf}	v_{div}	v_{af}	v_{pf}
Ver.	39.86	15.56	44.62	33.93	17.40	33.93	28.93	-	25.92	25.85	-	19.78
p-k	39.86	15.56	44.62	33.95	17.40	33.94	28.93	-	25.95	25.80	-	19.82

2.10.3. Verification of the optimisation procedure

The wing design that leads to the most favorable aeroelastic characteristics is found by an optimisation procedure. The second part of the verification is the verification of the optimisation procedure. The first step in the verification of the optimisation procedure is the check of the flutter solutions with the plots in the paper by Drazumeric et al. [3]. The flutter solutions show contour plots for which the real and imaginary part of the determinant are zero for a specific reduced frequency versus flow speed range.

Since equal models are exploited as in the paper by Drazumeric et al. [3] for similar system properties, the flutter solutions should be exactly identical to each other. The geometric system properties used are $l = 0.18m$, $l_p = 0.12m$, $x_0 = 32mm$, $x_T = 11mm$. The mass and inertia terms of the system

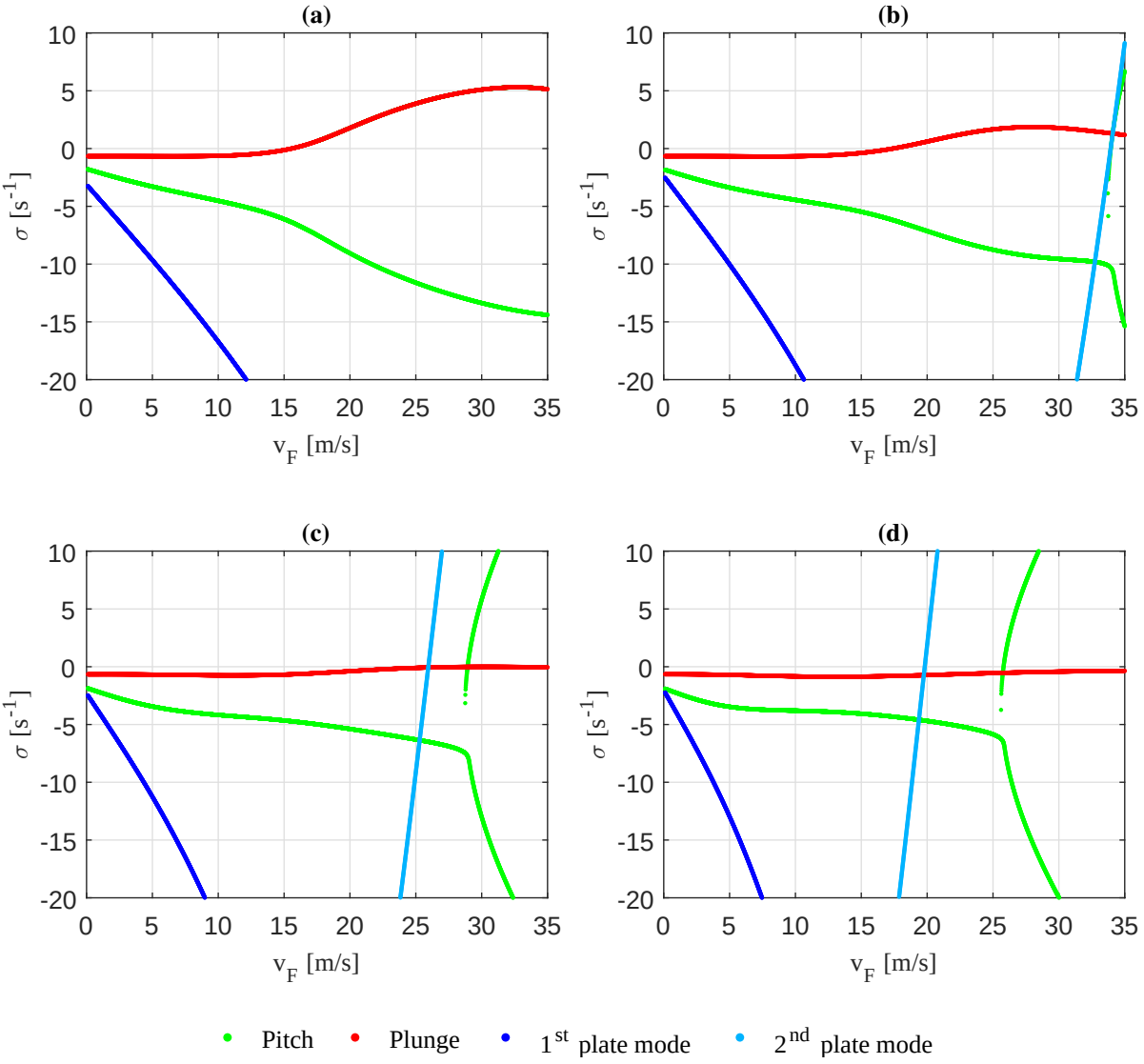

Figure 2.10: Damping plots obtained using the p-k method for various plate thicknesses: (a) $n_p = 6.0$, (b) $n_p = 5.2$, (c) $n_p = 4.22$, and (d) $n_p = 3.0$.

are given by $m = 1.179kg$, $m_0 = 0.511kg$, and $J_0 = 0.00161kgm^2$. The support system properties are defined as $k_y = 2230N/m$, $k_\alpha = 0.57Nm/rad$, $d_y = 1.26Ns/m$, and $d_\alpha = 0.0064Nms/rad$. The previously defined parameters are kept constant during the verification of the optimisation procedure. The plate properties however are varied. The plate properties shown in table 2.3 are experimentally obtained in the paper by Drazumeric et al. [3]. The plate properties are used as continuous functions by interpolating the discrete identified values by cubic splines.

Table 2.3: Dynamic properties of the flexible plate experimentally obtained by Drazumeric et al. [3].

n_p	1	2	3	4	5	6
$\sigma_p[kg/m^2]$	0.169	0.307	0.427	0.527	0.637	0.801
$D_p[Nm]$	1,01e-3	1.22e-2	3.34e-2	5.18e-2	9.43e-2	1.77e-1
$C_p[Nms]$	5.73e-6	1.77e-5	3.50e-5	4.61e-5	5.02e-5	8.09e-5

Figure 2.12 shows the verification of the flutter solution for plate thicknesses 6.0, 5.2, 4.22, and 3.0. As can be seen the flutter solutions found by the current model and the model by Drazumeric et al. [3] are identical. These verification plots give confidence that the determinant is calculated correctly over the domain shown and for different plate thicknesses. Furthermore from the plots the instability

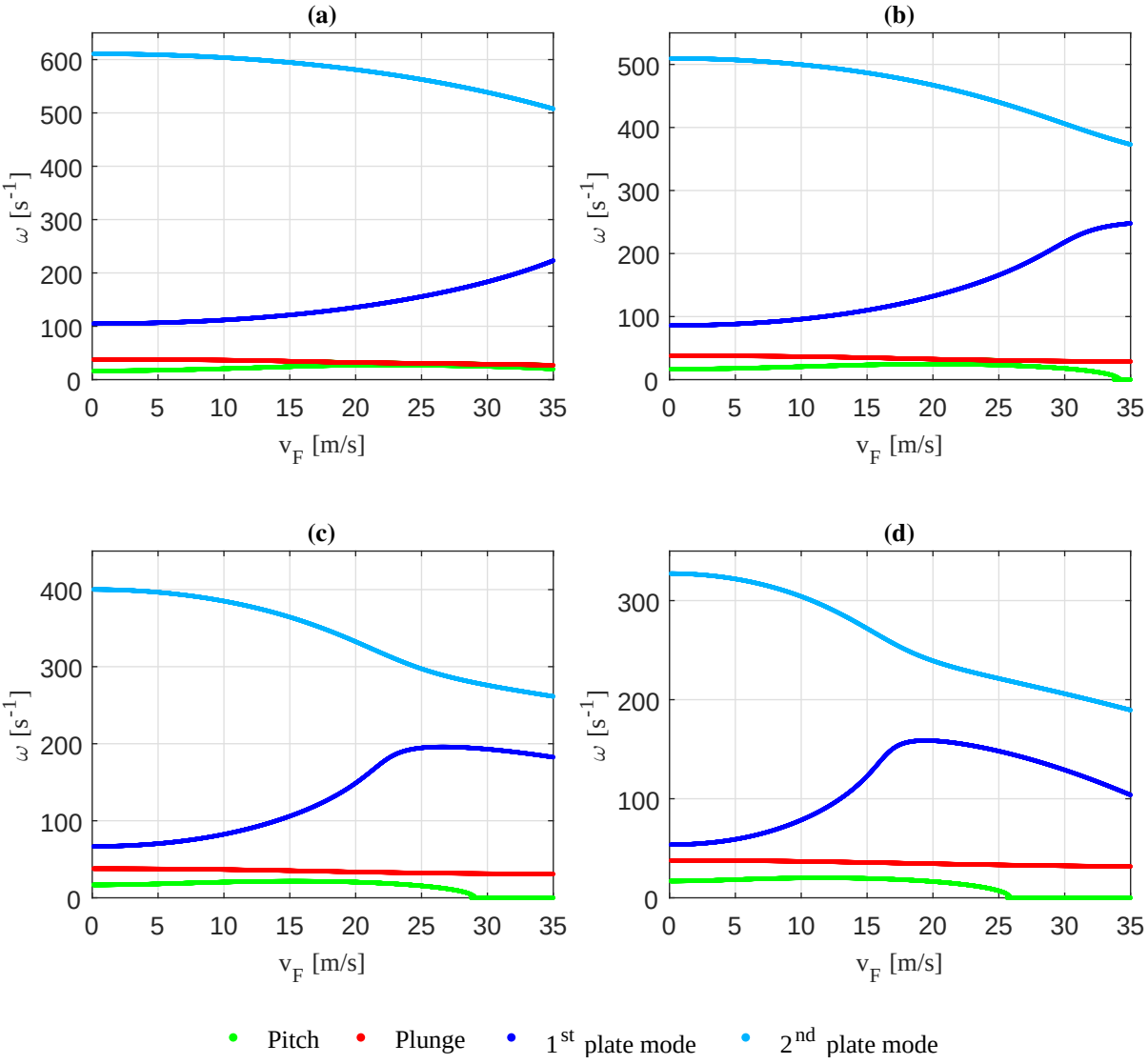

Figure 2.11: Frequency plots obtained using the p-k method for various plate thicknesses: (a) $n_p = 6.0$, (b) $n_p = 5.2$, (c) $n_p = 4.22$, and (d) $n_p = 3.0$.

points can be observed where both the real and imaginary parts of the determinant are zero for the same combination of the reduced frequency k and flow velocity v_F. In other words the instability occurs where the contours for the real and imaginary parts cross.
The instability points in the optimisation procedure are determined using the characteristic equation. For verification four aeroelastic systems are compared each having a different number of plate plies: 6.0, 5.2, 4.22, and 3.0. The characteristic equation is solved by using the $fsolve$ function, which is a built-in MATLAB function that minimises an equation. The comparison between the instability points calculated with the two previously mentioned methods and the verification model by Drazumeric et al. are presented in Table 2.4.

Table 2.4: Comparison instability points between the results found in the paper by Drazumeric et al. [3] and the results determined with the characteristic equation.

	$n_p = 6.0$			$n_p = 5.2$			$n_p = 4.22$			$n_p = 6.0$		
	v_{div}	v_{af}	v_{pf}	v_{div}	v_{af}	v_{pf}	v_{div}	v_{af}	v_{pf}	v_{div}	v_{af}	v_{pf}
Ver.	39.86	15.56	44.62	33.93	17.40	33.93	28.93	-	25.92	25.85	-	19.78
Ch. eq.	39.59	15.45	44.24	33.73	17.15	33.64	28.78	25.57	25.72	25.73	-	19.63

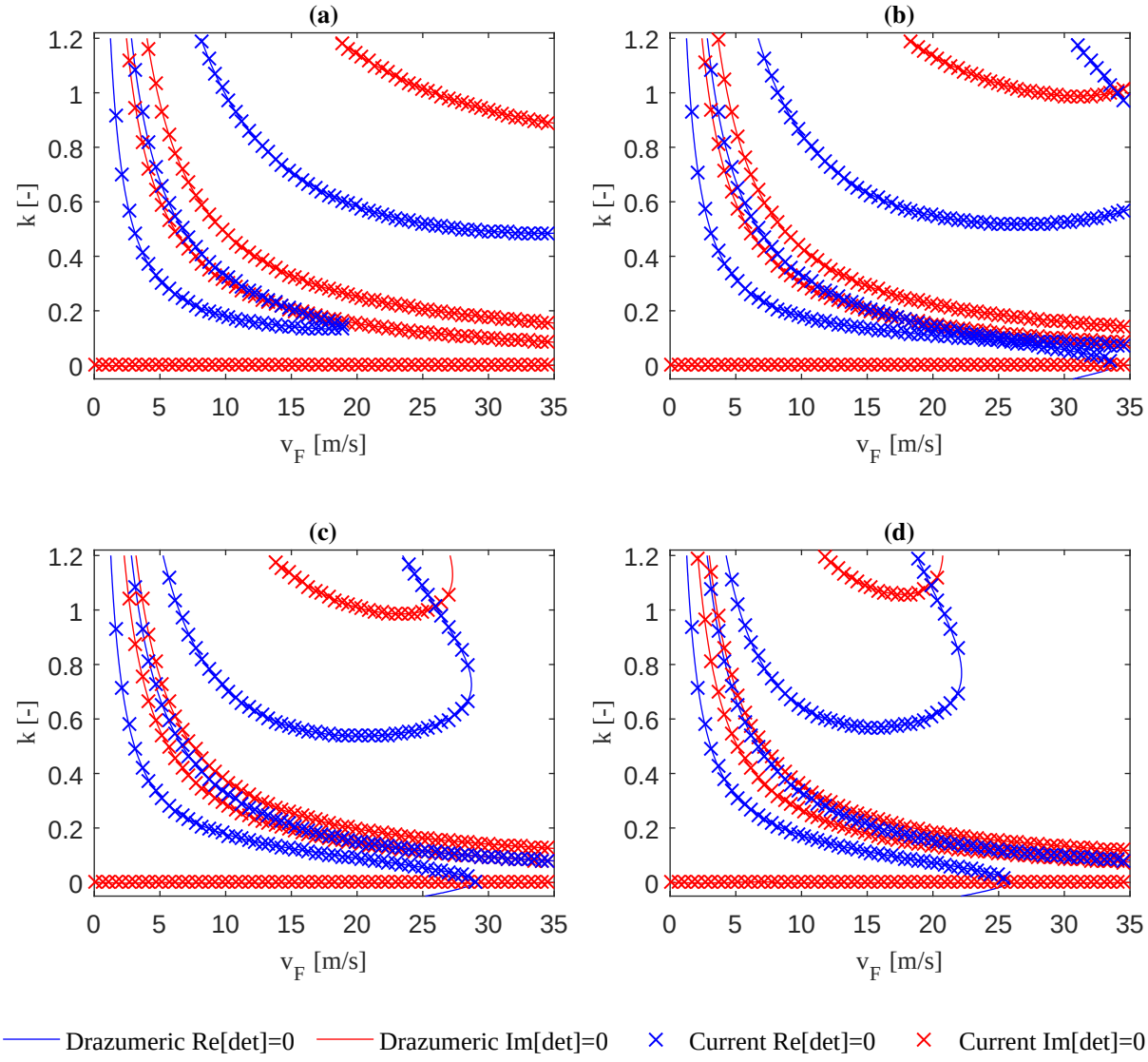

Figure 2.12: Verification flutter solution for various plate thicknesses: (a) $n_p = 6.0$, (b) $n_p = 5.2$, (c) $n_p = 4.22$, and (d) $n_p = 3.0$.

From Table 2.4 it can be concluded that a very good agreement with the verification model is obtained. It can be seen that the results obtained with the characteristic equation are slightly lower, however this difference is negligible. Note that the only difference worth mentioning is found for the airfoil flutter mode for $n_p = 4.22$ where no solution is found in the verification model while a solution is found when solving the characteristic equation. This difference originates from the fact that the MATLAB $fsolve$ function tries to minimise the function and therefore always finds a solution. However in theory the system just not encounter flutter.

3

Optimisation

In this chapter the optimisations and its results are presented. Previous literature by Drazumeric et al. [3] and Gjerek et al. [20] has proven the feasibility of increasing the critical speed of an aeroelastic system by attaching a flexible composite plate to the trailing edge of a rigid leading edge. As stated in Section 1.3 the main objective of this thesis is to investigate the feasibility of increasing the critical flow speed by introducing a thickness distributed trailing edge compared to the critical flow speed of a section with a constant thickness flexible trailing edge. To this extent a piecewise constant thickness distributed trailing edge is assumed. The optimisation is continued for an increasing number of plate sections, which each can have different thickness, until a converged critical flow speed is reached; meaning that adding more sections does not lead to an increase in critical flow speed.

The chapter begins with a discussion on the optimisation strategy in Section 3.1. In this section an explanation is given of the procedure how the critical flow speed for a single aeroelastic system is determined. Moreover genetic algorithms are discussed on a basic level and the bounds during the optimisation procedure are set. In the second section a study is done how the design variables that are kept constant during the optimisations influence the aeroelastic behaviour of the airfoil. In Section 3.3 the airfoil configurations used during the optimisations are defined. The results for two different airfoil sections are presented and elaborated in Sections 3.4 and 3.5. Lastly, Section 3.5.3 shows an applicability study of airfoil flexibility.

3.1. Optimisation Strategy

In this section the optimisation strategy is discussed. As mentioned in the chapter introduction, the main objective of this research is investigation of increasing the critical flow speed at which aeroelastic instabilities occur by introducing a thickness distributed flexible trailing edge. In this research three aeroelastic instabilities are considered, namely section divergence, airfoil flutter, and plate flutter. These three instability modes are calculated independently using the characteristic equation. The number of plate sections is increased until a convergence in critical flow speed has been reached.

The plate thickness distribution is not directly present in the equations of motion derived in Section 2.6. However it has has a direct relation with respect to the plate stiffness D_p, areal density σ_p, and the viscoelastic material damping C_p. Since the plate is made out of composite materials, the stiffness of the plate is a function of the number of plies and the ply angle. How ply angle variation is taken into account is explained in section 3.1.2. The remaining design variables are kept constant during the optimisations.

3.1.1. Optimisation procedure

A genetic algorithm is used to determine the optimal thickness distribution of the flexible trailing edge. Three main arguments to use a genetic algorithm for the optimisation procedure in the current procedure are:

- a genetic algorithm is very likely to find a local optimum,

- for every airfoil configuration the critical of three independent instability points have to be calculated,
- genetic algorithms are very effective when dealing with discontinuous variables [41].

The optimisation procedure is schematically shown in Figure 3.1. The genetic algorithm starts with generating an initial population. Next this initial population is used as input for the *Critical speed function* in which the fitness of each individual of the population is calculated. The fitness is determined in three steps:

- the critical points for each of the three instability modes considered are determined,
- the critical flow speed is defined as the minimal speed at which one of the instabilities occurs,
- the fitness is defined as $1/v_{cr}$.

Next a check is performed if the stopping criterion is met. In case the stopping criterion is not met, a new generation of individuals is generated and the analysed. When the stopping criterion is met, the optimisation ends.

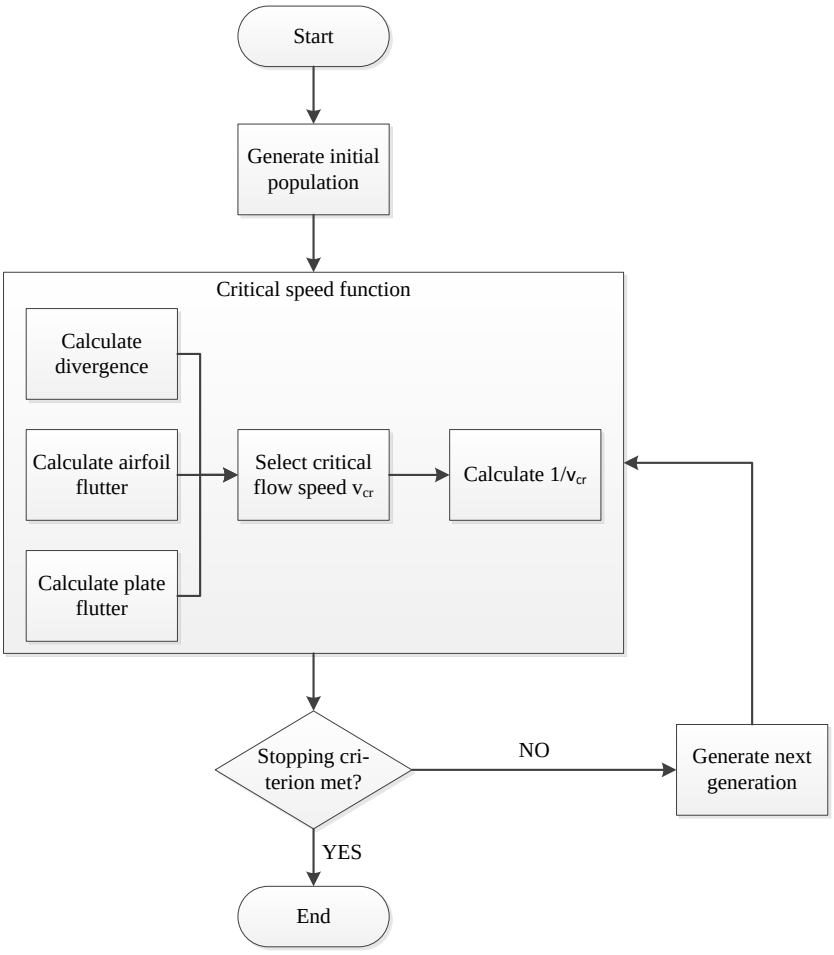

Figure 3.1: Schematic representation of the optimisation procedure.

3.1.2. Optimisation Bounds

The optimisation procedure is continued for an increasing number of sections until a convergence in critical flow speed has been achieved. Every section is defined using two design variables; the section thickness expressed as the number of plies and the ply angle rotation. The ply angle rotation is modelled by multiplying a ply rotation factor $r_{D,i}$ with the flexural rigidity of each section separately. By multiplying the flexural rigidity of a section with $r_{D,i}$, the mass-to-stiffness ratio of each composite section can be varies separately. During the optimisations, an independent multiplication factor is used for every section to determine sectional stiffness. Therewith the number of variables during optimisation is equal to two times the number of sections in which the flexible plate is divided.

Optimisation bounds need to be set for the ply angle variation and the number of plies. In practice the number of plies obviously is an integer, nevertheless in the numerical model the number of plies is treated as a continuous variable. The number of plies is treated as a continuous variable in order to get a more extensive insight into the flexible airfoil characteristics. The number of plies in the optimisation will be varied from one to six plies. The lower bound one is obviously the smallest number of plies physically possible, while the upper bound is determined by studying the results shown in the paper by Drazumeric et al. where it can be seen that the optimal plate design is not limited by the upper bound of six plies [3].

The bending stiffness in chordwise direction for a composite layer as function of the ply angle is given as:

$$\overline{Q}_{11}(\theta) = Q_{11}cos^4\theta + 2(Q_{12} + 2Q_{66})sin^2\theta cos^2\theta + Q_{22}sin^4\theta \tag{3.1}$$

where

$$Q_{11} = \frac{E_1}{1 - \nu_{12}\nu_{21}}, Q_{22} = \frac{E_2}{1 - \nu_{12}\nu_{21}}, Q_{12} = \frac{\nu_{12}E_1}{1 - \nu_{12}\nu_{21}}, Q_{66} = G \tag{3.2}$$

It is assumed that every single section has a constant ply angle. In order to determine the bounds for the multiplication factor, the upper and lower limit for the stiffness have to be determined over the range of possible ply angles. As the composite plate is composed out of plain weave fabric plies, the maximal stiffness is obtained for a ply in the $0/90$ direction, while minimal stiffness is obtained for the $-45/45$ direction. In order to be able to determine the bending stiffness for both cases, material properties are needed. The paper by Gjerek et al. [20] does not state material properties, therefore comparable properties for a glass fibre material are obtained from the book [42], which are shown in Table 3.1.

Table 3.1: Mechanical properties E-Glass/Epoxy Fabric (M10E/3783) [42].

V_f [-]	$\rho[g/cm^3]$	E_1 [GPa]	E_2 [GPa]	G [GPa]	ν_{12} [-]
0.50	1.90	24.5	23.8	4.7	0.11

Substitution of the material properties from Table 3.1 into the equations given in 3.2 results in:

$$Q_{11} = 24,8GPa, Q_{22} = 24,1GPa, Q_{12} = 2.7GPa, Q_{66} = 4.7GPa \tag{3.3}$$

Using the glass fiber properties from Equation 3.3 the reduced stiffneess for bending in chordwise direction can be determined for $\theta = [0/90]$ and $\theta = [-45/45]$.

$$\overline{Q}_{11}([0/90]) = 24.8GPa, \overline{Q}_{11}([-45/45]) = 18.3GPa \tag{3.4}$$

Translating these values for the stiffness values into stiffness multiplication factors, the range of the stiffness multiplication factor ranges from $0.7374 - 1$. Where the lower bound is determined by dividing $\overline{Q}_{11}([-45/45])$ by $\overline{Q}_{11}([0/90])$ and the upper bound is simply one by dividing $\overline{Q}_{11}([0/90])$ by itself.

3.2. Design Variables

The objective of this section is to gain insight in the effects of the design variables on the aeroelastic behaviour of the flexible airfoil. The insights are used for explanation of the results generated with the

optimisations and to design airfoil configurations that are used during the optimisations. The section is divided into two sub-sections; the first sub-section shows the effects of location of the elastic axis, plate length, and plate stiffness on divergence, while the second sub-section shows the effects of plate length, plate stiffness, the location of the center of gravity, and the bending to torsion natural frequency ratio of the elastic support on the flutter behaviour. The other parameters are treated as constants. The values of the design variables treated as constants in this section are shown in Table 3.2. In this section a multi-section plate is not considered.

Table 3.2: Variables treated as constants during the design variable study.

l [m]	b [m]	m_0 [kg]	m [kg]	$J_0[kgm^2]$	k_y [N/m]	k_α [Nm/rad]	d_y [Ns/m]	d_α [Nms/rad]
0.18	0.355	0.80	0.50	0.0006	2200	0.50	1.00	0.001

3.2.1. Divergence Study

Divergence is the static point of instability where the aerodynamic forces and moments are in balance with the elastic forces and moments. As stated in the chapter introduction the spring stiffnesses of the elastic support are kept constant. The aerodynamic forces and moments on the aeroelastic system however can be influenced by changing structural parameters. The structural parameters that have an effect on the aerodynamic forces are the position of the elastic axis x_0, plate stiffness D_p, and plate length l_p. The effects of these parameters on the divergence speed and benignity of the divergence onset are studied in this section.

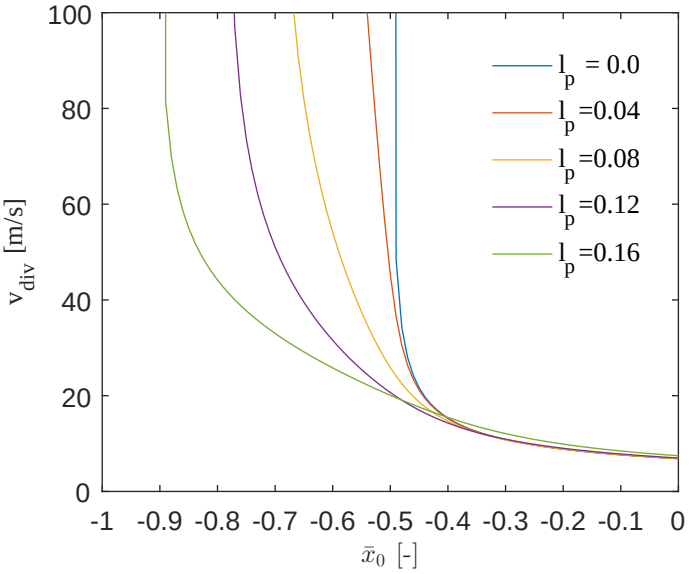

Figure 3.2: Divergence speed versus location of the elastic axis for multiiple flexible plate lengths.

The center of pressure is the location on the chord where the resulting aerodynamic force acts. The location of the center of pressure can be determined by dividing the total aerodynamic moment by the total aerodynamic force [33]. The pressure distribution over the airfoil governs the location of the center of pressure since the center of pressure is dependent on the aerodynamic moment. For a symmetrical rigid airfoil it is known that by placing the elastic axis at a quarter chord point, hence at the center of pressure, divergence vanishes. This is also seen from equation 3.5 from the book by Hodges which is the equation to determine the dynamic pressure at which divergence occurs [31].

$$q_D = \frac{GJ}{eca}\left(\frac{\pi}{2l}\right)^2 \tag{3.5}$$

where e indicates the distance between the center of pressure and the elastic axis. Obviously when e approaches zero, the divergence dynamic pressure goes to infinity and thus the divergence speed. The presence of a flexible trailing edge alters the pressure distribution over an airfoil and hence changes

the location of the center of pressure and therewith the divergence behaviour of the aeroelastic system. In Figure 3.2 the divergence speed is plotted against the location of the elastic axis for multiple flexible plate lengths and $n_p = 6.00$ with a corresponding flexural rigidity of $D_p = 1.741e^{-1}Nm$.

For a rigid airfoil ($l_p = 0$) it can be seen that divergence disappears as expected at a quarter chord point ($\bar{x}_0 = -0.5$) where the elastic axis is located in the center of pressure. As can be seen, the longer the plate, the closer the elastic axis has to be moved to the leading edge to make divergence disappear. This implies that the flexible plate moves the center of pressure forward. Figure 3.3 shows a comparison between two similar aeroelastic sytems with $l_p = 0.12$, but each with a different plate thickness and thus a different flexural stiffness $D_p = 2.176e^{-2}Nm$ for $n_p = 3.00$ and $D_p = 1.741e^{-1}Nm$ for $n_p = 6.00$. It can be seen that for a range of approximately -0.8 to -0.4 of the elastic axis position, the airfoil with a lower flexural rigidity has a significanty lower divergence speed. The location of the center of pressure however is unchanged.

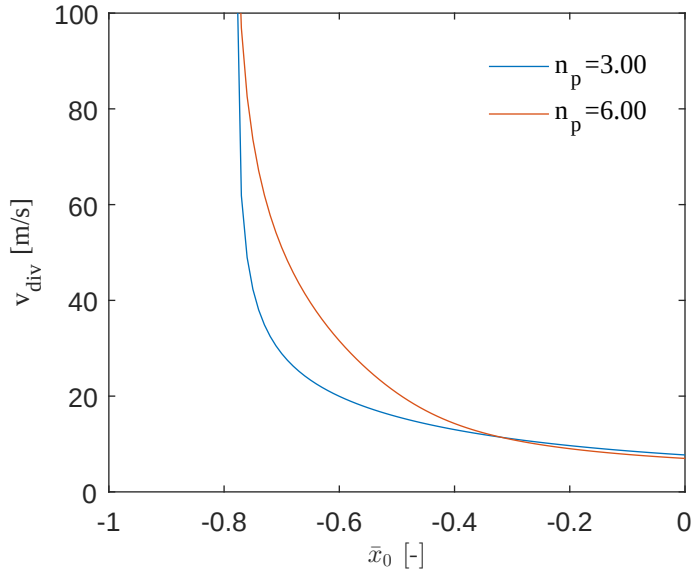

Figure 3.3: Divergence speed versus location of the elastic axis for $l_p = 0.12$ and two plate thicknesses.

The difference in divergence speed shown in Figure 3.3 can be explained by visualising the divergence modes for similar aeroelastic systems with a different flexural stiffness of the flexible plate. Again aeroelastic systems with $n_p = 3.00$ and $n_p = 6.00$ with $\bar{x}_0 = -0.6$ are compared with each other and their corresponding divergence modes are shown in Figure 3.4. Two most obvious differences are the larger plate deflection for the aeroelastic system with the softer plate shown in figure 3.4(a) while the plunge motion is larger for the stiffer plate shown in Figure 3.4. The softer plate shows a larger plate bending which leads to a lower upward pressure over the plate. Consequently the total aerodynamic force is smaller resulting in a smaller plunge displacement. A second result of the larger plate bending is a smaller aerdynamic nose down moment due to a smaller upward pressure over the plate and therewith resulting in a lower divergence speed $20.01m/s$ for $n_p = 3.00$ and $31.57m/s$ for $n_p = 6.00$. These conclusions only yield in the cases where the elastic axis is positioned in front of the location where the plate is attached to the airfoil, which for a plate length of $l_p = 0.12$ lies at $\bar{x} = -0.3333$.

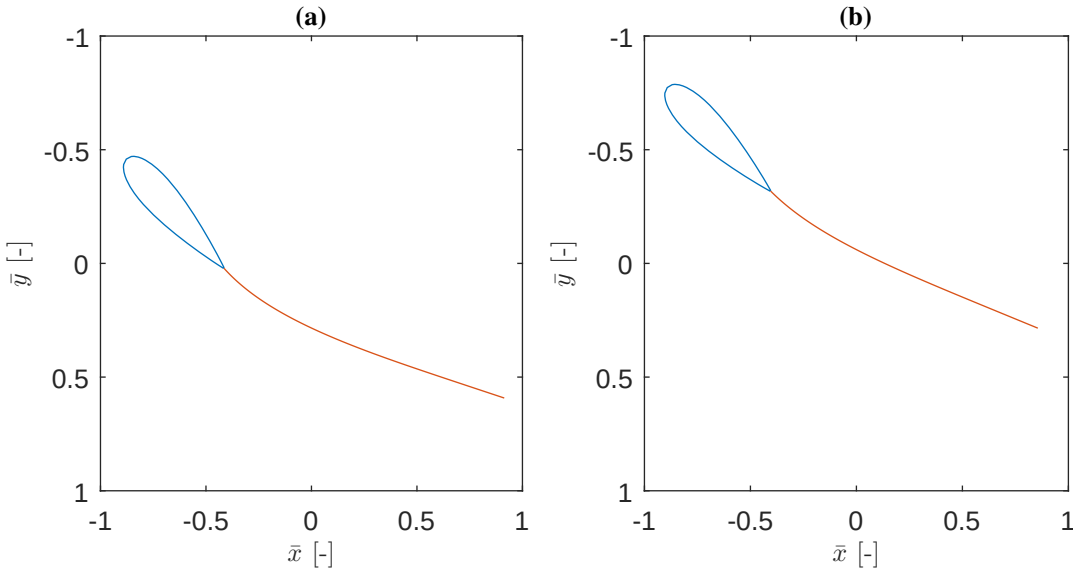

Figure 3.4: Divergence mode for an aeroelastic system with $\bar{x}_0 = -0.6$, $l_p = 0.12$ and with: (a) $n_p = 3.00$, and (b) $n_p = 6.00$.

3.2.2. Flutter Study

Flutter is the dynamic instability where aerodynamic, elastic, and inertial forces and moments interact with each other. This section presents a study to the effects of important design variables on the flutter bahaviour of an elastically supported airfoil. The geometric parameters that are varied are the plate length l_p, the flexural rigidity of the plate D_p, the areal density of the plate σ_p, the location of the center of gravity x_T, and the bending to torsion natural frequency ratio.

Variation of the plate length, stiffness, and density

One of the objectives of this research is to investigate the effects of a flexible trailing edge on the aeroelastic characteristics of an airfoil. The effects on the divergence behaviour has been discussed in the previous sub-section. In this sub-section the effects of plate length, and plate thickness is investigated for three different materials whose properties are presented in Table 3.3. The properties are defined as the flexural rigidity per ply D_n and the areal density per ply σ_n. The total flexural stiffness of a ply is detemined by $D_p = D_n \cdot n^3$ and the total areal density by $\sigma_p = \sigma_n \cdot n$.

Table 3.3: Flexural stiffness and areal density per ply for fiberglass, aramid, and carbon.

	Fiberglass	Aramid	Carbon
$D_n[Nm]$	$8.06e^{-4}$	$1.55e^{-3}$	$9.61e^{-3}$
$\sigma_n[kg/m^2]$	0.13	0.12	0.19

The critical flutter speed results for an aeroelastic system with $x_0 = 0.15$, $x_T = 0.25$, and $\alpha = 0.004$ are shown in Figure 3.5. In Subfigure (a) for $l_p = 0.04$ it can be seen that plate flutter is not critcal for the plate thickness range considered. A second observation that can be made is that the relieving effect of airfoil flexibility on airfoil flutter is only visible for a very small range and with a limited effect.

For longer flexible plates it can be seen that the critical plate flutter speed decreases as expected. The phenomenon of the mode jump seen in Section 2.10, can also be seen in Subfigures (c) and (d) where for a small number of plies the critical plate flutter speed first decreases for an increasing number of plies and after increases again.

Considering the airfoil flutter speed versus the number of plies, it is obvious that for a smaller amount of plies the airfoil flutter speed increases and for a certain number of plies the instability vanishes. This effect is stronger for longer plates and for plates with a lower stiffness. The increase in critical airfoil flutter speed can be accounted to the flexible plate having a relieving effect on the aerodynamic forces.

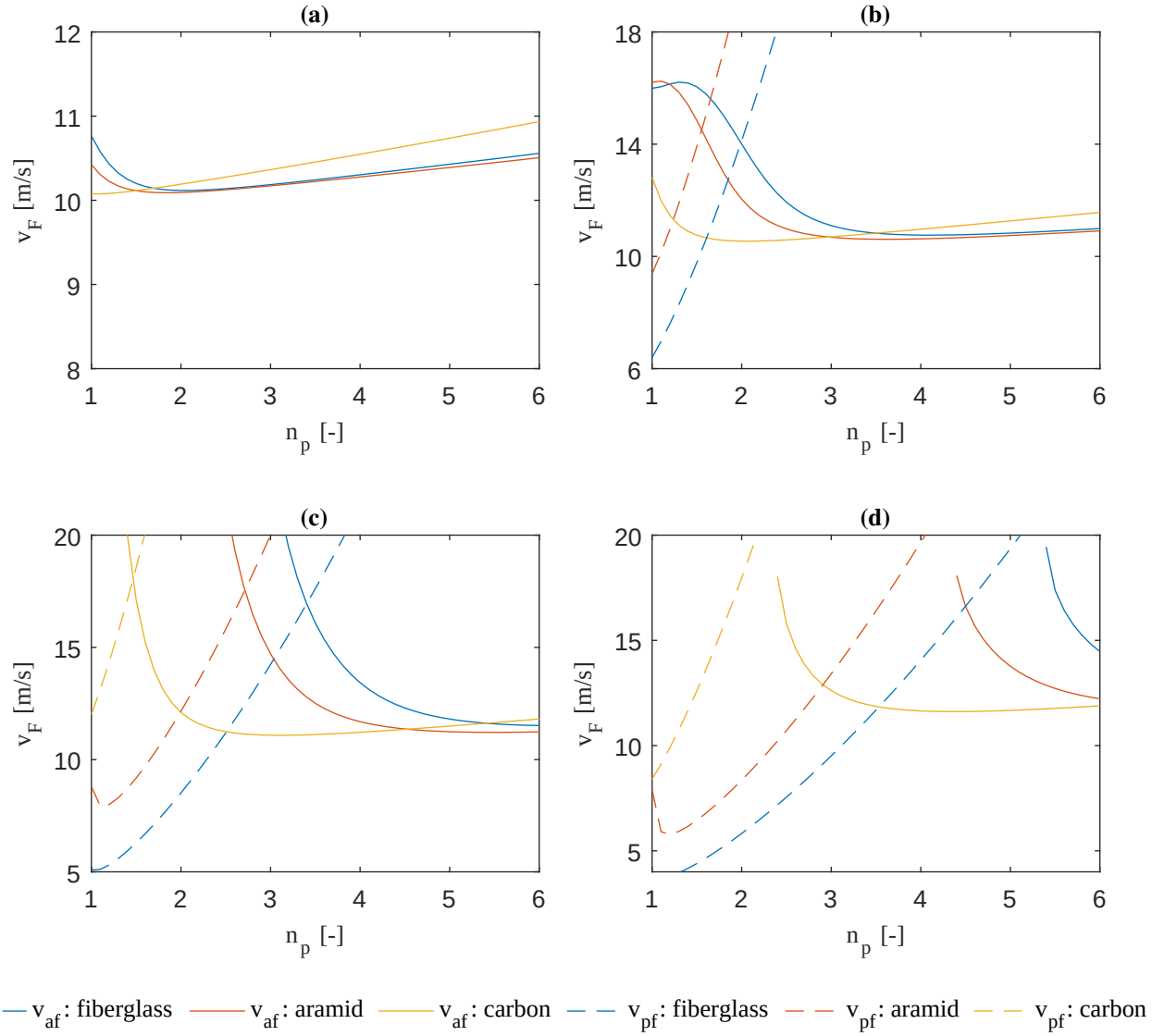

Figure 3.5: Flutter characteristics versus the number of plies for aeroelastic systems with different flexible plate materials and various plate lengths of: (a) $l_p = 0.04$, (b) $l_p = 0.08$, (c) $l_p = 0.12$, (d) $l_p = 0.16$.

In Figure 3.6 the airfoil flutter modes for a system with $n_p = 3.00$ in Sub-figure (a) and $n_p = 6.00$ in Sub-figure (b) are shown. It can be seen that the plate with a lower flexural rigidity undergoes more bending in the airfoil flutter mode and thus has a bigger relieving effect. This leads to a critical flow speed $v_{af} = 23.67 m/s$ for the system with $n_p = 3.00$ against a critical flow speed $v_{af} = 11.52 m/s$ for the system with $n_p = 6.00$.

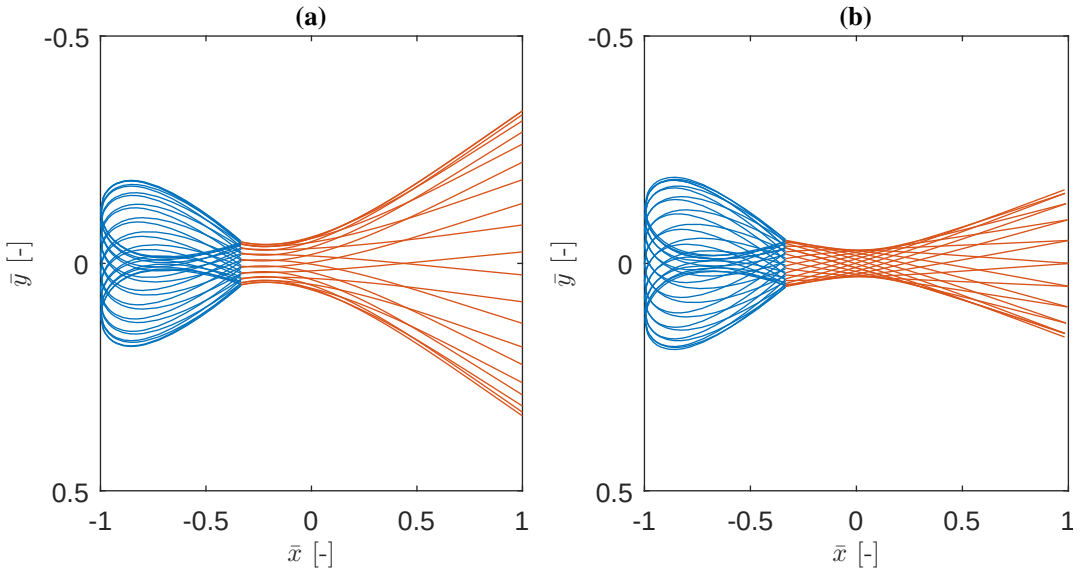

Figure 3.6: Airfoil flutter modes for an aeroelastic system with $x_0 = 0.15$, $x_t = 0.25$, and $l_p = 0.12$ for: (a) $n_p = 3.00$ and (b) $n_p = 6.00$.

Variation of the location of the center of gravity

As stated in the section introduction, the airfoil flutter phenomenon is an interaction between aerodynamic, elastic, and inertial forces and moments. The inertial force of the airfoil can be influenced by changing the mass and/or the location of the elastic axis. For this study the location of the center of gravity is varied in order to keep the mass of the system constant.

Changing the location of the center of gravity solely has an influence on the airfoil flutter mode, therefore plate flutter is not needed to take into consideration. Using the parameters as shown in Table 3.2 the plot for the airfoil flutter for a varying location of the center of gravity was obtained as shown in Figure 3.7(b). At a first glance the trend was not wat was expected, since in literature plots where airfoil flutter is plotted against a varying location of the center of gravity show a decreasing trend. However, Figure 3.7(b) is plotted for an airfoil for which the plunging frequency is higher than the pitching frequency. Now creating the same plot but for an airfoil where the pitching frequency is higher than the plunging frequency results in the trend shown in Figure 3.7, showing a similar trend as plots in literature. The airfoil flutter speed is very sensitive to varying the location of the center of gravity. Depending on the bending to torsion natural frequency ratio the airfoil flutter speed either increases or decreases.

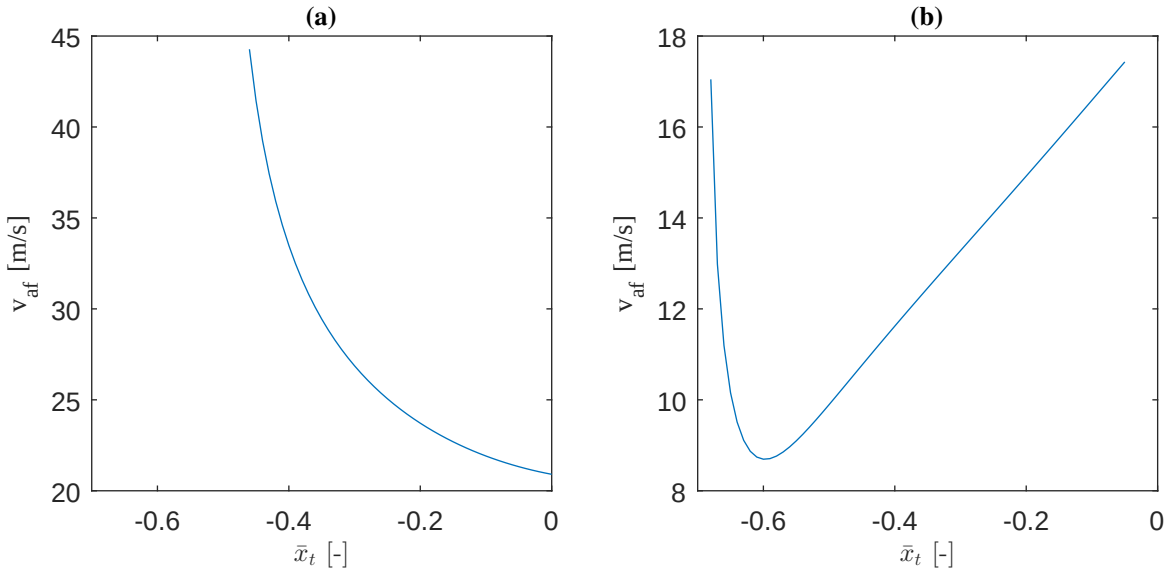

Figure 3.7: Airfoil flutter speed of a rigid airfoil section for $\overline{x}_0 = -0.7$ and an aft moving center of gravity for (a) a conventional airfoil configuration, and (b) an unconventional airfoil configuration.

Variation of the natural frequency ratio

The research by Gjerek et al. showed that the airfoil flutter mode is highly sensitive to the uncoupled natural frequency ratio of the elastic support. The natural frequencies can be altered by changing the total mass of the system, the total moment of inertia, the plunging stiffness, and the torsional stiffness. To limit the design variable study, the torsional stiffness stiffness is varied solely. This leads to a changing natural torsion frequency and therewith the ratio of the uncoupled natural frequency ratio is altered.

The result of varying the torsional stiffness from $k_\alpha = 6.77 Nm/rad$ where $\omega_h/\omega_\alpha = 0.4$ to $k_\alpha = 0.75 Nm/rad$ where $\omega_h/\omega_\alpha = 1.2$ results in the plot shown in Figure 3.8. It can be seen that the critical flow speed decreases until a bending to torsion natural frequency ratio of one where the natural plunging frequency is equal to the natural pitching frequency and after rises again. This can be explained by the fact that up to $\omega_h/\omega_\alpha = 1.0$, the pitching stiffness is higher than the plunging frequency. By reducing the torsional stiffness, the natural frequency of both modes are brought closer to each other, therefore the critical flow velocity decreases. After $\omega_h/\omega_\alpha = 1.0$ the natural frequency of the modes are separated and the critical flow velocity increases again. Varying the the bending to torsion natural frequency ratio by changing the rotational stiffness, increases the airfoil flutter speed when the frequencies of the modes are separated and vice versa.

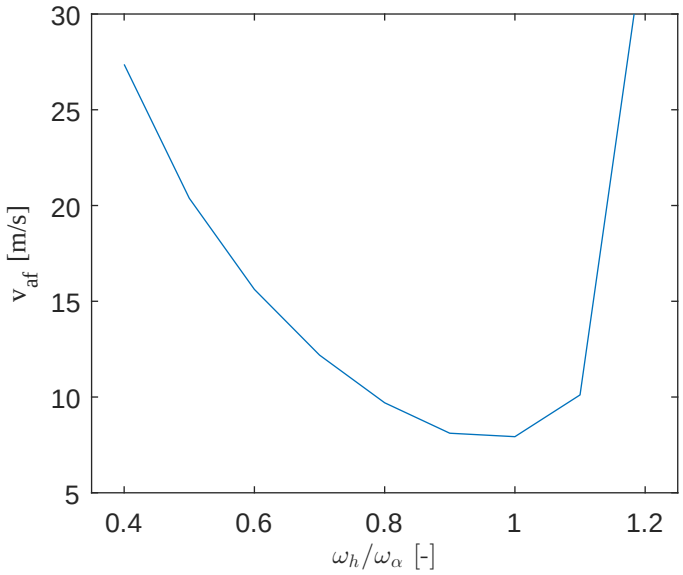

Figure 3.8: Airfoil flutter speed for a rigid airfoil for an increasing bending to torsion natural frequency ratio of the elastic support.

3.2.3. Synopsis

In this section the influence of some important design variables was presented. This synopsis is meant to summarise observations that were made with respect to the influence of the design variables on the aeroelastic behaviour. Firstly, the influence of the design variables studied on the divergence behaviour are summarised:

- moving the elastic axis towards the leading edge increases the divergence speed of an airfoil. In case the elastic axis is moved in front of the center of pressure the divergence mode vanishes.
- addition of a flexible plate to the trailing edge of an elastically supported rigid leading edge moves the center of pressure towards the leading edge. The longer the flexible plate, the more the center of pressure is moved forward.
- increasing the stiffness of the flexible plate results in an increase in divergence speed, the location of the center of pressure is not altered.

Regarding the airfoil flutter mote the following statements can be made based on the design variable study:

- adding flexibility to an airfoil section has a relieving effect on the airfoil flutter mode. Flexibility can be increased either by increasing the flexibility fraction or reducing the thickness of the flexible plate.
- varying the the bending to torsion natural frequency ratio by changing the rotational stiffness, increases the airfoil flutter speed when the frequencies of the modes are separated and vice versa.

3.3. Formulation of the Airfoil Sections

In this section there is elaborated on the design variables of the airfoils used during the optimisations. Optimisations are executed for two airfoil sections with different properties. The first airfoil section that is optimised for has properties comparable to the airfoil section properties found in the papers by Drazumeric et al. and Gjerek et al. [3, 20, 27, 36]. An airfoil section with comparable properties to the ones found in the here fore mentioned research is chosen since it was shown that adding flexibility to this specific configuration has a great potential. This airfoil configuration is unconventional since the plunging natural frequency is higher than the pitching natural frequency, while for conventional airfoil configurations found in literature the torsional frequency is significantly higher. In the remainder of the

research airfoils with a bending to stiffness ratio greater than one are referred to as the unconventional airfoil sections.

The second airfoil configuration is obtained from from the book *Introduction to Structural Dynamics and Aeroelasticity* Section 5.2 by Hodges [31]. The airfoil described by Hodges has design parameters based on conventional airfoils. The aifoil has a natural frequency ratio for pitching whch is significantly higher that the plunging natural frequency ratio. In the remainder of this research this airfoil configuration is referred to as the conventional airfoil configuration. The airfoil configuration in the book by Hodges is described using the following parameters: a, e, r, σ, and μ. These parameters are converted to the parameters used in the current research using the following relations:

$$\begin{aligned} x_0 &= (1+a)b \\ x_t &= (1+e)b \\ r^2 &= \frac{J_\alpha}{m_y b^2} \\ \sigma &= \frac{\omega_h}{\omega_\alpha} \\ \mu &= \frac{m_y}{\rho \pi b^2} \end{aligned} \tag{3.6}$$

This configuration is referred to as the conventional configuration in the remainder of the report.

The flexible trailing edge is modelled to be a fiberglass material. The stiffness and areal density properties used are presented in Table 3.3 and are obtained from measurements done in the paper by Gjerek et al. [20]. In Section 2.9 the influence of the viscoelastic material damping on the stability of the aeroelastic system has been shown. The material damping is defined in a similar manner as in the verification section and thus indirectly is a function of the number of plies. The value of non dimensional viscoelastic material damping coefficient is set to the value used in the paper by Tang and Paidoussis; being $\alpha = 0.004$ [23]. The material damping coefficient is set to a constant value since this is a material specific property.

3.3.1. Unconventional Airfoil Section Properties

An important paramer that influences the aeroelastic behaviour of an elastically supported airfoil significantly is the uncoupled natural frequency ratio of the elastic support. To be more specific, the airfoil flutter stability boundary is sensitive to a change in the uncoupled natural frequemcy ratio of the elastic support. The dependency of the critical airfoil flutter speed on the natural frequency ratio is shown for multiple Mach numbers in Figure 9.15 in the book $Aeroelasticity$ by Bisplinghoff et al. [43]. The paper by Gjerek et al. moreover shows that the airfoil flutter stability boundary sensitivity to a changing number of plies of the flexible plate is dependent on the frequency ratio [20]. By executing optimisations for airfoils with $\omega_h/\omega_\alpha = 0.5$, $\omega_h/\omega_\alpha = 1.0$, $\omega_h/\omega_\alpha = 1.5$, and $\omega_h/\omega_\alpha = 2.0$ it can be seen from Figure 3.9 that for frequency ratio's of 1.5 the biggest increase in critical flow speed can be achieved.

The values for the design variables used during the optimisations for the unconventional airfoil are found in Table 3.4. The mass, inertia, torsional spring stiffness, and plunging spring stiffness are determined as such that the bending to torsion natural frequnecy ratio of the elastic support is close to 1.5. The location of the elastic axis and center of gravity are set at $x_0 = 0.25$ and $x_t = 0.4$ of the chord.

Table 3.4: Constant design variables for the conventional airfoil configuration used during optimisations.

l [m]	b [m]	m_0 [kg]	m [kg]	$J_0[kgm^2]$	k_y [N/m]	k_α [Nm/rad]	d_y [Ns/m]	d_α [Nms/rad]
0.18	0.355	0.20	0.60	0.001	1800	1.50	1.00	0.001

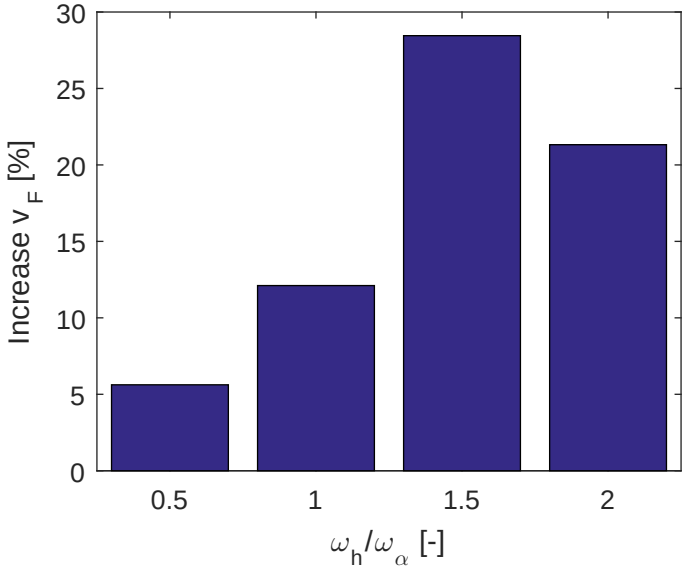

Figure 3.9: Relative increase in critical speed by optimisation compared to the most rigid sections considered $n_p = 6.00$) for different natural frequency ratio's.

3.3.2. Conventional Airfoil Section Properties

In the previous section it was shown that by adding flexibility to an airfoil section with unconventional properties the critical flow speed can be increased significanty. In this section an airfoil section is defined that possesses conventional properties. The airfoil section properties are obtained from Section 5.2 of the book *Introduction to Structural Dynamics and Aeroelasticity* by Hodges et al. [31]. The values of the non-dimensional parameters used in the book by Hodges are: $a = -1/5$, $e = -1/10$, $r^2 = 6/25$, $\sigma = 0.4$, and $\mu = 20$. These values can be rewritten to the current notation using equations 3.6.

The values for the design variables used during the optimisations of the conventional airfoil are shown in Table 3.5. The natural frequency ratio of the elastic support for the conventional configuration is thus set to 0.4. Using equations 3.6 the locations of the elastic axis and the center of gravity are $x_0 = 0.4$ and $x_t = 0.45$ of the chord.

Table 3.5: Constant design variables for the conventional airfoil configuration used during optimisations.

l [m]	b [m]	m_0 [kg]	m [kg]	$J_0[kgm^2]$	k_y [N/m]	k_α [Nm/rad]	d_y [Ns/m]	d_α [Nms/rad]
0.18	0.355	0.0	0.60	0.0011664	240	2.916	1.00	0.001

3.4. Unconventional Airfoil Section Results

In this section the results of the optimisations for the unconventional airfoil configuration are presented and discussed. The properties of the unconventional airfoil section are introduced in Sub-section 3.3.1. A reference critical flow speed is set by analysing the aeroelastic behaviour of a rigid airfoil section with equal values for the design variables as used during the optimisations for the unconventional airfoil. After the analysis of the rigid airfoil section results, the results of the optimisations for flexible airfoils are presented. Optimisations were executed for flexible airfoils with three different plate lengths, namely $l_p = 0.04m$, $l_p = 0.08m$, and $l_p = 0.12m$.

Before going to the results, let us first look into the notation of the plate designs that is used in this report. As was discussed earlier on in the chapter, there are two design variables per section. First is obviously the thickness expressed as the number of plies $n_{p,i}$ and the second is the ply angle rotation $r_{D,i}$. So $n_{p,i}$ is the thickness of the i^{th} section where counting starts from the clamp, and $r_{D,i}$ is the ply angle multiplication factor. The ply angle multiplication factor is multiplied with the flexural rigidity

D_p. The notation of a two section plate is as follows: $[r_{D,1}\ n_{p,1};\ r_{D,2}\ n_{p,2}]$ where $r_{D,1}$ is the multiplication factor of the first section, $n_{p,1}$ the thickness of the first section, $r_{D,2}$ the multiplication factor of the second section, $n_{p,2}$ the thickness of the second section.

3.4.1. Rigid section results unconventional airfoil

In order to be able to quantify the increase in critical flow speed by adding flexibility to the airfoil, results for the rigid section are defined. The aeroelastic matrix for the rigid section reduces to a two-by-two matrix since the influence of the plate is zero. Straightforwardly the aeroelastic system has two eigenvalues, and two corresponding eigenvectors which describe the motion of the rigid airfoil.

The flutter solution of the rigid airfoil with unconventional properties is shown in Figure 3.10. The divergence speed for the rigid section is infinite due to the fact that the elastic axis is located at the quarter-chord-point (the center of pressure). This result was obtained in the design variable study and presented in Figure 3.2. The critical speed is determined to be $v_F = 15.38m/s$ at a corresponding reduced frequency of $k = 0.2788$ ($\omega = 47.64rad/s$.). The critical aeroelastic mode is airfoil flutter. The critical flow speed for the rigid section is used as a reference value in the remainder of the sub-section.

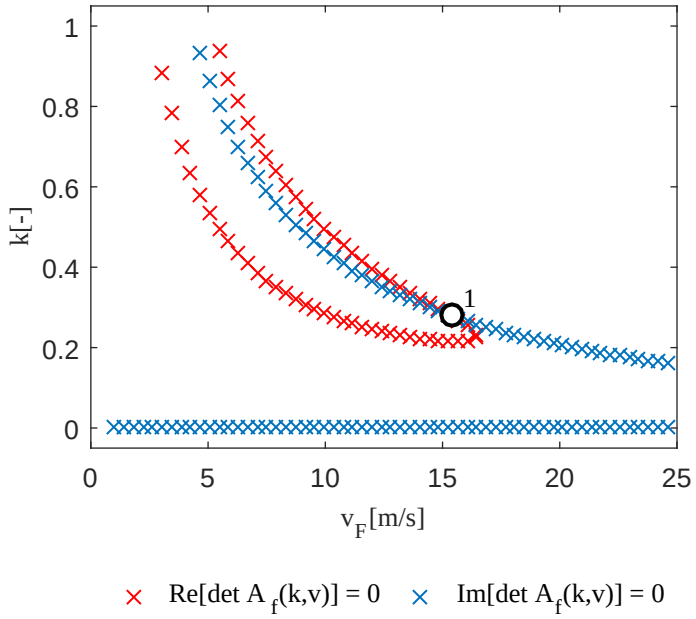

Figure 3.10: Flutter solution for a rigid airfoil section with unconventional properties.

3.4.2. Optimisation results unconventional airfoil

The first optimisation was executed for an unconventional airfoil with $l_p = 0.04m$. During the optimisation the number of plate sections S was increased until a convergence was obtained. The optimised plate designs for one to four plate sections together with the instability speeds are presented in Table 3.6. The corresponding flutter solutions of the aeroelastic systems with the optimised plate designs are shown in Figure 3.11.

The critical speeds in the table show that a convergence has been obtained for $S = 2$; increasing the number of plate sections to 3 or 4 does not increase the critical flow speed. Comparing the critical flow speed for one section with the critical flow speed for two sections an increase of $0.65m/s$ (3.7%) with respect to the constant plate is achieved. Another observation that is made is that the divergence speed is much higher than the airfoil flutter speed and the plate flutter speed. This is what could be expected because the plate is short, therefore the airfoil system possesses little flexibility. This observation is in agreement with what was shown in figures presented in Sub-section 3.2.1 Divergence study. The flutter solutions show that an optimal plate design has been obtained, when plate flutter and airfoil

flutter occur at the same time: the bimodal solution. This result is in agreement with the results that was observed by Drazumeric et al. in their research to partially flexible airfoils [3].

Table 3.6: Optimised plate designs and the corresponding instability speeds for an unconventional flexible airfoil with $l_p = 0.04m$.

S	v_{div} [m/s]	v_{af} [m/s]	v_{pf} [m/s]	Plate design
1	30.04	17.72	17.72	[0.8851 1.3174]
2	29.38	18.37	18.40	[0.8125 1.7643; 0.7382 1.0071]
3	29.35	18.34	18.46	[0.9928 2.4474; 0.8335 1.1156; 0.7999 1.0154]
4	29.23	18.42	18.67	[0.7407 4.2072; 0.9208 1.0345; 0.8595 1.0128; 0.7374 1.000]

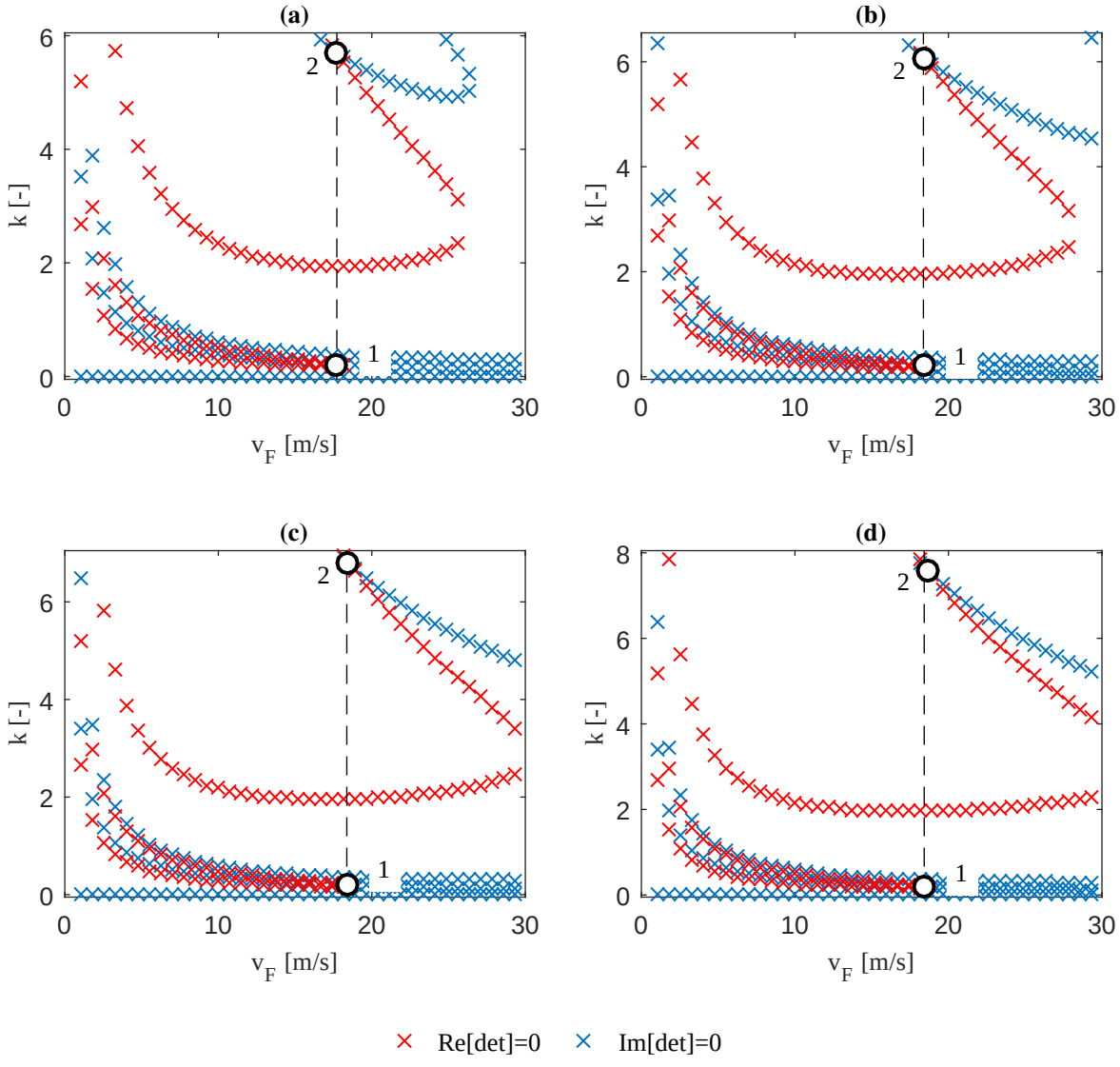

Figure 3.11: Optimisation results for flexible airfoils with unconventional properties for a flexible plate of $l_p = 0.04m$ with (a) $S = 1$, (b) $S = 2$, (c) $S = 3$, and (d) $S = 4$.

The second optimisation was executed for the an unconventional airfoil with $l_p = 0.08m$. All other design variables are kept constant. The optimised plate designs for one to four sections together with the instability speeds are presented in Table 3.7. The corresponding flutter speeds for one to our sections are shown in Figure 3.12.

Considering convergence a similar observation is made, namely that the critical flow speed for an increasing number of sections has converged for two sections. Comparing the critical speeds for the

constant plate with the plate divided in two sections, an increase of $4.61m/s$ (22.1%) with respect to the constant plate is seen. Contrary to the unconventional system with $l_p = 0.04m$ where an optimal design has been arrived at when airfoil flutter and plate flutter occur simultaneously, for this configuration an optimal design is obtained for the case where divergence and airfoil flutter occur simultaneously. The divergence speed is lower than in the previous system, due to the increased flexibility of the system.

Table 3.7: Optimised plate designs and the corresponding instability speeds for an unconventional flexible airfoil with $l_p = 0.08m$.

S	v_{div} [m/s]	v_{af} [m/s]	v_{pf} [m/s]	Plate design
1	26.24	20.85	20.85	[1.0000 2.6879]
2	25.46	25.50	43.28	[0.9261 5.9844; 0.9069 1.0366]
3	25.40	25.41	29.03	[0.8145 4.9135; 0.8982 3.8666; 0.8383 1.0476]
4	25.42	25.50	38.49	[0.8496 1.3018; 0.9929 5.6419; 0.9504 1.7006; 0.8169 1.1512]

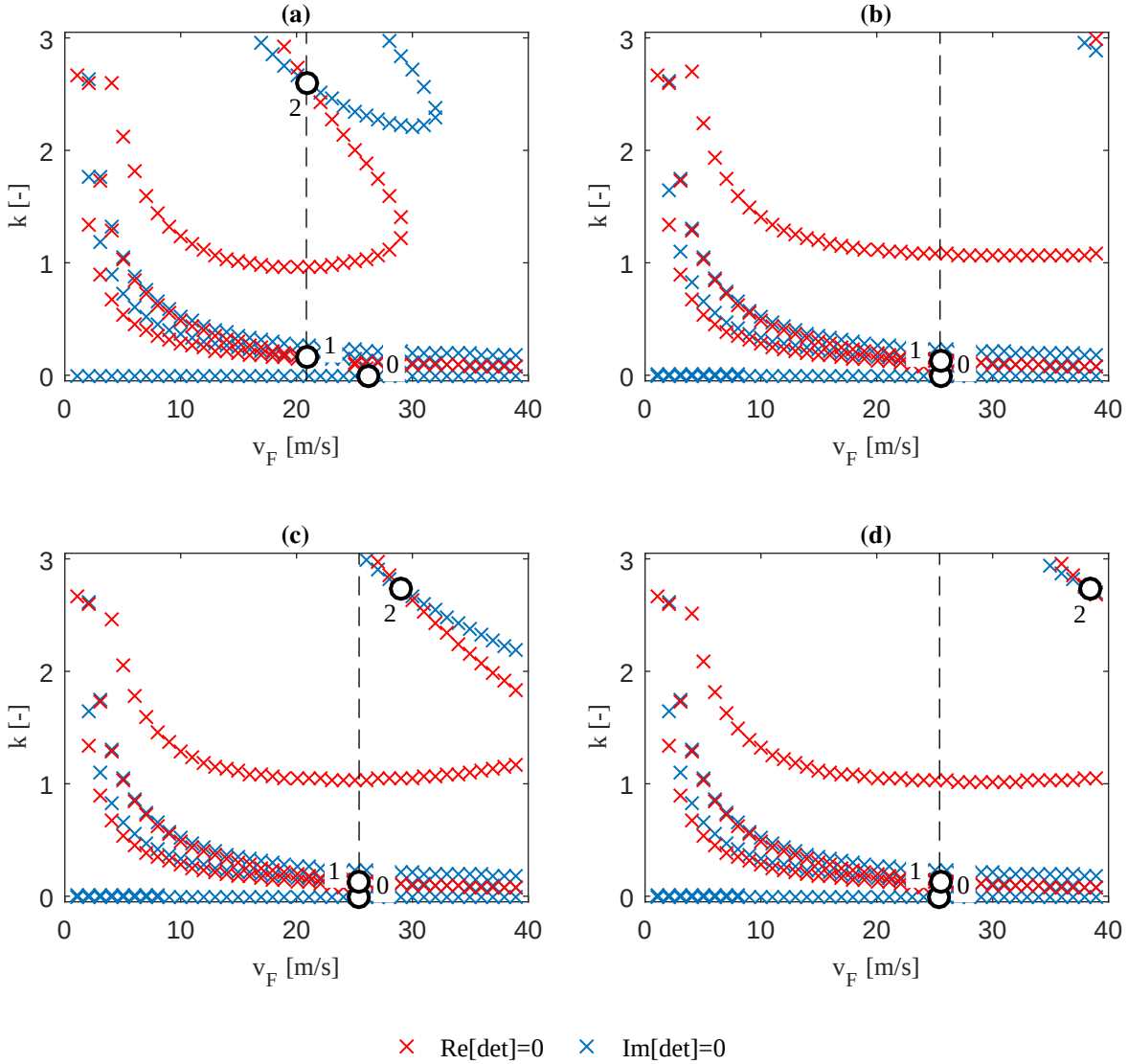

Figure 3.12: Optimisation results for flexible airfoils with unconventional properties for a flexible plate of $l_p = 0.08m$ with (a) $S = 1$, (b) $S = 2$, (c) $S = 3$, and (d) $S = 4$.

Again, an optimisation is executed for a similar airfoil configuration with an increased plate length of $l_p = 0.12m$. The results for the optimal plate designs with the critical speeds are presented in Table

3.8. The corresponding flutter solutions for one to four sections are shown in Figure 3.13.

Looking at the critical flow speeds in Table 3.8 it can be seen that the critical flow speed has converged for two plate sections similarly to the two other unconventional configurations considered. The critical speed has increased by $3.11m/s$ (13%) when comparing the critical speeds of the constant and the two-section plates. For the converged solutions it can be seen that the onset of divergence, airfoil flutter, and plate flutter occurs for (almost) similar flow speed. This solution will be called the trimodal solution in the remainder of the report.

Table 3.8: Optimised plate designs and the corresponding instability speeds for an unconventional flexible airfoil with $l_p = 0.12m$.

S	v_{div} [m/s]	v_{af} [m/s]	v_{pf} [m/s]	Plate design
1	27.31	23.93	23.93	[0.7944 4.7364]
2	27.04	27.12	27.63	[0.9507 5.6810; 0.9955 4.2132]
3	27.02	27.03	27.67	[0.8120 1.0464; 0.8621 5.8683; 0.9432 3.9748]
4	27.09	27.10	27.16	[0.7692 3.4821; 0.9937 5.9044; 0.8067 2.1782; 0.8920 4.8035]

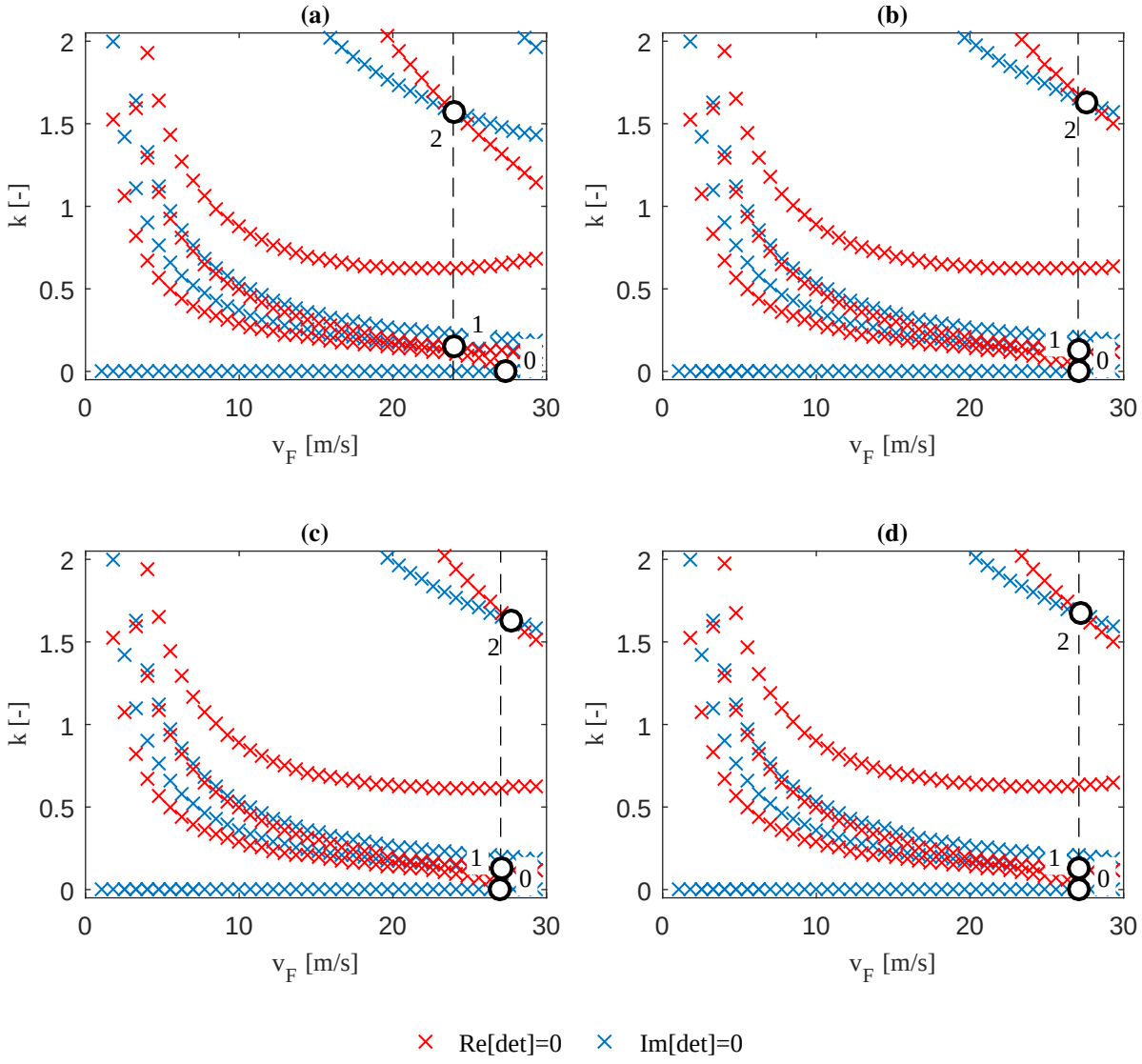

Figure 3.13: Optimisation results for flexible airfoils with unconventional properties for a flexible plate of $l_p = 0.12m$ with (a) $S = 1$, (b) $S = 2$, (c) $S = 3$, and (d) $S = 4$.

The configuration considered during this last optimisation is most similar to the aeroelastic system used

in the paper by Drazumeric et al. who also used a flexible plate with length $0.12m$ [3]. Drazumeric et al. employed a constant plate and their results should therefore be compared with Figure 3.13(a), which is the result for a constant plate. The results obtained are in agreement that the optimal solution for a constant plate is found for the case where airfoil flutter and plate flutter occur simultaneously; the bimodal solution.

To summarise the results of the optimisations for the unconventional airfoil sections, the normalised critical speeds for one to four section plates for the three different plate lengths considered are shown in Figure 3.14. The normalisation is performed with respect to the critical flow speed for the rigid section, which was determined to be $15.38m/s$. It can be seen that increases in critical flow speeds can be obtained up to 76%.

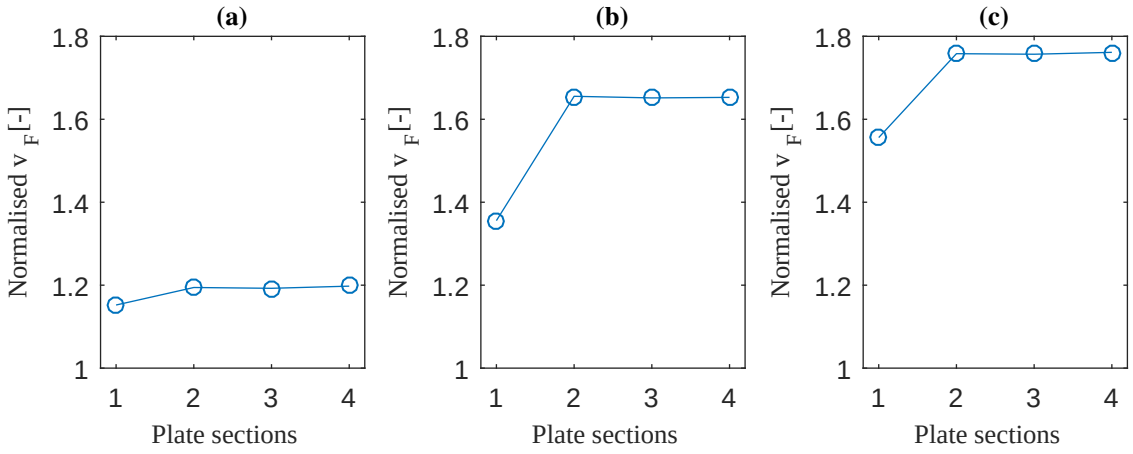

Figure 3.14: Normalised critical flow speed for unconventional airfoil sections for an increasing number of plate sections with (a) $l_p = 0.04m$, (b) $l_p = 0.08m$, and (c) $l_p = 0.12m$. The flow speeds are normalised with the critical flow speed for a rigid section.

3.5. Conventional Airfoil Section Results

In this section the results of the optimisations for the conventional airfoil configuration are presented and discussed. The properties of the conventional airfoil section are introduced in Sub-section 3.3.2. A similar procedure is followed as for the unconventional airfoil section. A reference critical flow speed is set by analysing a rigid airfoil section with equal values for the design variables as used during the optimisations. After the analysis of the rigid section, the results of the optimisations for flexible airfoil sections are presented. Optimisations were executed for flexible airfoils with two different plate lengths, namely $l_p = 0.04m$ and $l_p = 0.08m$. The number of plate sections was increased until a convergence in critical flow speed was obtained. A plate length of $0.12m$ is not used for the conventional airfoil optimisations, since this would lead to an unrealistic flexible fraction.

3.5.1. Rigid section results conventional airfoil

The flutter solution of the rigid airfoil with conventional properties is shown in Figure 3.15. In this flutter solution plot both instability modes of the rigid airfoil can be seen. The flow speed for divergence is calculated to be $21.35m/s$, but this mode is not critical. The difference in the divergence behaviour compared to the unconventional rigid section results from the more aft position of the elastic axis. Again, an aft moving elastic axis increases the aerodynamic moment and therefore decreases the divergence speed as shown in Figure 3.2. The critical aeroelastic mode is the airfoil flutter mode which occurs for a critical flow speed of $15.83m/s$ with a reduced frequency of $k = 0.1747$ ($\omega = 30.73rad/s$). The critical flow speed for the rigid section is used as a reference value in the remainder of the sub-section.

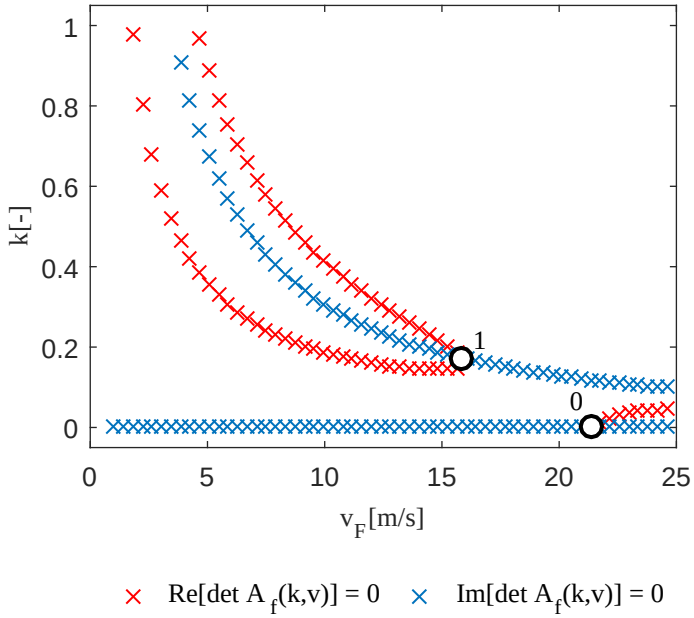

Figure 3.15: Flutter solution for a rigid airfoil section with conventional properties.

3.5.2. Optimisation results conventional airfoil

In the previous sub-section, where the results for the unconventional airfoil section were presented, adding flexibility to an airfoil looks very promising to increase the critical aeroelastic speed. However the airfoil configuration used is unconventional in a way that the natural frequency ratio between bending and torsional is unusual and moreover the elastic axis position is too close to the leading edge compared to conventional airfoils.

The results for the optimal plate design and the critical flow speeds for the conventional airfoil with $l_p = 0.04m$ are presented in Table 3.9. The corresponding flutter solutions for one and two sections are shown in Figure 3.16. It can be seen that no significant improvement in critical speed for the conventional airfoil section can be obtained by adding a plate of $0.04m$ compared to the rigid section. The introduction of a second plate section does not lead to an increase of the critical flow speed either.

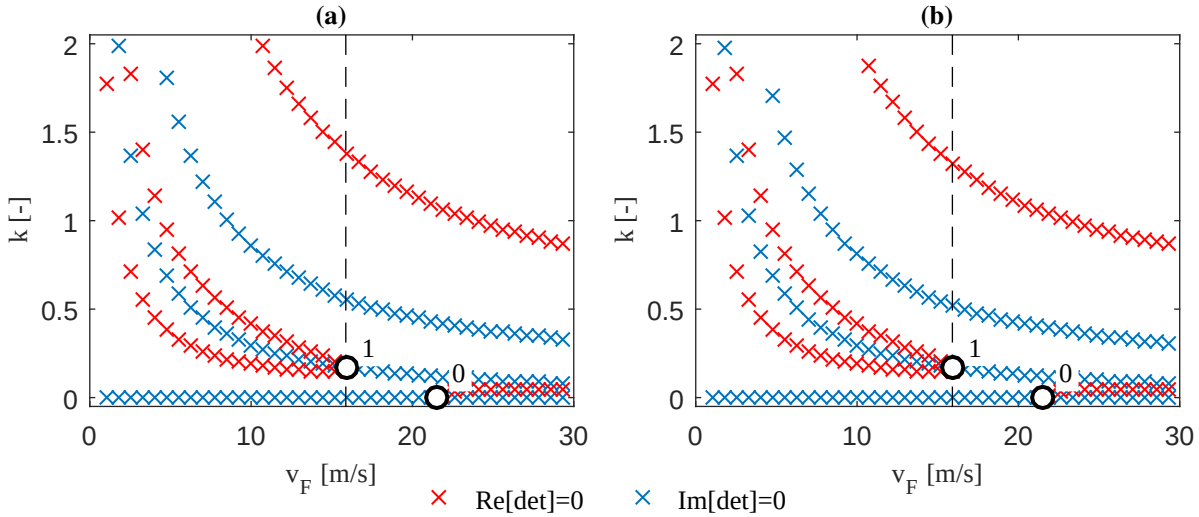

Figure 3.16: Optimisation results for flexible airfoils with conventional properties for a flexible plate of $l_p = 0.04m$ with (a) $S = 1$, (b) $S = 2$, (c) $S = 3$, and (d) $S = 4$.

Lastly an optimisation is executed for a conventional airfoil configuration with $l_p = 0.08$. The optimal

Table 3.9: Optimised plate designs and the corresponding instability speeds for a conventional flexible airfoil with $l_p = 0.04m$.

S	v_{div} [m/s]	v_{af} [m/s]	Plate design
1	21.47	15.87	[0.7407 5.9996]
2	21.53	15.91	[0.7400 1.0481; 0.7508 5.7079]

plate design and the critical speeds are presented in Table 3.10. The corresponding flutter solutions for one to four plate sections are shown in Figure 3.17.

It can be seen that a convergence has been reached for one section already, meaning a constant thickness plate. Compared to a rigid section where a critical flow speed of $15.83m/s$ was found, a limited increase in critical flow speed is observed. Airfoil flutter and plate flutter are the critical modes when the optimal plate designs are found, while for the unconventional airfoil configuration it was observed that divergence and airfoil flutter are critical.

Table 3.10: Optimised plate designs and the corresponding instability speeds for a conventional flexible airfoil with $l_p = 0.08m$.

S	v_{div} [m/s]	v_{af} [m/s]	v_{pf} [m/s]	Plate design
1	21.63	16.39	16.40	[0.9727 2.2881]
2	21.53	16.47	17.89	[0.8977 3.1082; 0.7517 1.0435]
3	21.52	16.49	17.79	[0.9809 4.4439; 0.8041 1.0553; 0.7862 1.0120]
4	21.52	16.48	16.48	[0.7695 1.5729; 0.9935 2.8713; 0.8137 1.0144; 0.7616 1.0591]

The normalised critical speeds for the conventional airfoil configurations with $l_p = 0.04m$ and $l_p = 0.08m$ are shown in Figure 3.18. The results show that a limited increase up to 4.1% is achieved for the system with $lp = 0.08m$.

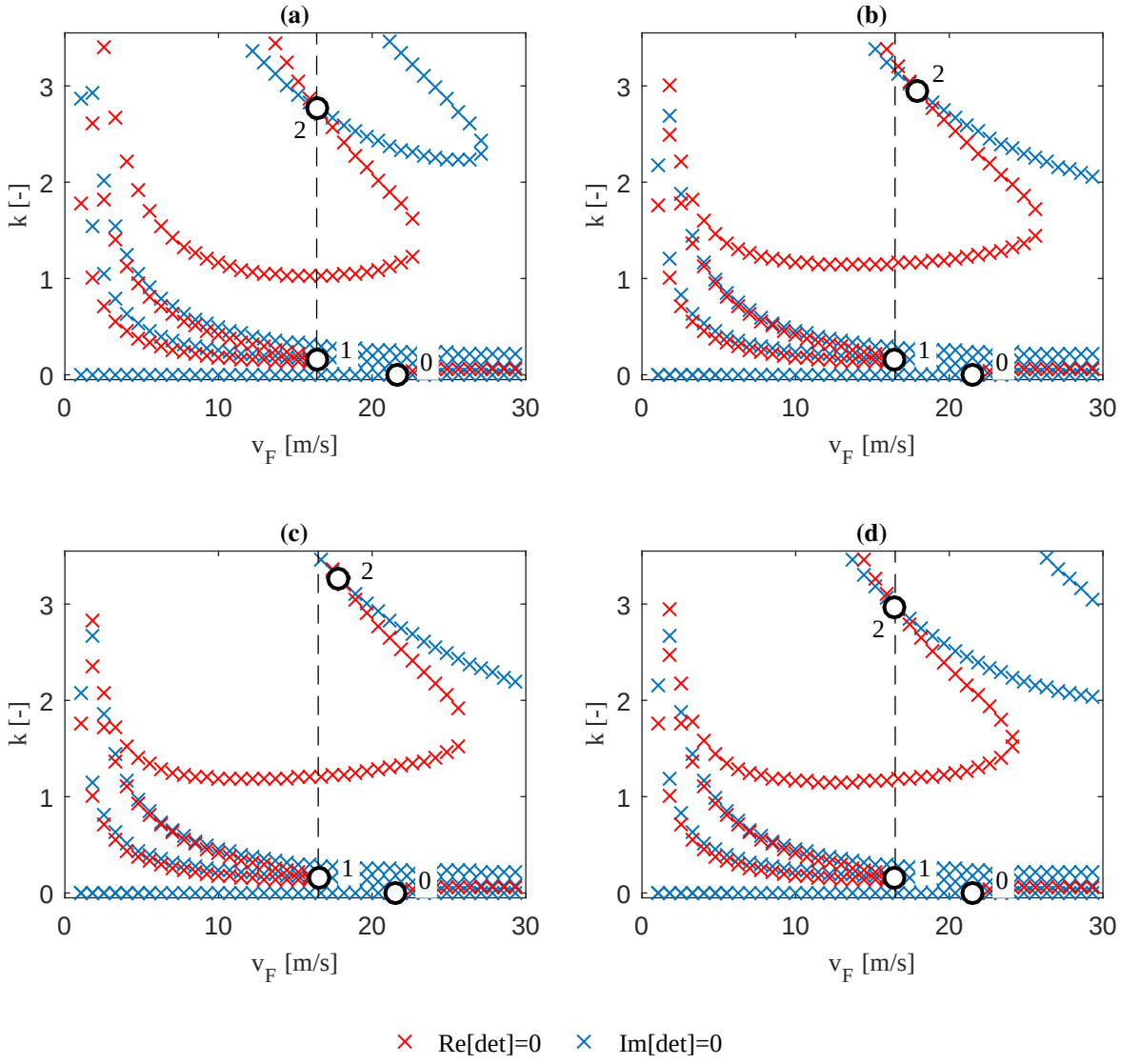

Figure 3.17: Optimisation results for flexible airfoils with conventional properties for a flexible plate of $l_p = 0.08m$ with (a) $S = 1$, (b) $S = 2$, (c) $S = 3$, and (d) $S = 4$.

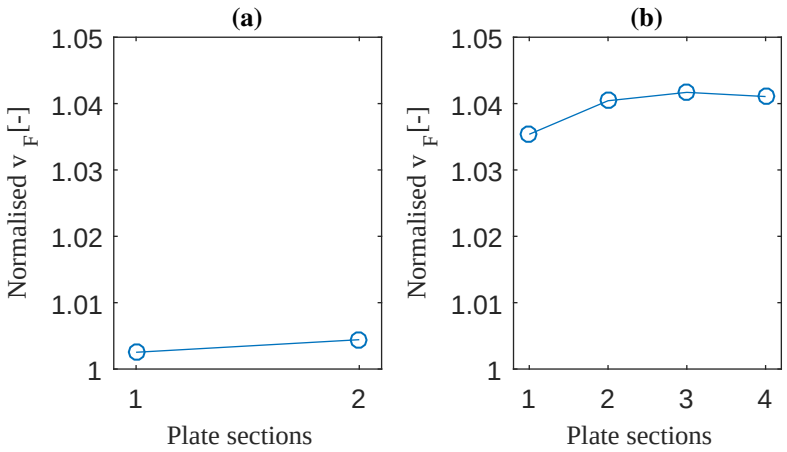

Figure 3.18: Normalised critical flow speed for conventional airfoil sections for an increasing number of plate sections with (a) $l_p = 0.04m$, and (b) $l_p = 0.08m$. The flow speeds are normalised with the critical flow speed for a rigid section.

3.5.3. Torsional Stiffness Variation

In this section the applicability of adding flexibility to an airfoil section is examined. Conventional airfoils posses a torsional stiffness that is significantly higher than the bending frequency. The results for the unconventional airfoil ($\omega_h/\omega_\alpha = 2.0$) and conventional airfoil ($\omega_h/\omega_\alpha = 0.4$) show that adding flexibility has a much higher beneficial effect for unconventional airfoil sections. Considering the afore mentioned, the results give rise to the question whether the critical flow speed can be increased by decreasing the torsional stiffness and adding flexibility to the airfoil. The advantage of lowering the torsional stiffness is that potentially lighter wings can be designed by adding flexibility, while the critical flow is not reduced by adding flexibility.

The applicability study of adding flexibility to an airfoil configuration for a varying natural frequency ratio begins with generating the critical flow speed boundary for a rigid section. For a rigid section yields that $l_p = 0m$, the remaining design variables that are kept constant during the applicability study are summarised in Table 3.11. The torsional stiffness is reduced from $k_\alpha = 18.225Nm/rad$ for which $\omega_h/\omega_\alpha = 0.4$ to $k_\alpha = 0.729Nm/rad$ for which $\omega_h/\omega_\alpha = 2.0$.

Table 3.11: Constant design variables for the applicability study of adding flexibility to an airfoil.

l [m]	b [m]	x_0 [m]	x_T [m]	m_0 [kg]	m [kg]	$J_0[kgm^2]$	k_y [N/m]	d_y [Ns/m]	d_α [Nms/rad]
0.18	0.355	0.072	0.081	0.0	0.60	0.0011664	1500	1.00	0.001

The resulting boundary for the critical speed for the rigid airfoil is shown by the blue line in Figure 3.19. It can be observed that by reducing the torsional stiffness, the critical flow speed reduces quickly until a minimum flow speed is reached where the torsional and bending natural frequencies are equal. This is as could be expected, since the the bending and torsional modes show strong interaction for this configuration. After reaching this minimum, the critical speed increases up until a natural frequency ratio of approximately 1.2. From approximately 1.2 to 2.0 the critical speed shows a decreasing trend. Since the torsional stiffness is decreased, the critical flow speed at which divergence occurs reduces and becomes the critical mode after the 'jump'.

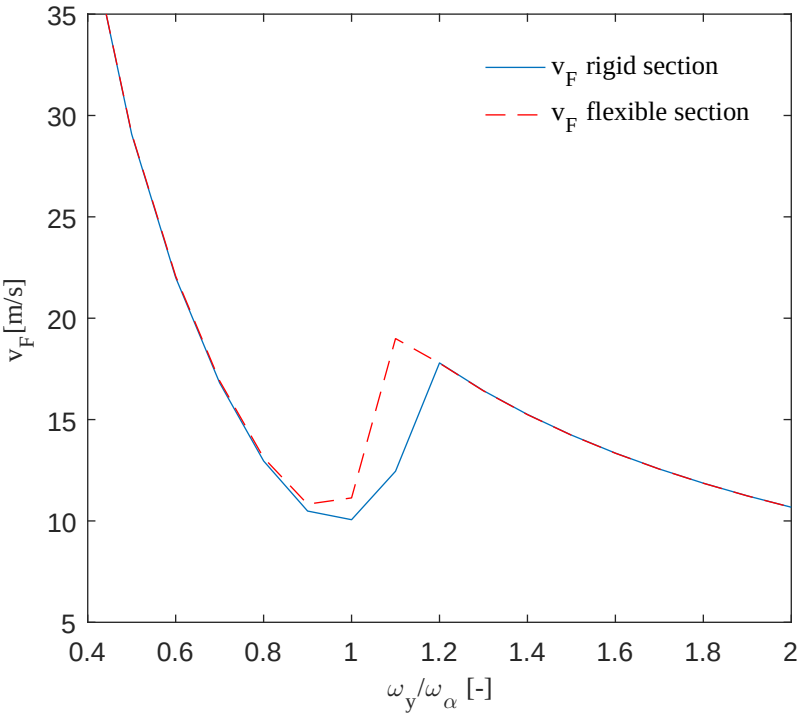

Figure 3.19: Critical flow speed plotted against a varying uncoupled natural frequency ratio of the elastic support for a rigid section and a flexible airfoil with a $l_p = 0.04m$ plate with an optimised thickness.

The next step is to add flexibility to the airfoil and optimise the thickness of the flexible trailing edge for the range of bending to torsional natural frequency ratio's considered. A constant thickness flexible plate with a length of $l_p = 0.04m$ was used during the optimisation. The resulting boundary for the critical speed for the optimised flexible airfoil configuration is shown by the dashed red line in Figure 3.19. The optimisation results for every natural frequency ratio are presented in Table B.1 in Appendix B.

As expected, adding a flexible plate of $l_p = 0.04m$ for low natural frequency ratio's does not increase the critical flow speed. This is an observation that was already seen in the optimisation results for the conventional airfoil sections. For natural frequency ratio's between 0.9 and 1.2 it is seen that the flexible plate has relieving effect on the critical airfoil flutter mode. At higher ratio's adding the flexible plate does not increase the critical flow speed. This last observation arises from the fact that the divergence mode is critical which can be increased by increasing the plate thickness as was observed from Figure 3.3. In Table B.1 in Appendix B it can be seen that the optimiser increases the thickness of the plate to the upper bound as was expected. Hence, when divergence is the critical mode, the critical speed can not be increased by adding flexibility.

The paper by Gjerek et al. presented increases up to 79% for a flexible airfoil with $l_p = 0.12$ and a natural frequency ratio of 1.7. The airfoil configuration used in the optimisation did not suffer from divergence for this high natural frequency ratio due to placing the elastic axis at 18% of the chord thus close to the leading edge. Remembering that Figure 3.2 showed that by moving the elastic axis towards the leading edge, divergence is mitigated. The difference in the location of the elastic axis is the explanation why in Figure 3.19 no increases in critical flow speed are observed for high bending to torsional natural frequencies.

4

Conclusions and Recommendations

In this chapter conclusions are drawn regarding the research objective. In Chapter 1 the research objective was presented, repeated in this chapter for convenience. The research objective was formulated as follows:

"Optimising the chordwise thickness distribution of a flexible composite trailing edge to postpone the onset of aeroelastic instabilities. For the optimisation a two-dimensional numerical model will be developed."

The research objective is divided into three sub-objectives.

1. Development of a two-dimensional numerical aeroelastic analysis methodology that accounts for airfoil flexibility and thickness-tailoring
2. Executing a verification of the developed aeroelastic analysis tool
3. Carrying out an optimisation which will provide an optimal stiffness distribution of the flexible trailing edge

In this section conclusions are drawn to what extend the sub-objectives are fulfilled.

4.1. Conclusions

The section is divided into four sub-sections, one for every sub-objective and in the last section the main objective is reflected on.

4.1.1. Sub-objective 1: Development aeroelastic model

An aeroelastic model has been developed to determine the aeroelastic characteristics of an elastically supported flexible airfoil. The model allows for a constant and a piecewise constant thickness distributed trailing edge. The thin airfoil is assumed to harmonically oscillate with small amplitudes. The aerodynamic forces and moments are calculated by adopting the Küssner and Schwarz model which relates the pressure distribution over the airfoil to the downwash [4]. The transverse motion of the plate is modelled as an Euler-Bernoulli beam under the assumption that no span-wise deformations in the flexible trailing edge occur. The aeroelastic stability boundary is obtained by solving a complex eigenvalue problem in matrix form. The solutions to the system of equations are obtained as couples of the reduced frequency with the corresponding critical flow speed. A deeper understanding of the physical mechanism of the instability point can be obtained by applying the p-k method to the aeroelastic system of interest.

4.1.2. Sub-objective 2: Verification of the aeroelastic model

A verification of the developed aeroelastic model has been performed. The verification consists of two parts: a verification of the aeroelastic model and a verification of the optimisation procedure. The

aeroelastic model is verified by comparison of the flutter boundary with results found in papers by Huang [18], De Breuker et al. [15], and Tang and Païdoussis [23]. A very good agreement between the results obtained with the current model and the results by the Tang and Païdoussis model is found for a non-dimensional material damping coefficient equal to 0.004. This model uses a vortex lattice model for representing the fluid loading, which is a fundamentally different method compared to the aerodynamic model used in this research. Comparing the flutter boundary for zero viscoelastic damping with the flutter boundary for zero damping obtained from the research by De Breuker et al. and Huang, significant differences are observed. Two discrepancies observed are the location of the mode jump and the trend of the reduced critical flow which are significantly different. No explanation has been found for the above mentioned discrepancies.

4.1.3. Sub-objective 3: Optimisation thickness distribution

The aeroelastic model is used to tailor the thickness distribution of the flexible trailing edge to optimise for the critical flow speed. Optimisations are executed for airfoil sections with conventional sectional parameters and with unconventional sectional parameters. In all cases it can be seen that a convergence in critical flow velocities was obtained for a trailing edge divided in two sections each with a constant thickness.

The optimisations for the unconventional airfoil configurations show good results in terms of the critical aeroelastic flow speed. During the optimisations it was shown that for a flexibility fraction of 2/3 an increase of 76% has been achieved. It was observed that an optimal critical flow speed is arrived at when divergence and airfoil flutter occur simultaneously. The addition of flexibility has a relieving effect on the airfoil flutter mode, in general it was observed that the airfoil flutter speed increases for a decreasing plate thickness. Contrary, the divergence speed increases for an increasing plate thickness. Therefore an optimum is reached as soon as divergence and airfoil flutter occur simultaneously because in order to increase the divergence speed the airfoil requires less flexibility, while more flexibility is required to increase the airfoil flutter mode. Here conflicting requirements are met and thus the optimum flow speed is achieved.

Optimisations for conventional wing parameters do not show much improvement in critical speed. Optimisations show that the critical flow speed for the conventional configuration with a flexibility fraction of 4/9 can be increased up to 4.1%. On one hand it can be concluded by adding flexibility to an airfoil the critical aeroelastic flow speed can only slightly be increased, but on the other hand adding flexibility, when well designed does not lower the critical flow speed and hence there is possibility to exploit this flexibility for aircraft control.

The optimisation results for the unconventional airfoil with a bending to torsional natural frequency ratio of 2.0 and the conventional airfoil with an uncoupled natural frequency ratio of 0.4 show that adding flexibility has a much higher beneficial effect for the unconventional airfoil configurations. This gave rise to the question if by adding a flexible plate to a wing while reducing the torsional stiffness of the airfoil, the critical aeroelastic flow velocity could be maintained or even improved. It can be concluded that for a conventional configuration with a reduced torsional stiffness it is not possible to increase the critical speed by adding flexibility. Since the torsional stiffness is decreased, the critical flow speed at which divergence occurs reduces and becomes the critical mode. Based on this study one can conclude that, as soon as the divergence becomes the critical aeroelastic instability no further improvements in terms of critical velocity can be achieved by reducing the flexibility of the flexible trailing edge.

4.1.4. Main objective: Postponing the aeroelastic instabilities

The main objective of the research was to postpone the aeroelastic instability boundary by introducing a chordwise thickness distribution over the flexible plate comprising the trailing edge. It has been shown that it is possible to postpone aeroelastic instabilities using a thickness-tailored flexible trailing edge. However, the increase in critical flow speed is highly dependent on the airfoil configuration as said in the conclusion on the third sub-objective. Within the thickness distribution study a convergence study was performed which investigated the effect of the number of chord-wise design regions in the flexible trailing edge on the critical speed. it was observed that no significant improvement could be achieved by introducing more than two design regions.

4.2. Recommendations

Important recommendations for future research efforts based on the current work are discussed in this section.

In the verification section a flutter boundary plot was created. Very good agreement was obtained when comparing the results between the current model and the results found in the paper by Tang and Païdoussis [23] for a plate with $\alpha = 0.004$. However, differences are observed for a plate which contains zero damping. Hence, further investigation of the implemented aeroelastic model is required to fully understand the origin of the observed differences.

The implemented aeroelastic model was verified against several flutter studies available in the literature. However, there is only limited literature available for the verification of the result obtained in the performed design studies. Hence, a validation is required in order to build more confidence in the obtained results.

Based on the optimisation results it is suggested to add flexibility to a three-dimensional wing with sweep and reduced torsional stiffness. The wing sweep is applied to increase the divergence speed of the wing, while a flexible fraction has a relieving effect to airfoil flutter. However, since a wing with a reduced torsional stiffness is considered, control reversal has to be taken into account in the investigation.

Look into the possibility to include flutter severity into the optimisation procedure. Not only the flow speed where the aeroelastic instability occurs is important, but also the severity of the onset. Severity is defined as the gradient with respect to the flow velocity of the damping at the point of instability. The gradient at the point of instability can be obtained using the p-k method.

Investigate a system where the plate mass is a significant fraction of the total mass. By increasing the mass significance of the flexible plate, the aeroelastic behaviour is more sensitive to the mass to stiffness ratio of the plate. Therewith an extra design variable is obtained which can be used to improve the aeroeastic behaviour.

Bibliography

[1] S.H. Kim and I. Lee. Aeroelastic Analysis Of A Flexible Airfoil With A Freeplay Non-Linearity. *Journal of Sound and Vibration*, 193(4):823–846, 1996.

[2] J. Murua, R. Palacios, and J. Peiró. Camber effects in the dynamic aeroelasticity of compliant airfoils. *Journal of Fluids and Structures*, 26:527–543, 2010.

[3] R. Drazumeric, B. Gjerek, F. Kosel, and P. Marzocca. On bimodal flutter behavior of a flexible airfoil. *Journal of Fluids and Structures*, 45:164–179, 2014.

[4] H.G. Küssner and L. Schwarz. The oscillating wing with aerodynamically balanced elevator. *Luftfahrtforschung*, 17(991):11–12, 1940.

[5] E.H. Dowell, R. Clark, D. Cox, H.C. Curtis Jr., and J.W. Edwards. *A Modern Course in Aeroelasticity*. Kluver Academic Publishers, Dordrecht, fourth rev edition, 2005.

[6] T. Buhl, M. Gaunaa, and C. Bak. Potential Load Reduction Using Airfoils with Variable Trailing Edge Geometry. *Journal of Solar Energy Engineering*, 127(4):503, 2005.

[7] L. Bergami and M. Gaunaa. Stability investigation of an airfoil section with active flap control. *Wind Energy*, 13:151–166, 2010.

[8] B Lambie, M Jain, and C Tropea. Passive Camber Change for Windturbine Load Alleviation. Number January, Orlando, 2011.

[9] R Srivastava, M.A. Bakhle, T.G. Keith Jr, and D. Hoyniak. Aeroelastic analysis of turbomachinery Part I– phase lagged boundary condition methods. *International Journal of Numerical Methods for Heat & Fluid Flow*, 14(3):382–402, 2004.

[10] R. Srivastava, M.A. Bakhle, T.G. Keith Jr, and D. Hoyniak. Aeroelastic analysis of turbomachinery: Part II – stability computations. *International Journal of Numerical Methods for Heat & Fluid Flow*, 14(3):382–402, 2004.

[11] P.P. Sarkar, N.P. Jones, and R.H. Scanlan. Identification of Aeroelastic Parameters of Flexible Bridges. *Journal of Engineering Mechanics*, 120(8):1718–1742, 1994.

[12] P.P. Sarkar, L. Caracoglia, F.L. Haan, H. Sato, and J. Murakoshi. Comparative and sensitivity study of flutter derivatives of selected bridge deck sections, Part 1: Analysis of inter-laboratory experimental data. *Engineering Structures*, 31(1):158–169, 2009.

[13] G.A.A. Thuwis, R. De Breuker, M.M. Abdalla, and Z. Gürdal. Aeroelastic tailoring using lamination parameters : Drag reduction of a Formula One rear wing. *Structural and Multidisciplinary Optimization*, 41(4):637–646, 2010.

[14] J.R. Wright and J.E. Cooper. *Introduction to Aircraft Aeroelasticity and Loads*. John Wiley & Sons. Ltd, Chichester, first edition, 2008.

[15] R. De Breuker, M.M. Abdalla, and Z. Gürdal. Flutter of Partially Rigid Cantilevered Two-Dimensional Plates in Axial Flow. *AIAA Journal*, 46(4):936–946, 2008.

[16] T. Theodorsen. General Theory of Aerodynamic Instability and the Mechanism of Flutter. Technical report, NASA, 1935.

[17] A. Kornecki and E.H. Dowell. On the aerodynamic forces involved in aeroelastic instability of two-dimensional panels in uniform incompressible flow. *Journal of Sound and Vibration*, 80(3):437–439, 1976.

[18] L. Huang. Flutter of cantilevered plates in axial flow. *Journal of Fluids and Structures*, 9:127–147, 1995.

[19] D.M. Tang, H. Yamamoto, and E.H. Dowell. Flutter and limit cycle oscillations of two-dimensional panels in three-dimensional axial flow. *Journal of Fluids and Structures*, 17:225–242, 2003.

[20] B. Gjerek, R. Drazumeric, and F. Kosel. Flutter behavior of a flexible airfoil: Multiparameter experimental study. *Aerospace Science and Technology*, 36:75–86, 2014.

[21] L.K. Shayo. The Stability of Cantilever Panels in Uniform Incompressible Flow. *Journal of Sound and Vibration*, 68(3):341–350, 1980.

[22] D. Tang and E.H. Dowell. Limit cycle oscillations of two-dimensional panels in low subsonic flow. *International Journal of Non-Linear Mechanics*, 37:1199–1209, 2002.

[23] L. Tang and M.P. Païdoussis. On the instability and the post-critical behaviour of two-dimensional cantilevered flexible plates in axial flow. *Journal of Sound and Vibration*, 305(1-2):97–115, 2007.

[24] C. Kassapoglou. *Design and Analysis of Composite Structures*. John Wiley & Sons. Ltd, Chichester, first edit edition, 2010.

[25] C. Semler, G.X. Li, and M.P. Païdoussis. The Non-linear Equations of Motion of Pipes Conveying Fluid. *Journal of Sound and Vibration*, 169(5):577–599, 1994.

[26] D. Tang, J.K. Henry, and E.H. Dowell. Limit cycle oscillations of delta wing models in low subsonic flow. *AIAA Journal*, 37(11):1355–1362, 1999.

[27] R. Drazumeric, B. Gjerek, and F. Kosel. Aeroelastic Characteristic of an Airfoil Containing Laminated Composite Plate. *AIAA*, (January):1–15, 2014.

[28] M. Gaunaa. Unsteady two-dimensional potential-flow model for thin variable geometry airfoils. *Wind Energy*, 13:167–192, 2010.

[29] M. Mesarič and F. Kosel. Unsteady airload of an airfoil with variable camber. *Aerospace Science and Technology*, 8:167–174, 2003.

[30] N.P.M. Werter, J. Sodja, and R. De Breuker. Design and Testing of an Aeroelastically Tailored Wing under Manoeuvre Loading. pages 1–16, Saint Petersburg, 2015.

[31] D H Hodges. *Introduction to structural dynamics and aeroelasticity*. First edition, 2011.

[32] J. Roesler, H. Harders, and M. Baeker. *Mechanical Behaviour of Engineering Materials*. Springer, New York, 2007.

[33] J.D. Anderson. *Fundamentals Of Aerodynamics*. McGRAW-HILL, New York, fifth edition, 2010.

[34] T.H.G Megson. *Aircraft structures for engineering students*. 2007.

[35] Hilbert D. Courant, R. *Methods of Mathematical Physics*. Wiley, New York, 1989.

[36] B. Gjerek, R. Drazumeric, and F. Kosel. A Novel Experimental Setup for Multiparameter Aeroelastic Wind Tunnel Tests. *Experimental Techniques*, 38(6):30–43, 2014.

[37] Herman J Hassig. An Approximate True Damping Solution of the Flutter Equation by Determinant Iteration. *J. Aircraft*, 8(11):885–889, 1971.

[38] Ming Chen, Lai Bing Jia, Xiao Peng Chen, and Xie Zhen Yin. Flutter analysis of a flag of fractional viscoelastic material. *Journal of Sound and Vibration*, 333(26):7183–7197, 2014.

[39] Ming Chen, Laibing Jia, Siying Wang, and Xiezhen Yin. Effects of material damping on flag flutter. *Science China Technological Sciences*, 57(1):117–127, 2014.

[40] L. Tang, M. P. Païdoussis, and J. Jiang. Cantilevered flexible plates in axial flow: Energy transfer and the concept of flutter-mill. *Journal of Sound and Vibration*, 326(1-2):263–276, 2009.

[41] Haftka R.T. P. Hajela Gurdal, Z. *Design and Optimization of Laminated Composite Materials*. John Wiley & Sons. Ltd, Chichester, 1999.

[42] Ishai O. Daniel, I. M. *Engineering Mechanics of Composite Materials*. Oxford University Press, New York, 2006.

[43] Ashley H. Halfman R. L. Bisplinghoff, R. L. *Aeroelasticity*. Dover Publications, Inc, Mineola, New York, 1955.

A

Derivation Euler-Lagrange Equations

Energy methods have proven themselves to be useful methods to derive the dynamic equations of motion for an elastic body [5]. Newton's second law can also be used to derive the equations of motion of any elastic system, however for systems with many degrees of freedom it is more efficient to use the procedure based on Hamilton's principle or the Euler-Lagrange equations. One of the advantages of energy methods is that energy methods give a methodology of deriving the equations of motion without excessive bookkeeping of signs, which is quite challenging when Newton's second law is used. Secondly in energy methods we deal with work or energy scalars opposed to Newtonian mechanics where there is dealt with force and acceleration vectors [5].

When an object or particle in an elastic body moves from point 'a' to point 'b' the total work done on the system is defined as the action. The action thus depends on the starting and ending points of a path, and moreover on the actual trajectory of the path [5]. The value of the action is determined by integrating the functional for the action, which depends on the trajectory and all 't' in the interval. This dependence of the value for the action on the path makes the concept of Hamilton's principle useful. Hamilton's principle states that the actual motion is along the path for which the action is stationary. In other words the actual motion is along the path for which the derivative of the functional for the action is zero i.e. the path for which the action in minimal or maximal.

The functions for which Hamilton's principle is stationary are found by substituting Hamilton's principle into the Euler-Lagrange equation. The Euler-Lagrange equation is a second order partial differential equation which solutions are the functions for which a given functional is stationary. Therefore substituting the formulation for the action into the Euler-Lagrange equation results in the functions for which the action is stationary. The functions for which the action is stationary or minimal are called the equations of motion.

The general dynamic equations of motion are derived by using Hamilton's principle and the Euler-Lagrange equation. The derivation of Hamilton's principle for the action starts off with Newton's second law. Next the Euler-Lagrange equation is derived from Hamilton's principle. This procedure is followed to show that the Euler-Lagrange equation is basically a different way of writing Newton's second law with the advantage that it is invariant for coordinate transformations. Non-conservative forces and are introduced through virtual work.

A.0.1. Hamilton's Principle

The derivation of Hamilton's principle for the stationary action starts with Newton's second law. Newton's second law can be written as

$$m\frac{d^2\mathbf{r}}{dt^2} = \mathbf{F} \tag{A.1}$$

Rewriting,

$$m\frac{d^2\mathbf{r}}{dt^2} - \mathbf{F} = 0 \tag{A.2}$$

where $\mathbf{F}$ is the force vector and $\mathbf{r}$ the displacement vector of the airfoil, and m the mass. The deformations of an elastic structure vary continuously with time and are dependent on the location on the airfoil. Hence the displacement vector is a function of time t and position on the airfoil x, now the position vector of the airfoil is represented by $\mathbf{r}(t,x)$.

By introducing a set of generalized coordinates, the configuration of the aeroelastic system can uniquely be described at any point in time with respect to the reference system. A generalized coordinate is arbitrary and independent of other generalized coordinates. The set of generalized coordinates q_i, for the aeroelastic system described in section 2.1 consists of the plunge motion, the pitch motion, and the transverse plate bending defined by the symbols $y_0(t)$, $\alpha_0(t)$, and $w(x,t)$ respectively. Therefore the displacement of any point on the airfoil may be written as

$$\mathbf{r} = \mathbf{r}\left(y_0(t), \alpha_0(t), w(x,t)\right) \tag{A.3}$$

where q_i is the i^{th} generalized coordinate. The set of generalized coordinates covers the complete motion of the airfoil in two-dimensions. Splitting the position vector $r(t,x)$ into components

$$\mathbf{r} = u\mathbf{i} + v\mathbf{j} \tag{A.4}$$

where u is the horizontal displacement component, v the vertical displacement component, $\mathbf{i}$, and $\mathbf{j}$ the unit Cartesian vectors. The wing motion in horizontal direction is restricted and only small pitching angles are considered. Based on these assumptions the displacement components are approximated as

$$\left.\begin{aligned} u &= x\left[\cos\left(\alpha_0\right) - 1\right] \approx 0 \\ v = y_0 + \sin\left(\alpha_0\right)\left(x + \tfrac{l}{2} - x_0\right) - w &\approx y_0 + \alpha_0\left(x + \tfrac{l}{2} - x_0\right) - w \end{aligned}\right\} for\ a_0 \ll 1 \tag{A.5}$$

Hence the displacement vector for the aeroelastic system considered is equal to the vertical displacement component v. Now the aeroelastic system is defined and the displacement components are expressed in terms of generalised coordinates. The displacement vector r in equation A.2 can be replaced by the vertical velocity component v.

$$m\frac{d^2v}{dt^2} - F = 0 \tag{A.6}$$

Consider an adjacent path $v + \delta v$ where v is the virtual displacement. The variation of the virtual work δv is zero at $t = t_1, t_2$, the begin and end points of the path, since these locations are known.

$$\int_{t_1}^{t_2}\left(m\frac{d^2v}{dt^2}\cdot\delta v - F\cdot\delta v\right)dt = 0 \tag{A.7}$$

The first term is the virtual kinetic energy, which can be written in in a simpler fashion using integration by parts.

$$\begin{aligned} m\int_{t_1}^{t_2}\frac{d^2v}{dt^2}\cdot\delta v dt &= \cancel{m\frac{dv}{dt}\cdot\delta v\Big|_{t_1}^{t_2}} - m\int_{t_1}^{t_2}\frac{dv}{dt}\cdot\frac{d}{dt}\delta v dt \\ &= -m\int_{t_1}^{t_2}\frac{dv}{dt}\cdot\delta\frac{dv}{dt}dt \\ &= -\frac{m}{2}\int_{t_1}^{t_2}\delta\left(\frac{dv}{dt}\cdot\frac{dv}{dt}\right)dt \end{aligned} \tag{A.8}$$

where the first term on the right hand side is zero, since the variation of the virtual displacement δv is zero at times t_1 and t_2. The second term between brackets in equation A.7 is the virtual work done by conservative forces F_C. Substituting the final form of Equation A.8 into Equation A.7 result in,

$$\int_{t_1}^{t_2} \left[\frac{1}{2} m \delta \left(\frac{dv}{dt} \cdot \frac{dv}{dt} \right) + F_C \cdot \delta v \right] dt = 0 \tag{A.9}$$

The virtual work done by conservative forces can be divided into internal potential energy U and external potential energy V.

$$\int_{t_1}^{t_2} [\delta T - (\delta U + \delta V)]\, dt = 0 \tag{A.10}$$

Equation A.10 is the final form of Hamilton's variational principle for the action for conservative systems.

A.0.2. Euler-Lagrange Equation

By reversing the process by which Hamilton's principle was obtained from Newton's second law, the Euler-Lagrange equation will be derived. Remember that the Euler-Lagrange equation is used to find the functions for which a given functional is stationary. For the aeroelastic system there will be searched for the values for which the action of the system is stationary. Therefore taking the derivative of the functional for the action with respect to every single generalized coordinate gives the functions for which the action is stationary. The functions found are the equations of motion for the aeroelastic system considered.

A mathematical function called the Lagrangian is a function of the generalized coordinates, their time derivatives, and time, that contains information about the dynamics of the system. The Lagrangian for a dynamic aeroelastic system under consideration is given by,

$$\mathcal{L}(q_i, \dot{q}_i, t) = T - (U + V) \tag{A.11}$$

where

$$\begin{aligned} T &= T(\dot{q}_i(t)) \\ U &= U(q_i(t)) \\ V &= V(q_i(t)) \end{aligned} \tag{A.12}$$

In order to find the stationary functions that are the solutions to Hamilton's functional for the action, we take the total derivative of the Lagrangian and equate it to zero.

$$\sum_i \int_{t_1}^{t_2} \left[\frac{\partial \mathcal{L}(q_i, \dot{q}_i, t)}{\partial \dot{q}_i} \delta \dot{q}_i + \frac{\partial \mathcal{L}(q_i, \dot{q}_i, t)}{\partial q_i} \delta q_i \right] dt = 0 \tag{A.13}$$

The first term between brackets contains the variation of the time derivative of the generalised coordinates. In order to get rid of the time derivative, integration by parts is applied.

$$\sum_i \cancel{\frac{\partial \mathcal{L}(q_i, \dot{q}_i, t)}{\partial \dot{q}_i} \delta q_i \Big|_{t_1}^{t_2}} + \int_{t_1}^{t_2} \left[-\frac{d}{dt} \frac{\partial \mathcal{L}(q_i, \dot{q}_i, t)}{\partial \dot{q}_i} \delta q_i + \frac{\partial \mathcal{L}(q_i, \dot{q}_i, t)}{\partial q_i} \delta q_i \right] dt = 0 \tag{A.14}$$

The first term in equation A.14 has the bounds t_1 and t_2 for which we know that the variation of the path δq_i is zero and therefore the complete term is zero. Collecting terms,

$$\sum_i \int_{t_1}^{t_2} \left[-\frac{d}{dt} \frac{\partial \mathcal{L}(q_i, \dot{q}_i, t)}{\partial \dot{q}_i} + \frac{\partial \mathcal{L}(q_i, \dot{q}_i, t)}{\partial q_i} \right] \delta q_i dt = 0 \tag{A.15}$$

Since we know that the δq_i are independent and arbitrary it follows that the part between brackets must be zero. This results in the following form of the Euler-Lagrange equation,

$$-\frac{d}{dt}\frac{\partial \mathcal{L}\,(q_i, \dot{q}_i, t)}{\partial \dot{q}_i} + \frac{\partial \mathcal{L}\,(q_i, \dot{q}_i, t)}{\partial q_i} = 0 \tag{A.16}$$

This equation represents the general Euler-Lagrange equations for conservative systems. Since it is known that the kinetic energy is a function of the time derivatives of the generalised coordinates, and in turn the internal and external potential energy are a function of the generalised coordinates, the Euler-Lagrange equations can be simplified to,

$$\frac{d}{dt}\frac{\partial T}{\partial \dot{q}_i} + \frac{\partial (U+V)}{\partial q_i} = 0 \tag{A.17}$$

In the next section the Euler-Lagrange equations are modified to introduce non-conservative forces in the equations.

A.0.3. Modified Euler-Lagrange Equation

Not all forces acting on the aeroelastic system can be derived from potentials. The forces that cannot be derived from potentials are the non-conservative forces. Examples of forces that can't be derived from a potential are frictional, and aerodynamic forces. The non-potential forces are introduced in equation A.15 through virtual work. The virtual work done by non-conservative forces is given by

$$\delta W_{NC} = -Q_i \cdot \delta q_i \tag{A.18}$$

where Q_i represents the generalised forces which are a function of the generalised coordinates. Substitution of the virtual work due to the non-conservative forces at the right hand side of equation A.15 gives,

$$\sum_i \int_{t_1}^{t_2} \left[-\frac{d}{dt}\frac{\partial \mathcal{L}\,(q_i, \dot{q}_i, t)}{\partial \dot{q}_i} + \frac{\partial \mathcal{L}\,(q_i, \dot{q}_i, t)}{\partial q_i} \right] \delta q_i dt = -Q_i \cdot \delta q_i \tag{A.19}$$

Rearranging terms,

$$\sum_i \int_{t_1}^{t_2} \left[-\frac{d}{dt}\frac{\partial \mathcal{L}\,(q_i, \dot{q}_i, t)}{\partial \dot{q}_i} + \frac{\partial \mathcal{L}\,(q_i, \dot{q}_i, t)}{\partial q_i} + Q_i \right] \delta q_i dt = 0 \tag{A.20}$$

Again since we know that δq_i are arbitrary and independent, the term between brackets must be zero. The modified Euler-Lagrange equations now become,

$$-\frac{d}{dt}\frac{\partial \mathcal{L}\,(q_i, \dot{q}_i, t)}{\partial \dot{q}_i} + \frac{\partial \mathcal{L}\,(q_i, \dot{q}_i, t)}{\partial q_i} + Q_i = 0 \tag{A.21}$$

The modified Euler-Lagrange equations defined in equation A.21 are used to derive the equations of motion for the aeroelastic system.

B

Result Tables

Table B.1: Optimisation results flexible airfoil section with conventional properties and $l_p = 0.04m$.

ω_{nr} [-]	v_F [m/s]	r_D [-]	n_p [-]
0.4	39.27	0.7377	5.68
0.5	29.11	0.7386	1.97
0.6	22.08	0.8043	1.59
0.7	16.91	0.8446	1.30
0.8	13.12	0.7735	1.12
0.9	10.83	0.7383	1.00
1.0	11.14	0.7517	1.00
1.1	19.00	0.9963	1.48
1.2	17.78	0.9987	5.99
1.3	16.41	0.9973	5.99
1.4	15.24	0.9898	5.98
1.5	14.23	0.9967	5.99
1.6	13.34	0.9991	5.98
1.7	12.56	0.9926	6.00
1.8	11.86	0.9887	6.00
1.9	11.24	0.9976	5.99
2.0	10.67	0.9843	5.99